Study of water treatment using photocatalytic material

Tsuyoshi Sugita

Department of Production Science and Technology, Gunma University

(From April 2012 to March 2015, supervised by Professor Hideyuki Itabashi)

March 2015

Contents

Chapter 1

Introduction

1.1. Photocatalytic reaction as advanced oxidation technologies

Advanced Oxidation Technology (AOT) is characterized by production of the OH radical as a primary oxidant [1]. AOT is a method that uses the oxidizing power generated from environmentally friendly chemicals, for the effective and economical removal of pollutants at room temperature [2]. The oxidizing power of AOT is mainly derived from OH radicals, ozone [3,4], and semiconducting metal oxides [5]. The OH radical generated from an oxidant has stronger oxidizing power (oxidation potential: 2.80 eV) than other oxidants in water (**Table. 1-1**), and can decompose organic pollutants into relatively harmless compounds. Various studies about sources of the OH radical including semiconducting metal oxides have been reported. Prasad *et al.* have studied the organic photodecomposition of sulfur mustard by ZnO [6], and Guo *et al.* have studied photodecomposition of acid orange 7 and phenol using Fe_2O_3 [7]. Other metal oxides such as Nb_2O_5, $BiTiO_3$, $SrTiO_3$, $ZnWO_4$, and WO_3 have been studied [8,9].

Among these metal oxides, anatase-type TiO_2, which acts as a photocatalyst, is especially attractive owing to its high stability, low cost, and low toxicity [10]. **Fig. 1-1** shows the schematic illustration of the photocatalytic redox reaction of TiO_2. An electron in a filled valence band (VB) is excited into a vacant conduction band (CB) when the irradiated photon energy is greater than the gap energy between the VB and CB, a band gap, to give a photoexcited electron (e^-) and a hole (h^+) in the CB and VB,

respectively. These species, *i.e.*, charge carriers, in the CB and VB reduce and oxidize substrates adsorbed on the photocatalyst surface, respectively [11]. TiO_2-based photocatalysts can generate OH radicals semi-permanently, using only photoenergy (mainly UV radiation, without additional chemicals), and reduce the operating cost of redox reactions substantially.

On the other hand, water treatment used TiO_2 has not been demonstrated. The low luminous efficiency of TiO_2 prevents the TiO_2-based photocatalysts from acting as a decomposer for organic substances in water [12]. The main objective of this study is to overcome this challenge.

Table 1-1

Redox potentials of the major oxidizing agents used in water treatment technology [2].

Oxidizing agent	Oxidation potential /V	Relative oxidizing power*
OH radical	2.80	2.06
Ozone	2.07	1.52
Hydrogen peroxide	1.77	1.30
Perhydroxyl radical	1.70	1.25
Permanganate	1.68	1.24
Chlorine dioxide	1.57	1.15
Chlorine	1.36	1.00
Oxygen	1.20	0.88

*Oxidizing power relative to chlorine, which is assumed to have an oxidizing power of 1.

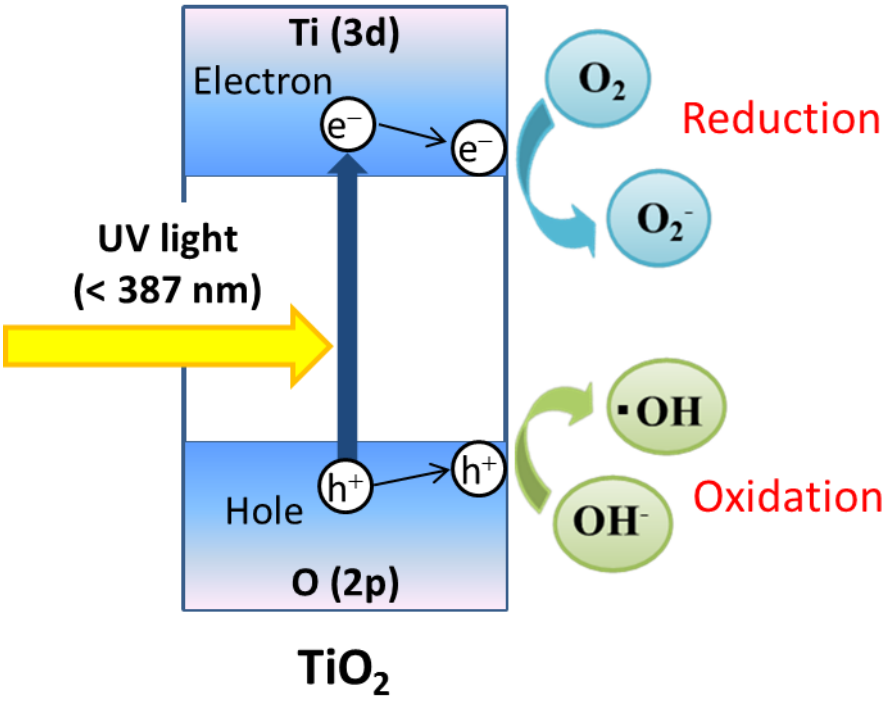

Fig. 1-1 Schematic illustration of the photocatalytic redox reaction in TiO_2.

1.2. Recent research on photocatalysts

Studies on photocatalysts have been performed since 1965, in a variety of research areas. Photocatalytic research is primarily focused on the efficient use of solar energy. Major applications of solar energy technology are solar batteries [13,14] or photocatalysis [15]. In 1972, Fujishima and Honda [16] reported the possibility of hydrogen production by water decomposition, facilitated water splitting by photocatalysis with solar energy. Since then, TiO_2 photocatalysis has been interested in the academic and industrial fields, and attempted to apply the property to hydrogen production [16], air cleaning [17], metal anti-corrosion [18,19], self-purification [20-22], antibacterial activity [23,24], and environmental purification [25]. **Fig. 1-2** summarizes the advances in research on photocatalysts [26], some of which have been released in the market.

Fig. 1-3 shows the numbers of papers on photocatalysis and related areas, published from 2000 to 2014 obtained by the Web of Science. The total number of papers obtained for the keyword “photocatalyst” was 13,213 comprising 4,412 on “energy”, 2,401 on “environmental purification”, and 1,627 on “water purification”. The majority of the published papers on water treatment using photocatalysts and related materials are from China (467), Japan (247), US (122), and Korea (108). Thus, the application of photocatalysis for water treatment is actively studied in the Asian region.

Based on the increase in the number of papers published on water treatment by photocatalytic reactions, from 2000 to 2014, this research field is expected to progress further by collaborations with other advanced technologies.

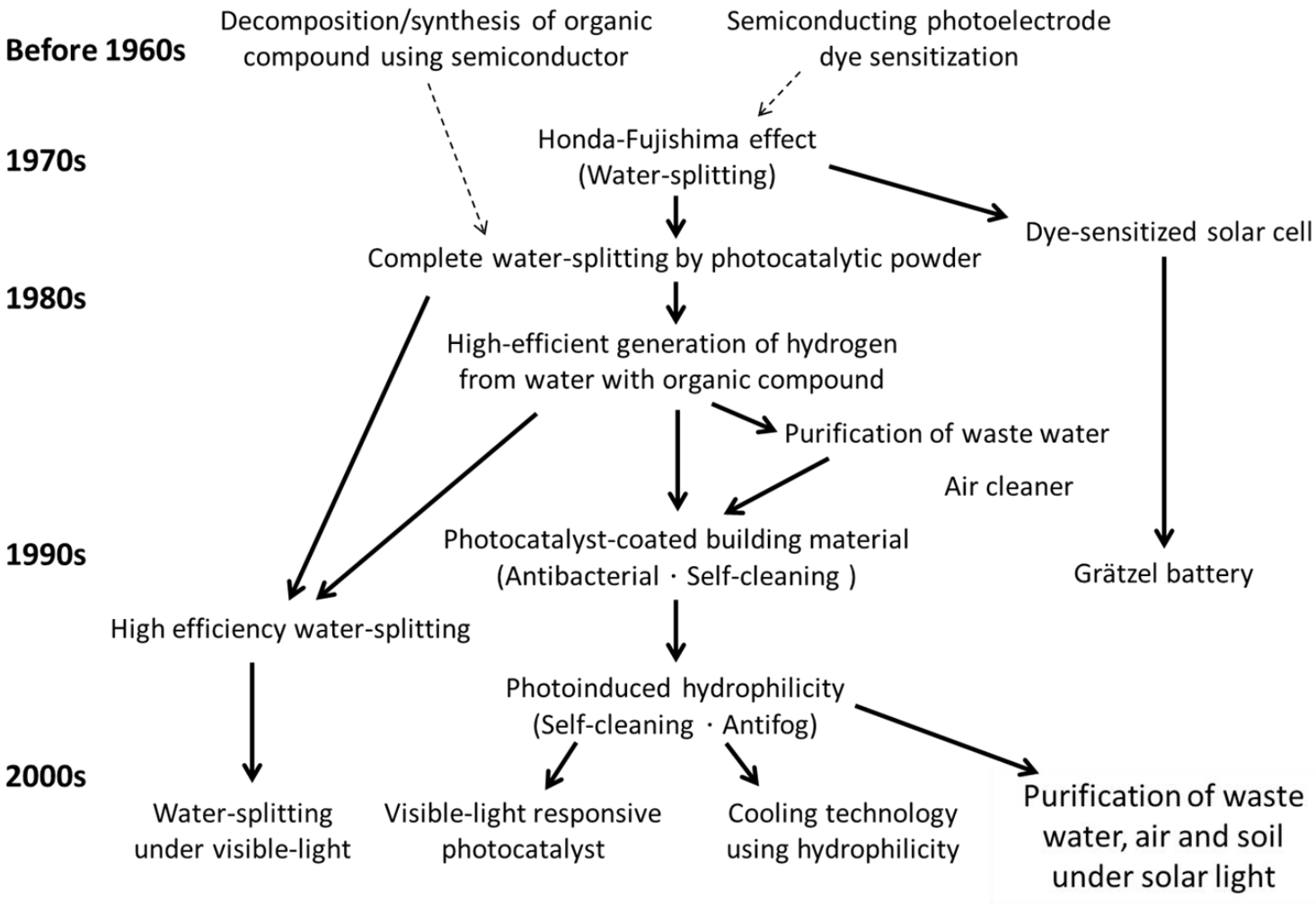

Fig. 1-2 Major advances in photocatalyst research.

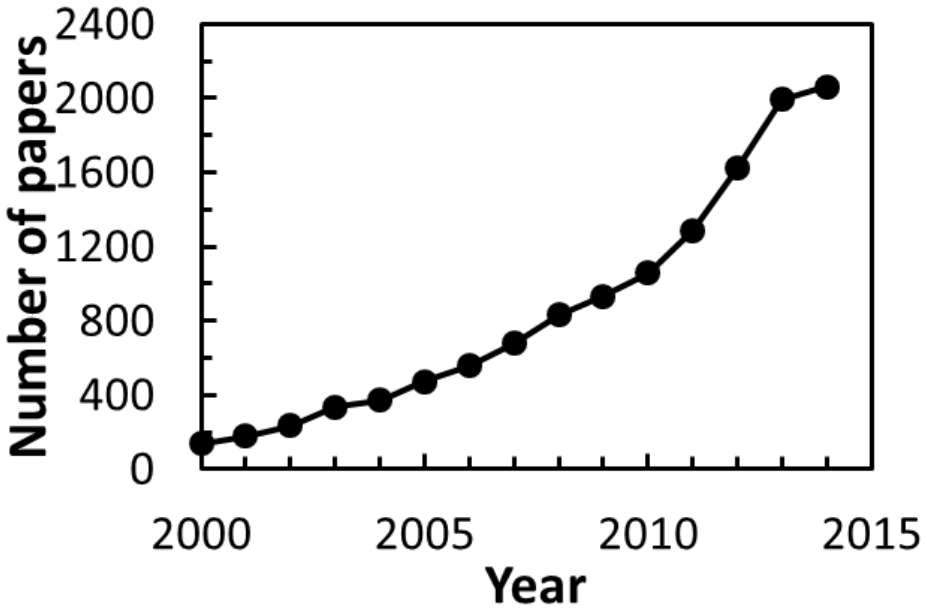

Fig. 1-3 Numbers of papers published in the area of photocatalysts since 2000.

1.3. Approach to water treatment technologies

In recent years, the rapid development of manufacturing technology and uncontrolled groundwater utilization has resulted in high levels of water pollution. The contamination of rivers and drinking water by organic compounds contained in waste water has become so severe that it cannot be mitigated by the natural cleansing cycle [28-30].

Current water treatment technology is mainly based on biological treatment with coagulation/precipitation techniques, and the Fenton oxidation treatment technology

[31-33]. In the coagulation and precipitation technique, suspended solids are precipitated by forming flocs upon addition of a polymer coagulator and inorganic coagulants, such as Fe and Al [34-36]. This treatment has high efficiency, but the use of chemicals causes secondary environmental problems; for example, pipe blockages and water deterioration.

The Fenton oxidation treatment technology decomposes organic matter by OH radicals, generated by a reaction of hydrogen peroxide and iron salts (Fenton's reagent) [37-41]. While this reaction process is simple to apply, and the cost of the reaction device is generally cheaper than those of other high-level oxidation methods, the amount of sludge produced is a disadvantage. Hence, a new water treatment technology that can rapidly treat waste water, without the generation of secondary contaminants, is strongly desired. While the decomposition of organic matter by photocatalysts can be potentially applied to water treatment, progress in this area has been hindered due to: 1) low diffusivity of the objective decomposition substance, 2) light shielding by water, and 3) complexity of the photocatalytic reaction.

To improve these drawbacks, Li *et al.* reported the water treatment using a BiOBr film-coated rotating disk photocatalytic reactor [42]. This method effectively decomposed organic dyes by the rotation of photocatalytic disk. The examinations of the shapes in the purifying device are energetically pursued to provide a highly efficient water purification using a photocatalyst material [43-45].

Also, the combination of the photocatalyst and ozone was widely reported as a method to increase the water treatment ability of the photocatalyst [46-47]. For example, Ochiai and coauthors attempted the enhancement of removal efficiency of *E. coli* and Qβ phage when concurrently using the photocatalyst and ozone [46]. In contrast,

researches that clarifiy the degradation pathway of organic dye using various reactors has been actively carried out [48-50].

We have addressed these drawbacks by three different approaches; 1) development of adsorptive-added photocatalysts that can respond under both UV and visible lights, 2) development of the coating method of photocatalyst onto a solid phase, and 3) establishment online analytical system to elucidate the ability of the developed photocatalytic materials and the decomposition of mechanism of target organic dyes.

The strategies on these approaches as mentioned above are described below in this section and chaptors 2 – 7, as well as the statuses of these studies.

1.3.1. Addition of adsorptivity

As described above, organic compounds are decomposed by the active oxygen radicals generated from the surface of the photocatalyst. However, these highly reactive radicals disappear immediately after the reaction. The development of highly adsorptive photocatalysts on which they remain for longer durations is required. Towards this end, highly adsorptive materials such as zeolite [51], activated carbon [52], and hydroxyapatite [53,54] were modified onto the photocatalyst. In addition, a composition containing TiO_2 along with porous silica was applied to the decomposition of organic compounds in gas and aqueous phases [55].

However, synthesis of these high-adsorptive photocatalysts generally required complicated procedures, resulting in relatively high manufacturing costs. Hence, development of more convenient and inexpensive synthetic methods is required for wide use of adsorptive photocatalysts.

1.3.2. Application of visible-light responsive photocatalyst

The band gap energies of the anatase and rutile phases of TiO_2 are 3.2 and 3.0 eV, respectively, and as a result, these materials display very little photocatalytic activity under visible light. To enhance the efficiency of TiO_2 under solar irradiation, it is necessary to modify nanomaterials to facilitate visible light absorption. The development of visible-light induced photocatalysts has been achieved through the doping of transition metals (such as Cr, V, and Fe), and non-metals (such as C, F, and S), into TiO_2 [56-60]. The ability of these photocatalysts to purify water and air has also been investigated [61]. In fact, the doping of TiO_2 by non-metals has shown high responsive to visible light, with nitrogen being the most promising dopant [62,63]. Since Sato first reported the synthesis of N-doped TiO_2 (NT) [64], it has been widely applied because of its ease of preparation [65-68]. Irie *et al.* [69] discovered that the photoactivity of NT under visible light could be manipulated by changing the amount of nitrogen doped into TiO_2. The doping of metal species into NT was considered to slow the rate of electric charge recombination in TiO_2, and these materials have been used to remove target substances in the gas phase. For example, the Fe^{III}/N co-doped TiO_2 exhibited efficient photocatalytic decomposition of 2-propanol under visible light irradiation [70]. Co-doping of Cu^{II} into NT produced a photocatalyst better suited for the decomposition of acetaldehyde than NT alone [71]. Furthermore, Higashimoto *et al.* [72] reported that V-modified NT could decompose volatile organic compounds under both UV and visible light irradiation.

There are fewer reports of the decomposition of dyes, endocrine disruptors, or humic acid (HA) in aqueous solutions by visible-light induced photocatalysis compared to those reporting their decomposition in air [73-75]. The activity of photocatalysts in

water is significantly lower than in air because of decreased photoabsorption and aggregation of the photocatalytic particles. To address these problems, TaON, Nb_2O_5, and WO_3 have been investigated as visible-light induced photocatalysts, and their mechanisms of activation have been elucidated [76-78].

However, these are expensive compared to TiO_2 and easily undergo autolysis in water. Accordingly, the development of a visible-light responsive photocatalyst with high dispersibility and structural stability in water is essential.

1.3.3. Coating of photocatalyst onto a solid phase

The photodegradation of pollutants in water samples has become an important topic of research in recent years, and numerous investigations have been conducted on the photodecomposition of natural organic matter (NOM) by TiO_2-based photocatalysts in environmental water samples such as surface and lake waters [79-86]. Similarly, the potential for the formation of disinfection byproducts (DBPs), such as trihalomethane (THM) and haloacetic acid (HAA), generated by the chlorination of NOM, HA, or fulvic acid has been recently analyzed [82,83]. TiO_2 materials, both commercial (Degussa P25 or Hombikat UV100) and in-house, are typically utilized in the form of powders, which are suspended in an aqueous solution containing the pollutant, resulting in troublesome recovery and recycling of the photocatalyst.

This drawback could be overcome by the approach of coating the powders onto solid materials such as ceramics, glasses, and fibers, which act as supports. Consequently, there is a growing interest in the development of a method to evaluate the efficiency of solid-supported TiO_2 photocatalysts in water purification applications.

One requirement for the practical use of photocatalysts in water purification is that

it is immobilized onto a solid substrate for repeated use of the photocatalyst. At present, photocatalyst immobilization techniques include sol-gel processing [87,88], sputtering [89,90], and a hydrothermal method [91]. Sol-gel processing is the most convenient method; however, the type of substrate is limited to those with high thermal resistance, such as silica glass beads, because a calcination step is necessary to deposit the photocatalyst on the substrate. Sputtering is an effective method for obtaining a homogeneous photocatalytic film, but cannot be used for coating photocatalysts onto a complicated structure with irregularities, and the process of sputtering requires a dedicated device. The hydrothermal method is convenient as it can coat a variety of substrates; however, uniform coating is difficult to achieve owing to aggregation of the photocatalyst particles during the particle-substrate interactions.

Thus, there is a requirement for a convenient method that can coat photocatalysts onto substrates with both complex and smooth structures. Furthermore, to be widely used in water purification, the development of photocatalytic materials that are responsive to visible light is also required. In general, during the synthesis of visible-light responsive TiO_2 photocatalysts, ionized nitrogen and argon are doped into photocatalyst-coated membranes using dedicated ion-imprinting equipment [92,93]. Recently, the formation of visible-light responsive photocatalytic films using one-step procedures based on sol-gel processing [94] and sputtering [95] have been reported, but the types of substrate that can be used are limited to heat-resistant materials because both methods involve a calcination step.

1.4. Purpose of this study

The main purpose of this study was to establish a water treatment method using photocatalysts on the effective photodecomposition of target organic pollutants in aqueous solution. This thesis describes the development of photocatalysts that induce adsorptivity, the development of a method coating the photocatalyst onto a solid material, and application to real water samples. Furthermore, we developed a new method for the evaluation of photocatalyst-coating materials used in water treatment, using flow-analytical method.

Chapter 2 describes synthesis and water treatment ability of a photocatalyst prepared by coating hydroxyapatite on TiO_2 particles, using a photoinduced superhydrophilic reaction, in order to achieve a highly efficient coating of the adsorbent on TiO_2. The hydroxyapatite-coated TiO_2 thus synthesized was evaluated through photocatalytic decomposition efficiency of the cationic dyes, methylene blue (MB), and dimethylsulfoxide (DMSO). This synthesis method of the photocatalyst was advantageous because of its short synthesis time, lower precursor concentration, and high crystallinity of the product.

Chapter 3 describes the performance of a photocatalyst that enhances the electrostatic adsorptivity by combining both vanadium and silica with TiO_2 in order to obtain high-adsorptivity for cationic species in aqueous solution. The silica-doped TiO_2, vanadium-modified TiO_2, and vanadium-silica-TiO_2 (VSiT) have strong negative charges in the range of weakly acidic pH to alkaline pH, and can adsorb cationic species. Consequently, these photocatalysts displayed a high decomposition efficiency of the target materials in aqueous phase.

Chapter 4 describes the synthesis and characterization of vanadium-modified N/Si co-doped TiO_2 (VNSiT) in order to obtain the same capability as VSiT, and to further improve the visible-light response. The efficiency of VNSiT in an aqueous solution was evaluated by the adsorption of several dyes in the dark, and their decompositions by UV-light irradiation. In addition, the capacity of the VNSiT for water purification, via the photoactivated decomposition of DMSO and MB dissolved in water, under visible-light irradiation, was evaluated.

Chapter 5 describes the development and evaluation of a TiO_2-coated ceramic foam filter, as a high-efficiency photocatalytic coating material, for the treatment of waste water. This material has a highly porous structure, and causes turbulence of water. The TiO_2-coated ceramic foam filter displayed a high photodecomposition efficiency of humic acid, and degradation of total organic carbon (TOC), as well as the suppression of formation of disinfection byproducts.

Chapter 6 describes the establishment of a novel evaluation system for water treatment efficiency using photocatalytic materials. In the evaluation of a quality test for the water treatment by photocatalysts, the photocatalytic reactor and the analytical devices were commonly separated. In this chapter, we equipped the flow analytical system with an online-combined photocatalytic reactor and spectrophotometer, and evaluated the as-prepared photocatalytic plate through the decomposition of organic dye and ibuprofen using this evaluation system.

Chapter 7 describes the coating of photocatalyst powder onto a solid material (glass plate) through electrostatic interactions using cationic silane-coupling reagent as a spacer. This method improved the stability of fixing of the photocatalyst onto a glass plate, without a calcination step. It is expected that the increasingly negative zeta

potential of photocatalyst induces the electrostatic dispersion in the aqueous solution, and could electrostatically bind to cationic silane-coated glass plates. The advantage of this method was to provide a uniform photocatalytic layer on the substrate surface, without burial of the photocatalyst, which typically occurs when using inorganic spacers such as mortar [96-98].

Chapter 8 summarizes the results obtained in each chapter.

1.5. References

[1] I. Hua, M.R. Hoffmann, Optivization of ultrasonic irradiation as an advanced oxidation technology, Environ. Sci. Technol. 31 (1997) 2237 – 2243.

[2] R. Ameta, S. Benjamin, A. Ameta, S.C. Ameta, Photocatalytic degradation of organic pollutants: A review, Materi. Sci. Forum 734 (2013) 247 – 272.

[3] W. Lei, D. Portehault, D. Liu, S. Qin, Y. Chen, A miniaturized implantable loop antenna at MICS and ISM bands for biomedical applications, Nat. Commun. 4 (2013) 1 – 3.

[4] B. Kasprzyk-Hordern, M. Ziolek, J. Nawrocki, Catalytic ozonation and methods of enhancing molecular ozone reactions in water treatment, Appl. Catal. B Environ. 46 (2003) 639 – 669.

[5] S.S.A. Amr, H.A. Aziz, M.N. Adian, S.Q. Aziz, Effect of Ozone and Ozone/Fenton in the Advanced Oxidation Process on Biodegradable Characteristics of Semi-aerobic Stabilized Leachate, Clean-Soil Air Water 41 (2013) 148– 152.

[6] S. Jagadevan, N.J. Graham, I.P. Thompson, Treatment of waste metalworking fluid by a hybrid ozone-biological process,J. Hazard. Mater. 244–245 (2013) 394 – 402.

[7] W. Tao, J. Chang, D. Wu, Z. Gao, X. Duan, F. Xu, K. Jiang,Solvothermal synthesis of graphene-Sb_2S_3 composite and the degradation activity under visible light, Mater. Res. Bull. 48 (2013) 538 – 543.

[8] T. Ghosh, K.Y. Cho, K. Ullah, V. Nikam, C.Y. Park, Z.D. Meng, W.C. Oh, High photonic effect of organic dye degradation by CdSe-graphene-TIO_2 particles, J. Ind. Eng. Chem. 19 (2013) 797 – 805.

[9] L.G. Devi, R. Kavitha, A review on non metal ion doped titania for the

photocatalytic degradation of organic pollutants under UV/solar light: Role of photogenerated charge carrier dynamics in enhancing the activity, Appl. Catal. B Environ. 140–141 (2013) 559 – 587.

[10] J. Yu, X. Yu, Hydrothermal Synthesis and Photocatalytic Activity of Zinc Oxide Hollow Spheres, Environ. Sci. Tech. 42 (2008) 4902 – 4907.

[11] J.L. Lyons, A. Janotti, C.G. van de Walle, The multidimensional character of electric systems storage, Semiconduct. Semimet. 88 (2013) 1 – 11.

[12] R. Wang, K. Hashimoto, A. Fujishima, M. Chikuni, E. Kojima, A. Kitamura, M.Shimohigoshi, T. Watanabe, Light-induced amphiphilic surfaces, Nature 288 (1997) 431 – 432.

[13] A. Nottrott, J. Kleissl, B. Washom, Energy dispatch schedule optimization and cost benefit analysis for grid-connected, photovoltaic-battery storage systems, Renew. Energ. 55 (2013) 230 – 240.

[14] N.S. Lewis, Toward Cost-Effective Solar Energy Use, Science 315 (2007) 798 – 801.

[15] Y. Shavisi, S. Sharifnia, S.N. Hosseini, M.A. Khadivi, Application of TiO2/perlite photocatalysts for degradation of ammonia in wastewater, J. Ind. Eng. Chem. 20 (2014) 278 – 283.

[16] A. Fujishima, K. Honda, Electrochemical Photolysis of Water at a Semiconductor Electrode, Nature 238 (1972) 37 – 38.

[17] J. Mo, Y. Zhang, Q. Xu, J.J. Lamson, R. Zhao, Photocatalytic purification of volatile organic compounds in indoor air: A literature review, Atmos. Environ. 43 (2009) 2229 – 2246.

[18] M.R. Hoffmann, S.T. Martin, W. Choi, D.W. Bahnemann, Environmental

Applications of Semiconductor Photocatalysis, Chem. Rev. 95 (1995) 69 – 96.

[19] C.K. Lee, Comparative corrosion resistance of electroless Ni-P/nano-TiO_2 and Ni-P/nano-CNT composite coatings on 5083 aluminum ally, Int. J. Electrochem. Sci. 7 (2012) 12941 – 12954.

[20] K. Nakata, M. Sakai, T. Ochiai, T. Murakami, K. Takagi, A. Fujishima, Antireflection and Self-Cleaning Properties of a Moth-Eye-Like Surface Coated with TiO_2 Particles, Langmuir 27 (2011) 3275 – 3278.

[21] K. Katsumata, S. Okazaki, C.E.J. Cordonier, T. Shichi, T. Sasaki, A. Fujishima, Preparation and characterization of self-cleaning glass for vehicle with niobiananosheets, ACS Appl. Mater. Inter. 2 (2010) 1236 – 1241.

[22] T. Shichi, K. Katsumata, Development of photocatalytic self-cleaning glasses utilizing metal oxide nanosheets, J. Surf. Finish. Soc. Jpn. 61 (2010) 30 – 35.

[23] H.R. Pant, D.R. Pandeya, K.T. Nam, W.I. Baek, S.T. Hong, H.Y. Kim, Photocatalytic and antibacterial properties of a TiO_2/nylon-6 electrospunnanocomposite mat containing silver nanoparticles, J. Hazard. Mater. 189 (2011) 465 – 471.

[24] J.Y. Choi, K.H. Kim, K.C. Choy, K.T. Oh, K.N. Kim, Photocatalytic antibacterial effect of TiO_2 film formed Ti and TiAg exposed to Lactobacillius acidophilus, Journal of Biomedical Materials Research Part B: Appl. Biomaterial. 80B (2006) 353 – 359.

[25] T. Ochiai, A. Fujishima, Photoelectrochemical properties of TiO_2 photocatalyst and its applications for environmental purification, J. Photochem. Photobio. C: Photocem. Rev. 13 (2012) 247 – 262.

[26] K. Hashimoto, B. Ohtani, A. kudo, Photocatalyst: Basic, material development and

application, (2005) N.T.S Ltd., Tokyo, p 24.

[27] A. Fujishima, X. Zhang, D.A. Tryk, TiO_2 photocatalysis and related surface phenomena, Surf. Sci. Rep. 63 (2008) 515 – 582.

[28] M. Heikkinen, H. Poutiainen, M. Liukkonen, T. Heikkinen, Y. Hiltunen, Subtraction analysis based on self-organizing maps for an industrial wastewater treatment process, Math, Comput. Simulat. 82 (2011) 450 – 459.

[29] A. Biati, F. Moattar, A.R. Karbassi, A.H. Hassani, Role of saline water in removal of heavy elements from industrial wastewaters, Inter. J. Environ. Res. 4 (2010) 177 – 182.

[30] L. Tajeddine, M. Nemmaoui, H. Mountacer, A. Dahchour, M. Sarakha, Photodegradation of fenamiphos on the surface of clays and soils, Environ. Chem. Lett. 8 (2010) 123 – 128.

[31] L. Liberatore, M. Bressan, C. Belli, G. Lustrato, G. Ranalli, Chemical and biological combined treatments for the removal of pestivides from wastewaters, Water, Air and Soil Pollution 223 (2012) 4751 – 4759.

[32] M.M. Ballesteros Martín, J.A. Sánchez Pérez, J.L. Casas López, I. Oller, S. MalatoRodríguez, Degradation of a four-pesticide mixture by combined photo-Fenton and biological oxidation, Water Res. 43 (2009) 653 – 660.

[33] M. Bressan, L. Liberatore, N. D'Alessandro, L. Tonucci, C. Belli, G. Ranalli, Improved combined chemical and biological treatments of olive oil mill wastewaters, J. Agr. Food Chem. 52 (2004) 1228 – 1233.

[34] M.S. Tahir, M. Saleem, S.R. Malik, J.R. Khan, M. Siebenhofer, An innovative and advanced oxidation process for effluent treatment through wet tube-type electrostatic precipitation, Chem. Eng. Process. 52 (2012) 16 – 20.

[35] L.B. Mansour, I. Kesentini, Treatment of effluents from cardboard industry by coagulation-electroflotation, J. Hazard. Material. 153 (2008) 1067 – 1070.

[36] Ö. Hanay, H. Hasar, Effect of anions on removing Cu^{2+}, Mn^{2+} and Zn^{2+} in electrocoagulation process using aluminum electrodes, J. Hazard. Material. 189 (2011) 572 – 576.

[37] G. Centi, S. Perathoner, T. Torre, M.G. Verdone, Catalytic wet oxidation with H_2O_2 of carboxylic acids on homogeneous and heterogeneous Fenton-type catalysts, Catal. Today 55 (2000) 61 – 69.

[38] P. Ghosh, A.N. Samanta, S. Ray, Reduction of COD and removal of Zn^{2+} from rayon industry wastewater by combined electro-Fenton treatment and chemical precipitation, Desalination 266 (2011) 213 – 217.

[39] S.H. Lin, C.C. Chang, Treatment of landfill leachate by combined electro-Fenton oxidation and sequencing batch reactor method, Water Res. 34 (2000) 4243 – 4249.

[40] O.B. Ayodele, B.H. Hameed, Synthesis of copper pillared bentonite ferrioxalate catalyst for degradation of 4-nitrophenol in visible light assisted Fenton process, J. Ind. Eng. Chem. 19 (2013) 966 – 974.

[41] J.M. Monteagudo, A. Duran, I.S. Martı´n, M. Aguirre, Effect of light source on the catalytic degradation of protocatechuic acid in a ferrioxalate-assisted photo-Fenton process, Appl. Catal. B Environ. 96 (2010) 486 – 495.

[42] K. Lia, H. Zhanga, Y. Tangb, D. Yingc, Y. Xud, Y. Wanga, J. Jia, Photocatalytic degradation and electricity generation in a rotating disk photoelectrochemical cell over hierarchical structured BiOBr film, Appl. Catal. B Environ. 164 (2015) 82 – 91.

[43] B. Stephan, L. Ludovic, W. Dominique, Modelling of a falling thin film deposited

photocatalytic step reactor for water purification: Pesticide treatment Chem. Eng. J. 169 (2011) 216 – 225.

[44] T. Ochiai, K. Nakata, T. Murakami, A. Fujishima, Y.Y. Yao, D.A. Tryk, Y. Kubota, Development of solar-driven electrochemical and photocatalytic water treatment system using a boron-doped diamond electrode and TiO_2 photocatalyst, Water Res. 44 (2010) 904 – 910.

[45] S. Malato, P. Fernández-Ibánez, M.I. Maldonado, J. Blanco, W. Gernjak, Decontamination and disinfection of water by solar photoatalysis: Recent overview and trends, Catal. Today 147 (2009) 1 – 59.

[46] T. Ochiai, H. Nanba, T. Nakagawa, K. Masuko, K. Nakata, T. Murakami, R. Nakano, M. Hara, Y. Koide, T. Suzuki, M. Ikekita, Y. Morito, A. Fujishima, Development of an O_3-assisted photocatalystic water-purification unit by using a TiO_2 modified titanium mesh filter, Catal. Sci. Technol. 2 (2012) 76 – 78.

[47] E. Menaa, A. Reya, B. Acedoa, F.J. Beltrána, S. Malatob, On ozone-photocatalysis synergism in black-light induced reactions: Oxidizing species production in photocatalytic ozonation versus heterogeneous photocatalysis, Chem. Eng. J. 204-206 (2012) 131 – 140.

[48] M.A. Rauf, M.A. Meetani, A. Khaleel, A. Ahmed, Photocatalytic degradation of Methylene Blue using a mixed catalyst and product analysis by LC/MS, Chem. Eng. J. 157 (2010) 373 – 378.

[49] S. Horikiri, N. Teshima, Y. Saruki, H. Nishikawa, T. Sakai, Decomposition of methylene blue by new porous photocatalysts and analysis of decomposed products using high-performance liquid chromatography and mass spectrometry, Bunseki Kagaku (Japanese) 52 (2003) 881 – 885.

[50] M. Vautier, C. Guilland, J. Herrmann, Photocatalytic degradation of dyes in water: Case study of indigo and indigo carmine, J. Catal. 201 (2001) 46 – 59.

[51] Y. Kuwahara, J. Aoyama, K. Miyakubo, T. Eguchi, T. Kamegawa, K. Mori, H. Yamashita, TiO_2 photocatalyst for degradation of organic compounds in water and air supported on highly hydrophobic FAU zeolite: Structural, sorptive, and photocatalytic studies, J. Catal. 285 (2012) 223 – 234.

[52] M. Janus, E. Kusiak, A. W. Morawski, Carbon Modified TiO_2 Photocatalyst with Enhanced Adsorptivity for Dyes from Water, Catal. Lett. 131 (2009) 506 – 511.

[53] H. Nakane, S. Aoki, T. Nonami, K. Tanaka, M. Mori, K. Tone, T. Kameyama, Synthesis and characterization of fluoride apatite in a simulated body fluid, J. Ceram. Soc. Jpn. 114 (2006) 838 – 843.

[54] H. Nakane, S. Aoki, T. Nonami, K. Tanaka, M. Mori, K. Sachimoto, K. Tone, T. Kameyama, Optimization on synthetic conditions of fluoride apatite coated titanium dioxide in simulated body fluid, J. Ceram. Soc. Jpn. 115 (2007) 151 – 155.

[55] H. Ozaki, K. Saito, S. Iwamoto, M. Inoue, Photocatalytic activities of nanocrystalline Si-modified titaniaxerogels prepared by the glycothermal method, J. Mater. Sci. 43 (2008) 2286 – 2292.

[56] W. Choi, A. Termin, M.R. Hoffmann, The role of metal ion dopants in quantumsizedTiO_2: correlation between photoreactivity and charge carrierrecombination dynamics, J. Phys. Chem. 98 (1994) 13669 – 13679.

[57] H. Yamashita, M. Harada, J. Misaka, M. Takeuchi, K. Ikeue, M. Anpo, Degradation of propanol diluted in water under visible light irradiation usingmetal ion-implanted titanium dioxide photocatalysts, J. Photochem. Photobiol. A Chem. 148 (2002) 257 – 261.

[58] X. Yang, C. Cao, L. Erickson, K. Hohn, R. Maghirang, K. Klabunde, Synthesis ofvisible-light-active TiO_2-based photocatalysts by carbon and nitrogen doping, J. Catal. 260 (2008) 128 – 133.

[59] X. Yang, C. Cao, L. Erickson, K. Hohn, R. Maghirang, K. Klabunde, Photo-catalyticdegradation of rhodamine B on C-, S-, N-, and Fe-doped TiO_2 under visible-lightirradiation, Appl. Catal. B Environ. 91 (2009) 657 – 662.

[60] C. Han, M. Pelaez, V. Likodimos, A.G. Kontos, P. Falaras, K. ÓShea, D.D. Dionysiou, Innovative visible light-activated sulfur doped TiO_2 films for watertreatment, Appl. Catal. B Environ. 107 (2011) 77 – 87.

[61] N. Murakami, Y. Fujisawa, T. Tsubota, T. Ohno, Development of a visible-lightresponsivetitania nanotube photocatalyst by site-selective modification withhetero metal ions, Appl. Catal. B Environ. 92 (2009) 56 – 60.

[62] A. Fujishima, X. Zhang, D.A. Tryk, TiO_2 photocatalysis and related surfacephenomena, Surf. Sci. Rep. 63 (2008) 515 – 582.

[63] M. Pelaez, N.T. Nolan, S.C. Pillai, M.K. Seery, P. Falaras, A.G. Kontos, P.S.M.Dunlop, J.W.J. Hamilton, J.A. Byrne, K. O'Shea, M.H. Entezari, D.D. Dionysiou, Areview on the visible light active titanium dioxide photocatalysts forenvironmental applications, Appl. Catal. B Environ. 125 (2012) 331 – 349.

[64] S. Sato, Photocatalytic activity of NO_x-doped TiO_2 in the visible light region, Chem. Phys. Lett. 123 (1986) 126 – 128.

[65] R. Asahi, T. Morikawa, T. Ohwaki, K. Aoki, Y. Taga, Visible-light photocatalysisin nitrogen-doped titanium oxides, Science 293 (2001) 269 – 271.

[66] T. Lindgren, J.M. Mwabora, E. Avendano, J. Jonsson, A. Hoel, C.G. Granqvist, S.E.Lindquist, Photoelectrochemical and optical properties of nitrogen

dopedtitanium dioxide films prepared by reactive DC magnetron sputtering, J. Phys. Chem. B 107 (2003) 5709 – 5716.

[67] Y. Suda, H. Kawasaki, T. Ueda, T. Ohshima, Preparation of high quality nitrogendoped TiO_2 thin film as a photocatalyst using a pulsed laser depositionmethod, Thin Solid Films 453 – 454 (2004) 162 – 166.

[68] K. Kobayashi, Y. Murakami, Y. Sato, Visible-light active N-doped TiO_2 preparedby heating of titanium hydroxide and urea, J. Photochem. Photobiol. A 170 (2005) 177 – 179.

[69] H. Irie, Y. Watanabe, K. Hashimoto, Nitrogen-concentration dependence onphotocatalytic activity of $TiO_{2-x}N_x$ powders, J. Phys. Chem. B 107 (2003) 5483 –5486.

[70] T. Ohno, Z. Miyamoto, K. Nishijima, H. Kanemitsu, F. Xueyuan, Sensitization ofphotocatalytic activity of S- or N-doped TiO_2 particles by adsorbing Fe^{3+} cations, Appl. Catal. A 302 (2006) 62 – 68.

[71] T. Morikawa, Y. Irokawa, T. Ohwaki, Enhanced photocatalytic activity of $TiO_{2-x}N_x$ loaded with copper ions under visible light irradiation, Appl. Catal. A 314 (2006) 123 – 127.

[72] S. Higashimoto, W. Tanihata, Y. Nakagawa, M. Azuma, H. Ohue, Y. Sakata, Effective photocatalytic decomposition of VOC under visible-light irradiationon N-doped TiO_2 modified by vanadium species, Appl. Catal. A 340 (2008) 98 – 104.

[73] Y. Ohko, I. Ando, C. Niwa, T. Tatsuma, T. Yamamura, T. Nakashima, Y. Kubota, A. Fujishima, Degradation of bisphenol A in water by TiO_2 photocatalyst, Environ. Sci. Technol. 35 (2001) 2365 – 2368.

[74] S. Liu, M. Lim, R. Fabris, C. Chow, K. Chiang, M. Drikas, R. Amal, Removal of

humic acid using TiO_2 photocatalytic process–Fractionation and molecularweight characterization studies, Chemosphere 72 (2008) 263 – 271.

[75] M. Janus, J. Choina, A.W. Morawski, Azo dyes decomposition on new nitrogenmodifiedanatase TiO_2 with high adsorptivity, J. Hazard. Mater. 166 (2009) 1 – 5.

[76] F. Kojin, M. Mori, Y. Noda, M. Inagaki, Preparation of carbon-coated $W_{18}O_{49}$ and its photoactivity under visible light, Appl. Catal. B 78 (2008) 202 – 209.

[77] R. Abe, Recent progress on photocatalytic and photoelectrochemical watersplitting under visible light irradiation, J. Photochem. Photobiol. C 11 (2010) 179 – 209.

[78] S. Furukawa, A. Tamura, T. Shishido, K. Teramura, T. Tanaka, Solvent-freeaerobic alcohol oxidation using Cu/Nb_2O_5: green and highly selectivephotocatalytic system, Appl. Catal. B 101 (2011) 216 – 220.

[79] P. Le-Clech, E-K. Lee, V. Chen, Hybrid photocatalysis/membrane treatmentfor surface waters containing low concentration of natural organic matters, Water Res. 40 (2006) 323 – 330.

[80] K-H Choo, R. Tao, M-J. Kim, Use of a photocatalytic membrane reactor forthe removal of natural organic matter in water: effect of photoinduceddesorption and ferrihydrite adsorption, J. Membrane Sci. 322 (2008) 368 – 374.

[81] X. Huang, M. Leal, Q. Li, Degradation of natural organic matter by TiO_2 photocatalytic oxidation and its effect on fouling of low-pressure membrane, Water Res. 42 (2008) 1142 – 1150.

[82] S. Liu, M. Lim, R. Fabris, C. Chow, K. Chiang, M. Drikas, R. Amal, Removalof humic acid using TiO_2 photocatalytic process – fractionation and molecularweight characterization studies, Chemosphere 72 (2008) 263 – 271.

[83] K.K. Philippe, C. Hans, J. MacAdam, B. Jefferson, J. Hart, S.A. Parsons, Photocatalytic oxidation of natural organic matter surrogates and the impact ontrihalomethane formation potential, Chemosphere 81 (2010) 1509 – 1516.

[84] V.B. Prilti, U.S.U. Demirel, M. Bekbolet, Response surface methodologicalapproach for the assessment of the photocatalytic degradation of NOM, J. Photochem. Photobio. A Chem. 225 (2011) 26 – 35.

[85] C.S. Uyguner-Demirel, M. Bekbolet, Significance of analytical parameters forthe understanding of natural organic matter in relation to photocatalyticoxidation, Chemosphere 84 (2011) 1009 – 1031.

[86] S. Valencia, J. Marin, J. Velasquez, G. Restrepo, F.H. Frimmel, Study of pH effects on the evolution of properties of brown-water natural organic matter asrevealed by size-exclusion chromatography during photocatalytic degradation, Water Res. 46 (2011) 1198 – 1206.

[87] T. Ban, Y. Tanaka, Y. Ohya, Fabrication of titania films by sol–gel method using transparent colloidal aqueous solutions of anatasenanocrystals, Thin Solid Films 519 (2011) 3468 – 3474.

[88] Z. Liu, X. Zhang, T. Murakami, A. Fujishima, Sol–gel SiO_2/TiO_2 bilayer films with self-cleaning and antireflection properties, Sol. Energ. Mat. Sol. C. 92 (2008) 1434 – 1438.

[89] M. Kitano, K. Funatsu, M. Matsuoka, M. Ueshima, M. Anpo, Preparation of nitrogen-substituted TiO_2 thin film photocatalysts by the radio frequency magnetron sputtering deposition method and their photocatalytic reactivity under visible light irradiation, J. Phys. Chem. B. 110 (2006) 25266 – 25272.

[90] Y. Yasuda, M. Tobisaka, K. Kamikuri, Y. Hoshi, Effect of ion bombardment on

low-temperature growth of TiO_2 thin films in DC reactive sputtering with two sputtering sources, Surf. Coat. Tech. 231 (2013) 439 – 442.

[91] J.H. Lee, M. Kang, S.J. Choung, K. Ogino, S. Miyata, M.S. Kim, J.Y. Park, J.B. Kim, The preparation of TiO_2 nanometer photocatalyst film by a hydrothermal method and its sterilization performance for *Giardia lamblia*, Water Res. 38 (2004) 713 – 719.

[92] R. Fernandes, N. Patel, R. Dholam, M. Adami, A. Miotello, Low energy ion-beam modification of TiO_2 photocatalyst thin film for visible light absorption, Surf. Coat. Technol. 203 (2009) 2579 – 2583.

[93] M. Takeuchi, Y. Onozaki, Y. Matsumura, H. Uchida, T. Kuji, Photoinducedhydrophilicity of TiO_2 thin film modified by Ar ion beam irradiation, Nucl. Instrum. Methods Phys. Res. B 206 (2003) 259 – 263.

[94] W. Mekprasart, T. Khumtong, J. Rattanarak, W. Techitdheera, W. Pecharapa, Effect of nitrogen doping on optical and photocatalytic properties of TiO_2 thin film prepared by spin coating process, Energy Procedia 34 (2013) 746 – 750.

[95] M. Kitano, K. Iyatani, E. Afsin, Y. Horiuchi, M. Takeuchi, S.H. Cho, M. Matsuoka, M. Anpo, Photocatalytic oxidation of 2-propanol under visible light irradiation on TiO_2 thin films prepared by an RF magnetron sputtering deposition method, Res. Chem. Intermed. 38 (2012) 1249 – 1259.

[96] A.H. Aissa, E. Puzenat, A. Plassais, J.M. Herrmann, C. Haehnel, C. Guillard, Characterization and photocatalytic performance in air of cementitious materials containing TiO_2. Case study of formaldehyde removal, Appl. Catal. B Environ. 107 (2011) 1 – 8.

[97] S.S. Lucas, V.M. Ferreire, J.L. Barroso de Aguiar, Incorporation of titanium

dioxide nanoparticles in mortars—Influence of microstructure in the hardened state properties and photocatalytic activity, Cem. Concr. Res. 43 (2013) 112 – 120.

[98] R. Sugrañez, J.I. Álvarez, M.C. Yusta, I. Mármol, J. Morales, J. Vila, L. Sánchez, Enhanced photocatalytic degradation of NO_x gases by regulating the microstructure of mortar cement modified with titanium dioxide, Build. Environ. 69 (2013) 55 – 63.

Chapter 2

Preparation of hydroxyapatite-coated anatase by photoinduced superhydrophilic reaction of TiO_2 for water purification

2.1. Introduction

TiO_2-based photocatalyst materials have been found to efficiently decompose and remove a variety of pollutants by means of oxidation reactions with active oxygen (e.g., OH radicals) generated *in situ* upon light irradiation [1,2]. Taking advantage of this inherent ability of TiO_2, self-cleaning materials [3]. Antibacterial [4] and antifungal [5] agents, air [6] and water [7, 8] purification systems, etc., have been developed. Research in our laboratory has focused on the photodegradation of pollutants in water, which has become an important topic of research in recent years. However, this practice usually leads to lower decomposition efficiency owing to lower diffusion in the aqueous phase than in air. Hence, the coatings or composites of TiO_2 with adsorbents such as carbon [9] or zeolite [10] have been vigorously investigated by many researchers. We synthesized hydroxyapatite (HAp: $Ca_{10}(PO_4)_6(OH)_2$) coated TiO_2 without autoclave and/or electric furnace, and investigated adsorptivity in the dark conditions and photocatalytic activity under UV-irradiation, in aqueous solution. HAp-coated TiO_2 has been studied over 10 years, and it has been known to provide high decomposition efficiency to nitrogen oxide, bacteria and positively charged organic compounds [11-14].

Our laboratory successfully induced crystallization of HAp from simulated body fluid (SBF) on TiO_2 under dark conditions in previously studies [11,12,15]. The HAp-coated anatase TiO_2 (HT) could decompose trimethylamine and butyric acid in water. the reproducibly preparation of the HT particles was not easy due to influences of various circumstances, such as temperature, humidity, or contamination in the laboratory, during formation of HAp on TiO_2 in SBF.

In this study, we propose a simple method for the preparation of HT employing the photoinduced superhydrophilic reaction of TiO_2 under UV irradiation (**Fig. 2-1)**. This coating method of HAp on surface of TiO_2 has been reported by Ueda, *et al.* [16]. They described that the formation of spherical HAp clusters on the surface of TiO_2 was obtained by the UV irradiation, based on the generations of Ti–OH or Ti–O groups and the electron-hole.

The chemical composition, crystalline state, and isoelectric point of the prepared HT particles were evaluated. The photocatalytic activities of the HT samples in the decomposition of dimethyl sulfoxide (DMSO) and methylene blue (MB) were also investigated to assess the abilities of HT for applications in water purification.

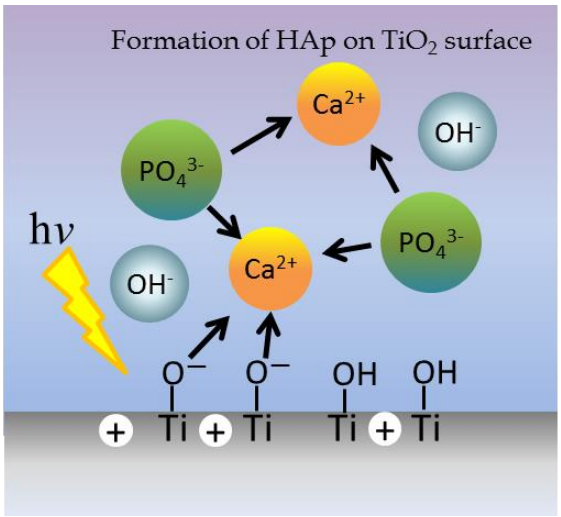

Fig. 2-1 Schematic illustration on coating of HAp-coating to TiO_2 in this study.

2.2. Experimental

2.2.1. Preparation of apatite-coated TiO_2

In the preparation of HT specimens, 5 mg of anatase TiO_2 (ST-01, Ishihara Sangyo Kaisha, Ltd.) was sintered at 500 °C in air for 1 h, then suspended in 100 mL of distilled-deionized water. Next, 2 mL of a $Ca(NO_3)_2$ solution was added to the suspension under UV irradiation (λ_{Max} = 365 nm). After stirring the solution for 20 min, 2 mL of an SBF mixture composed of CH_3COONa, KCl, KH_2PO_4, and Na_2HPO_4 was added and the resultant mixture was stirred for 20 min under UV irradiation. The sample obtained using SBF composed of 40 mM $Ca(NO_3)_2$, 60 mM CH_3COONa, 7 mM KCl, 1.5 mM KH_2PO_4, and 9 mM Na_2HPO_4 is denoted as HT1, and that obtained using SBF composed of 400 mM $Ca(NO_3)_2$, 600 mM CH_3COONa, 70 mM KCl, 15 mM KH_2PO_4, and 90 mM Na_2HPO_4 is denoted as HT2. The chemical compositions of SBF were from a previous study [12,13]. The suspensions were filtered using a membrane filter (0.45 μmϕ) and dried overnight. We also prepared a sample by immersion in the SBF used for synthesis of HT1 under dark conditions and this sample is denoted as HT1d.

2.2.2. Characterization of photocatalyst

Crystalline phases in the samples were identified from powder diffraction patterns collected using X-ray diffraction (XRD, Cu Kα radiation, Rigaku RINT2200VF). X-ray photoelectron spectroscopy (XPS) spectra were obtained on a Shimadzu AXIS-NOVA with an Al Kα source operating at 15 kV and 10 mA and used to determine the atomic and chemical composition of the sample surface. The Ca/Ti ratios are determined by X-ray fluorescence (EDX-700, Shimadzu).

Zeta potentials and hydrodynamic sizes were determined using a Zetasizer Nano ZS apparatus with an MRT-2 autotitrator (Malvern) through the measurement of the electrophoreticity and dynamic light scattering characteristics of the sample. For this experiment, a small amount of sample was dispersed in 10 mM NaCl, and the pH was adjusted with 0.1 M NaOH or 0.1 M HCl. The analysis was conducted after the suspension was ultrasonicated for 10 min.

2.2.3. Evaluation of photocatalyst in aqueous solutions

The ability of the photocatalysts to treatment water under UV light was evaluated via their ability to decompose DMSO [17,18], which has been used as an indicator of water quality in such experiments.

The test for the photocatalytic decomposition of DMSO was conducted by dispersion the synthesized photocatalyst (5 mg) in a 10 ppm DMSO solution (50 mL) and then stirring under dark condition for 1 h, and next, irradiating the suspension with UV lamps emitting for 3 h at 352 nm (National-FL20S-BLB lamp, Matsushita Electric Industrial Co., Ltd., Osaka, Japan). The light intensity of the UV lamps used in this study was *ca.* 2.0 mW/cm^2.

The concentration of DMSO and its products in solution were determined by ion chromatography (IC; Tosoh IC-2001, Tosoh Co., Japan). DMSO was isolated using a TSKgel Super-IC A/C-0.1 weakly acidic cation exchange column (150 mm × 6 mm i.d.) and 20 mM succinic acid as the eluent with a flow rate of 0.6 mL/min. UV detection was employed (195 nm). Methanesulfinic acid (MSI), methanesulfonic acid (MSA), and sulfuric acid (SA), which are byproducts generated during the photocatalytic decomposition of DMSO, were isolated using a TSKgel Super IC-AZ

strongly basic anion exchange column (150 mm × 4.6 mm i.d.) and 1.9 mM $NaHCO_3$ and 3.2 mM Na_2CO_3 as eluents with a flow rate of 0.8 mL/min. Suppressed conductimetric detection was used for these derivatives. In addition, evaluation of adsorptivity and water treatment efficiency in synthesized photocatalyst was carried out by photodecomposition of MB (basic dye).

The test for the photocatalytic decomposition of MB was conducted by dispersion the synthesized photocatalyst (5 mg) in a 5 ppm MB solution (50 mL) and then stirring under dark condition for 1 h, and next, irradiating the suspension with UV lamps emitting for 3 h (MB).

The dye concentration was determined on the basis of the change in the absorbance at 660 nm (MB) as a function of the irradiation time using a Hitachi U-3500 UV–Vis spectrophotometer. The decomposition experiments were also performed in the dark to evaluate the adsorptivity of the catalyst particles.

2.3. Results and discussion

2.3.1. Characterization of photocatalyst

In order to evaluate the properties of the obtained samples, the XRD patterns of HT were compared to those of anatase TiO_2 (ST-01) and pure HAp (Wako Pure Chemical Industries). **Fig. 2-2** show the XRD patterns of each sample. The peaks from HAp at 2θ = 31.8°, 32.2°, and 32.9° appear only in HT2. In contrast, the XRD patterns of HT1 and HT1d were almost the same as that of anatase TiO_2. Differences in peak intensities among the samples were not observed.

In the XPS spectra of HT1 and HT2, the Ca and P peaks, which originate from HAp, were distinctly observed, but the corresponding peaks in the spectrum of HT1d were less intense (**Fig. 2-3**). Moreover, the Ca/Ti ratios of HT1, HT1d, and HT2 estimated from XPS spectra were 0.08, 0.03, and 3.61, respectively. Additionally, the Ca/Ti ratios determined by EDX were 0.04, 0.03, and 0.38, respectively. Accordingly, this suggests that HT1d prepared without irradiation could bind Ca^{2+} to TiO_2 but the formation of HAp was insufficient.

Fig. 2-4 shows the zeta potential of each sample. The isoelectric points (pIs) of the HT samples were shifted to acidic pH compared to anatase TiO_2. The pIs of HT1 and HT1d were 3.9 while that of ST-01 was 5.6. The average hydrodynamic diameters of ST-01, HT1, and HT1d were 1850 nm, 780 nm, and 486 nm, respectively, in aqueous solution at pH 7.

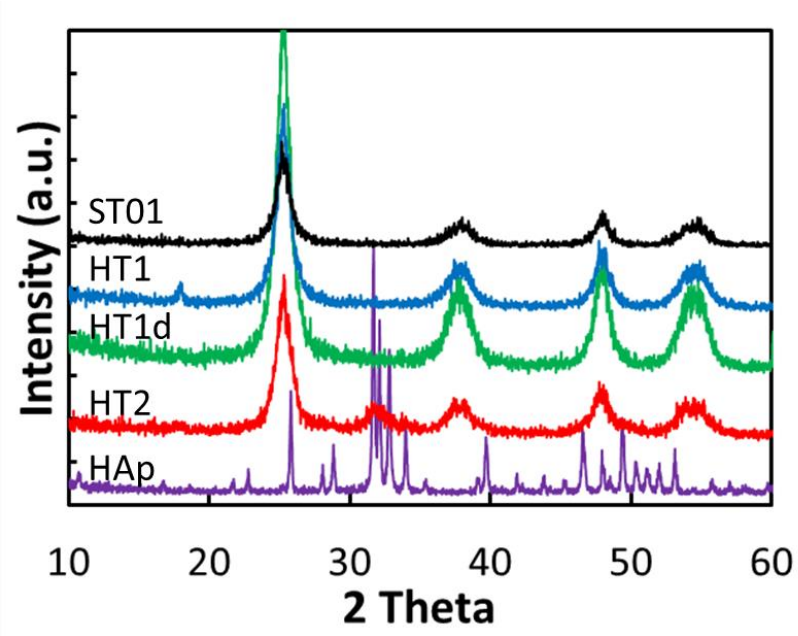

Fig. 2-2 XRD patterns of photocatalysts.

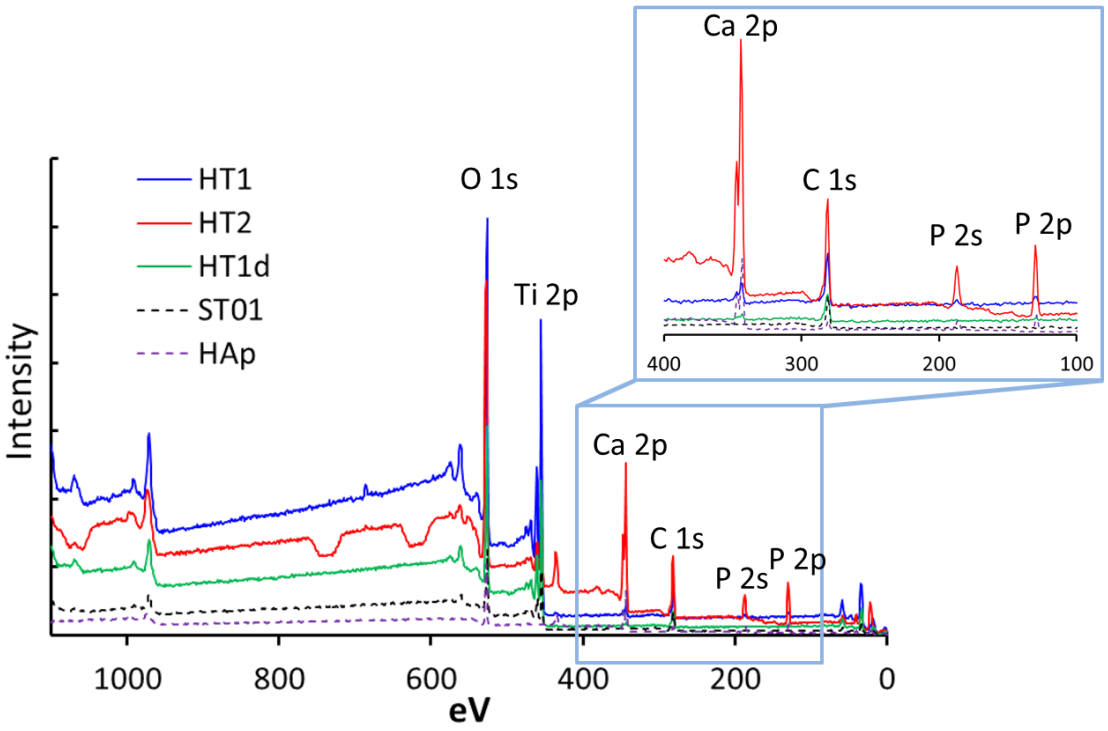

Fig. 2-3 XPS spectra of the catalysts.

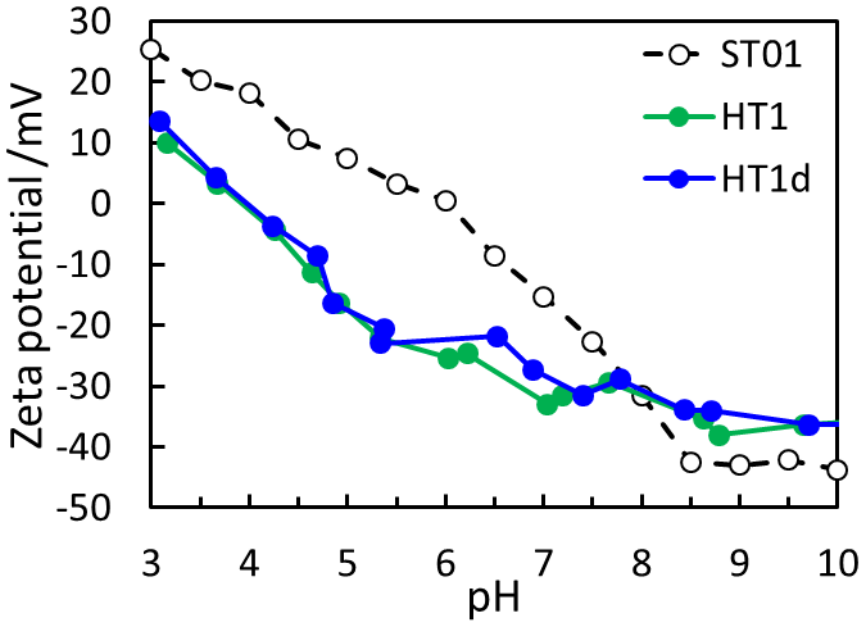

Fig. 2-4 Zeta potential of each catalyst as a function of solution pH.

2.3.2. Evaluation of water treatment ability

The results of the decomposition test are shown in **Fig. 2-5**. Adsorption of DMSO by HT1, HT1d, and HT2 under dark conditions was not observed. The decomposition rates (*k*) for DMSO under UV irradiation for 3 h were calculated from the slope of approximate curve in **Fig. 2-5**. The *k* values were in the order of ST01 (1.57 h^{-1}) > HT1 (0.866 h^{-1}) > HT1d (0.541 h^{-1}) > HT2 (0.371 h^{-1}). The difference between HT1 and HT1d in the decomposition of DMSO should be related to differences in the formation of HAp on TiO_2 with or without UV irradiation during preparation of the photocatalysts. The photocatalytic activity of HT2 would be reduced by large amounts of HAp coated on the surface of anatase TiO_2. In contrast, adsorption percentages of HT samples for MB under dark condition were 5–10%, while ST01 did not achieve adsorption. The *k* values for MB under UV irradiation for 3 h were in the order of HT1 (1.04 h^{-1}) > HT1d (0.679 h^{-1}) > HT2 (0.652 h^{-1}) > ST01 (0.386 h^{-1}).

The stronger acidity of HT1 compared to anatase TiO_2 (**Fig. 2-4**) would lead to stronger electric attraction for positively charged MB in the solution. Also, since the average hydrodynamic diameters can be used to predict the average sizes of particles aggregated in a solution, the small particle size in water was considered to be an important factor in the decomposition of pollutants in water, as were the crystalline states and amount of HAp formed on the TiO_2.

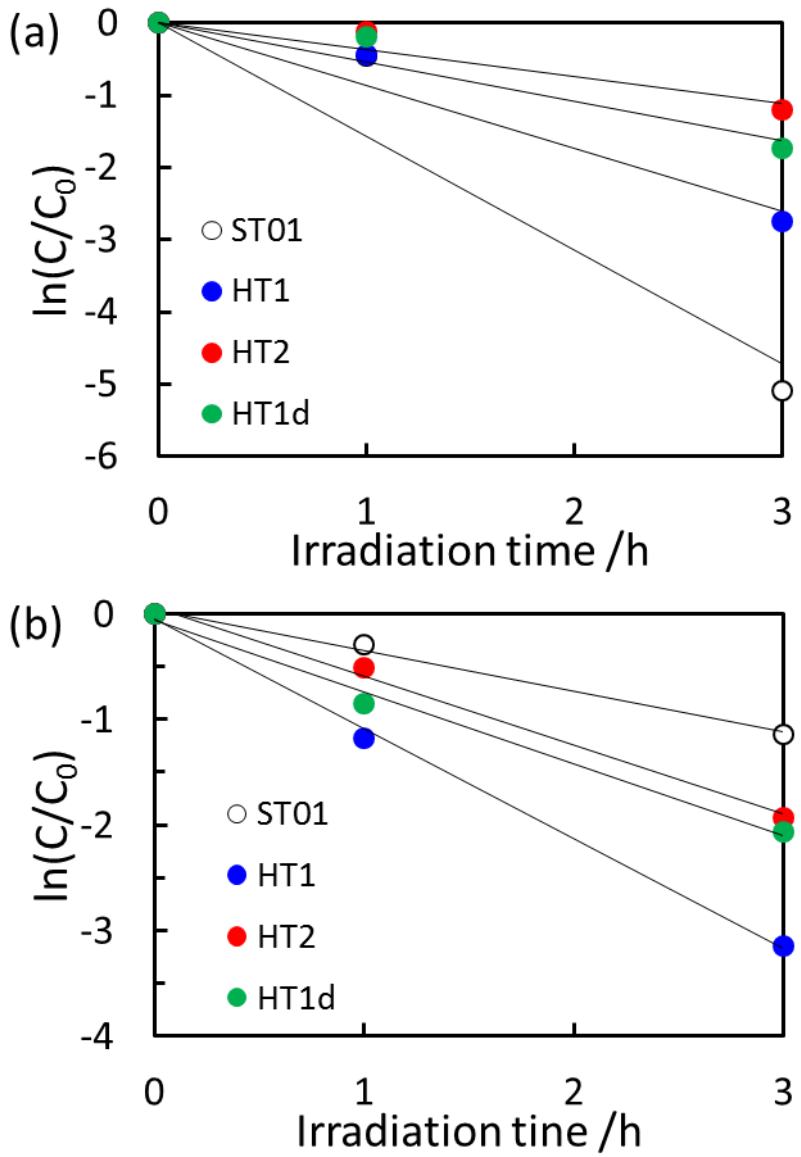

Fig. 2-5 Plots of $\ln(C/C_0)$ for (a) DMSO and (b) MB as a function of UV-irradiation time. C_0: initial concentration (DMSO: 10 ppm; MB: 5 ppm); and C: concentration at each sampling time.

2.4. Conclusions

The photoinduced superhydrophilic reaction under UV irradiation provided the formation of HAp with high crystallization on anatase TiO_2. The simple one-cycle preparation procedure was achieved by immersing TiO_2 in SBF solution with UV irradiation around 1 h. The crystalline states and amounts of HAp formed on TiO_2, as well as particle size, were related to the abilities of the catalysts in decomposition of DMSO and MB in water. Thus, HT1 was found to be most effective among the prepared HT catalysts in DMSO and MB decomposition. Inversely, the existence of large amounts of HAp on TiO_2 in the case of HT2 reduced its decomposition rates.

Further investigations will be conducted to enhance both photocatalytic activity and adsorptivity of HT through detailed optimization of the preparation procedure for practical applications in water purification.

2.5. References

[1] K. Kabra, R. Chaudhary, R. L. Sawhney, Treatment of hazardous organic and inorganic compounds through aqueous-phase photocatalysis: A review, Ind. Eng. Chem. Res. 43 (2004) 7683 – 7696.

[2] J.-M. Herrmann, Heterogeneous photocatalysis: State of the art and present applications, Top. Catal. 34 (2005) 49 – 65.

[3] Y. Cheng, T. Sakai, R. Moroi, M. Nakagawa, H. Sakai, T. Ogata, Y. Terada, Self-cleaning ability of a photocatalyst-containing denture base material, Dent. Mater. J. 27 (2008) 179 – 186.

[4] Y. Xing, X. Li, L. Zhang, Q. Xu, Z. Che, W. Li, Y. Bai, K. Li, Effect of TiO_2 nanoparticles on the antibacterial and physical properties of polyethylene-based film, Prog. Org. Coat. 73 (2012) 219 – 224.

[5] A. Markowska-Szczupak, K. Ulfig, B. Grzmil, A. Morawski, A preliminary study on antifungal effect of TiO_2-based paints in natural indoor light, Pol. J. Chem. Technol. 12 (2010) 53 – 57.

[6] I. Sopyan, M. Watanabe, S. Murasawa, K. Hashimoto, An efficient TiO_2 thin-film photocatalyst: Photocatalytic properties in gas-phase acetaldehyde degradation, J. Photochem. Photobiol. A 98 (1996) 79 – 86.

[7] E. Watanabe, M. Fukaya, H. Taoda, Generation of low-molecular-weight organic compounds in water by titania photocatalyst under UV-Vis light radiation, Res. Chem. Intermed. 34 (2008) 365 – 374.

[8] J. M. Dostanić, D. R. Lončarević, P. T. Banković, O. G. Cvetković, D. M. Jovanović, D. Z. Mijin, Influence of process parameters on the photodegradation of

synthesized azo pyridine dye in TiO_2 water suspension under simulated sunlight, J. Environ. Sci. Health A 46 (2011) 70 – 79.

[9] M. Janus, E. Kusiak, A. W. Morawski, Carbon Modified TiO_2 Photocatalyst with Enhanced Adsorptivity for Dyes from Water, Catal. Lett. 131 (2009) 506 – 511.

[10] Y. Kuwahara, J. Aoyama, K. Miyakubo, T. Eguchi, T. Kamegawa, K. Mori, H. Yamashita, TiO_2 photocatalyst for degradation of organic compounds in water and air supported on highly hydrophobic FAU zeolite: Structural, sorptive, and photocatalytic studies, J. Catal. 285 (2012) 223 – 234.

[11] H. Nakane, S. Aoki, T. Nonami, K. Tanaka, M. Mori, K. Tone, T. Kameyama, Synthesis and characterization of fluoride apatite in a simulated body fluid, J. Ceram. Soc. Jpn. 114 (2006) 838 – 843.

[12] H. Nakane, S. Aoki, T. Nonami, K. Tanaka, M. Mori, K. Sachimoto, K. Tone, T. Kameyama, Optimization on synthetic conditions of fluoride apatite coated titanium dioxide in simulated body fluid, J. Ceram. Soc. Jpn. 115 (2007) 151 – 155.

[13] A. Nakajima, K. Takakuwa, Y. Kameshima, M. Hagiwara, S. Sato, Y. Yamamoto, N. Yoshida, T. Watanabe, K. Okada, Preparation and properties of titania-apatite hybrid films, J. Photoch. Photobio. A 177 (2006) 94 – 99.

[14] M. Pratap Reddy, A. Venugopal, M. Subrahmanyam, Hydroxyapatite-supported Ag-TiO_2 as *Excherichia coli* disinfection photocatalyst, Water Res. 41 (2007) 379 – 386.

[15] T. Nonami, H. Hase, K. Funakoshi, Apatite-coated titanium dioxide photocatalyst for air purification, Catal. Today 96 (2004) 113 – 118.

[16] M. Ueda, M. Ikeda, M. Ogawa, Chemical-hydrothermal combined surface modification of titanium for improvement of osteointegration, Mater. Sci. Eng. C

29 (2009) 994 – 1000.

[17] M.N. Abellán, R. Dillert, J. Gimenez, D. Bahnemann, Evaluation of two types of TiO_2-based catalysts by photodegradation of DMSO in aqueous suspension, J. Photochem. Photobiol. A 202 (2009) 164 – 171.

[18] M. Mori, K. Tanaka, H. Taoda, M. Ikedo, H. Itabashi, Ion-exclusion/adsorption chromatography of dimethylsulfoxide and its derivatives for the evaluation to quality-test of TiO_2-photocatalyst in water, Talanta 70 (2006) 169 – 173.

Chapter 3

Preparation of vanadium/silica modified TiO_2 and its evaluation for water treatment ability

3.1. Introduction

Chapter 2 described the coating method of HAp onto photocatalyst surface to improve the adsorptivity in the aqueous phase. However, HAp-coated TiO_2 have declined the adsorptivity by the dissolution of the HAp during circulation with the solution containing a target chemical compound. We described adsorptivity and photocatalytic activity of photocatalyst that modified vanadium and silica to TiO_2. The effect expected in the developed photocatalyst is electrostatic adsorption for target compounds. The electrostatic adsorption in aqueous phase is generally stronger than hydrophobic adsorption by carbon-modified photocatalyst. Silicate and vanadium oxides have negative charges in neutral pH of water solution. When they are modified or doped to TiO_2, the pH that obtains the zero charge point are shifted to acidic pH [1]. Therefore, in neutral pH, TiO_2 photocatalyst modifying silicate or vanadium oxide has negatively charge.

This effectiveness of the silica or vanadium oxide-modified TiO_2 can provide high-dispersibility in water [1]. This feature is advantageous to obtain the high-efficient photodecomposition of a targeted organic compound due to increase of contact efficiency between photocatalyst and the compound.

In this study, we synthesized silica-doped TiO_2 (SiT), vanadium-modified TiO_2

(VT), and vanadium-modified silica-doped TiO_2 (VSiT), and evaluated the adsorptivities and the photodecomposition abilities by dimethyl sulfoxide (DMSO), methylene blue (MB), and indigo carmine (InC). DMSO, a highly polar organic solvent, is known to be an OH radical scavenger [2]. Upon oxidation of DMSO, MSI, MSA, and SA are generated stoichiometrically [3,4]. Thus, the generation of OH radicals using photocatalysts under irradiation can be indirectly observed through the oxidation of DMSO. MB and InC, basic and acidic dyes, have often been utilized to assess synthetic photocatalysts [5-8].

3.2. Experimental

3.2.1. Preparation of photocatalytic powders

Silica-doped TiO_2 with a Si/Ti charged ratio of 0.2 was prepared by the glycothermal method and collected as a xerogel [9]. The product was calcined in a box furnace in air at 500 ^{o}C for 30 min to remove surface organic species. This sample was designated as Si(0.2)–TiO_2 (SiT).

The vanadium modification of photocatalyst was carried out using an impregnation method in which the TiO_2 was added to an ammonium vanadate solution. The samples were dried at 70 °C, followed by calcination at 600 °C for 30 min. The vanadium species were mounted on the TiO_2 or SiT in V/Ti ratios (v/v) of 0.005, corresponding to values reported in previous studies by Ozaki *et al.* and previous study [10,11]. The base photocatalyst of vanadium modification used ST01 (anatase-type TiO_2: Ishihara Sangyo Kaisha Ltd., Osaka, Japan) and SiT. Those samples were named vanadium-modified

TiO_2 (VT) and vanadium-modified silica-doped TiO_2 (VSiT).

3.2.2. Characterization of photocatalysts

Crystalline phases in the samples were identified from powder diffraction patterns collected using X-ray diffraction (XRD, Cu Kα radiation, Rigaku RINT2200VF). Zeta potentials were determined using a Zetasizer Nano ZS (Malvern Instruments).

3.2.3. Photocatalytic decomposition of DMSO

The evaluation of the photocatalysts activity under UV light was performed via the decomposition of DMSO [3,4], which is used as an indicator on water quality-test in the standardized evaluation method [12].

The test for the photocatalytic decomposition of DMSO was conducted by dispersion the synthesized photocatalyst (5 mg) in a 10 ppm DMSO solution (50 mL) and then stirring under dark condition for 1 h, and next, irradiating the suspension with UV lamps emitting for 3 h at 352 nm (National-FL20S-BLB lamp, Matsushita Electric Industrial Co., Ltd., Osaka, Japan). The light intensity of the UV lamps used in this study was *ca.* 2.0 mW/cm^2.

The concentration of DMSO and its products in solution were described in experimental section of chapter 2.

3.2.4. Photocatalytic decomposition of organic dyes

The indicators to investigate both of adsorptivity and photodecomposition ability of synthesized photocatalyst employed MB (basic dye) and InC (acidic dye).

The using MB and InC were conducted by dispersion the synthesized photocatalyst (5 mg) in a 5 ppm MB or 20 ppm InC solution (50 mL) and then stirring under dark

condition for 1 h, and next, irradiating the suspension with UV lamps emitting for 3 h (MB) and 1 h (InC).

The dye concentration was determined on the basis of the change in the absorbance at 660 nm (MB) and 610 nm (InC) as a function of the irradiation time using a Hitachi U-3500 UV–Vis spectrophotometer. The decomposition experiments were also performed in the dark to evaluate the adsorptivity of the catalyst particles.

3.3. Results and discussion

3.3.1. Characterization of the synthesized photoatalysts

The photocatalysts were initially characterized using XRD. The diffraction patterns revealed peaks originating from anatase phase TiO_2 in all samples. However, the peaks from SiO_2 and V_2O_5 were not observed in VT, SiT or VSiT because of their low abundance (**Fig. 3-1**). **Fig. 3-2** shows the zeta potentials of the photocatalysts as a function of pH. The isoelectric points (pIs) of each photocatalysts were 6.0 in ST01, 4.5 in SiT, 4.2 in VT, 3.1 in VSiT. The shift to lower pI values of SiT was caused by the addition of Si, which is believed to be related to the pI of pure SiO_2 (pI *ca.* 2.0) [13]. The pI values of VT and VSiT were lowered by the addition of V, which are believed to be related to the hydration of vanadium in photocatalyst surface to vanadic acid [13].

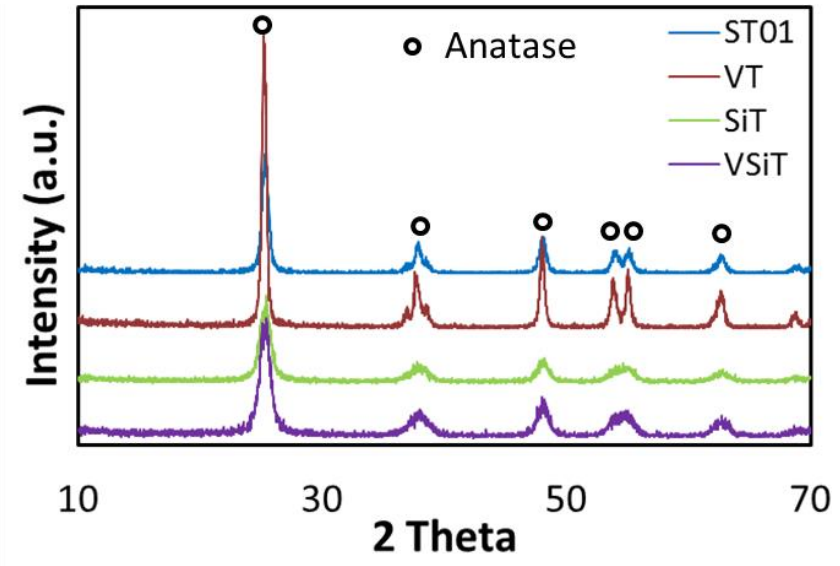

Fig. 3-1 XRD pattern of each photocatalyst powder.

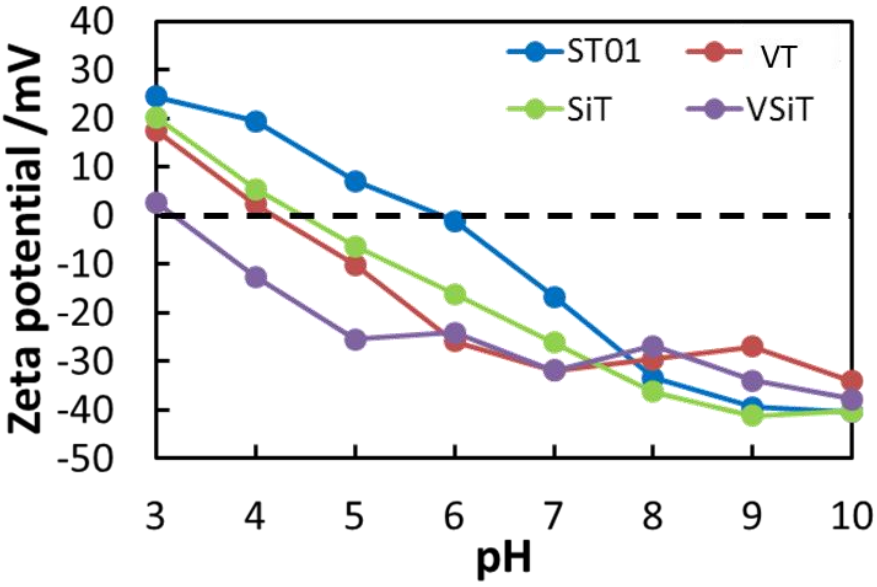

Fig. 3-2 Zeta potential of each photocatalyst.

3.3.2. Photocatalytic decomposition of DMSO

The water treatment efficiency of the synthesized photocatalysts were carried out by photodecomposition of DMSO under UV irradiation. As the result, no decrease in the DMSO concentration was observed under dark conditions. In addition, the self-decomposition of DMSO was not observed before or after light irradiation in the absence of photocatalyst. In contrast, UV light irradiation for 3 h in the presence of each photocatalyst decreased the concentration of DMSO in the test solution, as shown in **Fig. 3-3**. The formations of MSI and MSA was observed during the photocatalytic decomposition of DMSO, but SA was not detected. This might be because the decomposition of MSA was insufficient during the irradiation for 3 h (**Fig. 3-3**). The SiT exhibited high decomposition efficiency for DMSO, attaining 88.8% decomposition, compared to ST01 (72.7%), VT (38.7%) and VSiT (56.5%). The rate constants (*k*) for the decomposition rate, C/C_0, of DMSO under UV light irradiation for 3 h were calculated from the slope of the approximate curves (**Fig. 3-4**) and found to be 0.419 h^{-1} for ST01, 0.158 h^{-1} for VT, 0.690 h^{-1} for SiT and 0.268 h^{-1} for VSiT.

The formation of MSA was related to the decomposition efficiency of MSI. Also, SiT that shows the best decomposition efficiency of DMSO under UV irradiation relates the high dispersivity. However, the decomposition rates by using vanadium-modified TiO_2 such as VT and VSiT were not improved compared that by ST01 (**Fig. 3-4**). This relates two reasons as following: 1) reduction of dispersivity due to higher weight than SiT, and 2) decrease of decomposition rate by reduction of surface area.

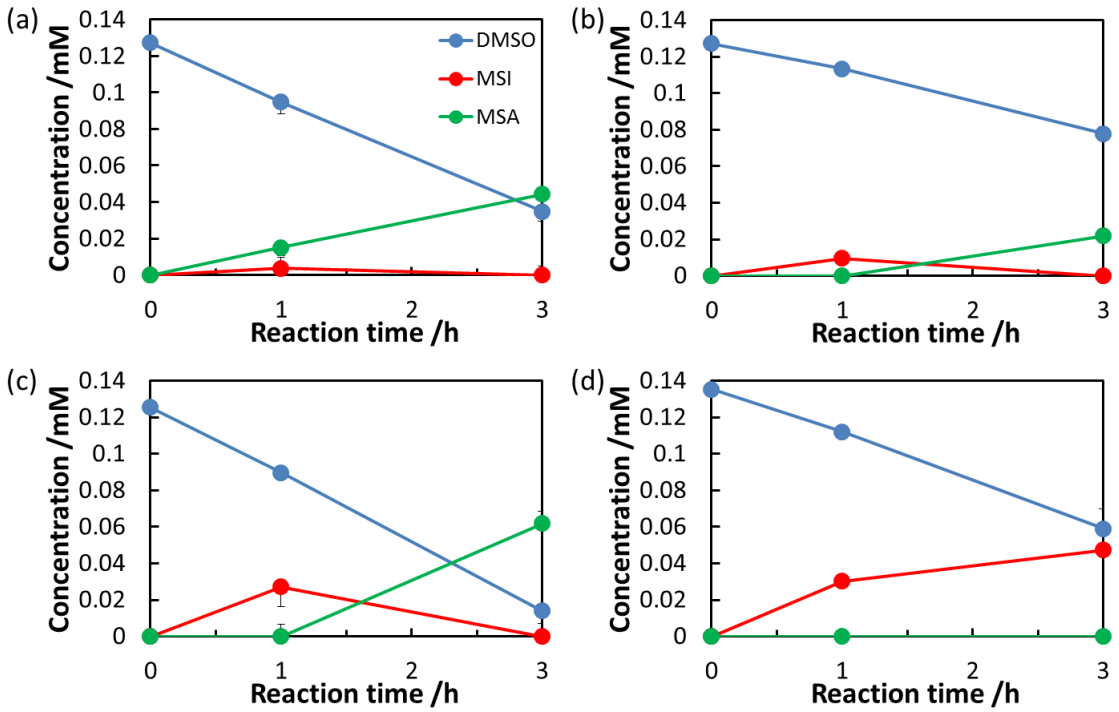

Fig. 3-3 Changes in DMSO, MSI and MSA concentrations by (a) ST01, (b) VT, (c) SiT and (d) VSiT as functions of irradiation time of UV light.

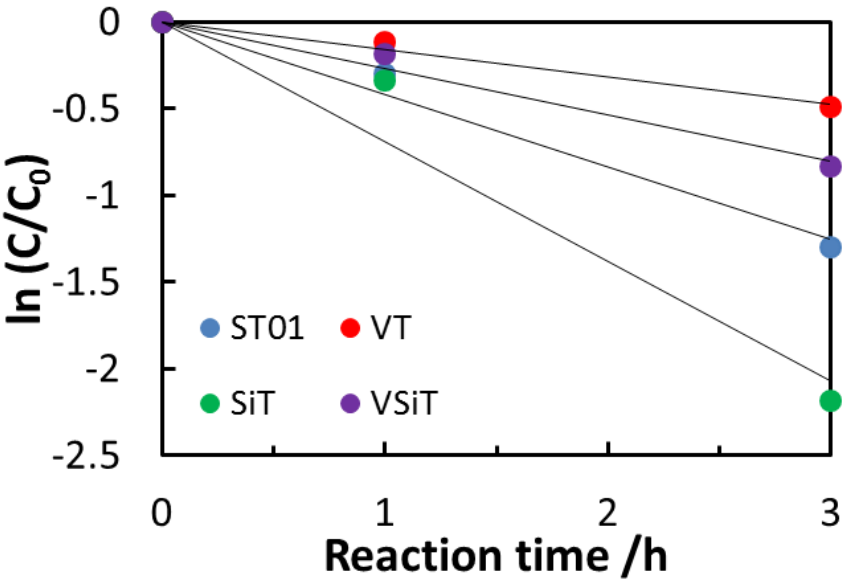

Fig. 3-4 Changes in $\ln(C/C_0)$ by the four different photocatalysts as functions of irradiation time of UV light for 3 h.

3.3.3. Photocatalytic decomposition of organic dyes

The ion adsorption and photodecomposition efficiencies of synthesized photocatalysts for organic dyes, MB and InC, were evaluated under UV irradiation.

In the dark conditions for 1 h, the SiT, VT and VSiT exhibited adsorptivities of 20%, 6.7% and 52% for MB, respectively. ST01, which is an anatase TiO_2, did not adsorb MB in the dark. These results were based on the electrostatic adsorption between the negatively charged photocatalyst and positively charged MB. Furthermore, total of adsorptivities and photodecomposition efficiencies of ST01, SiT, VT, and VSiT for MB were 44.0%, 94.6%, 85.2%, and 79.9%, respectively (**Fig. 3-5**). These results demonstrates that the adsorption for the target compound closely relate to the effective photodecomposition. However, the photodecomposition efficiency (*k*) of the VSiT under UV light irradiation following adsorption of MB was found to be lower than those of SiT and VT, by photodecomposition rate (*k*) estimated from plots in **Fig. 3-6**. The *k* values of ST01, SiT, VT, and VSiT for MB were 0.185, 0.959, 0.631, and 0.367 h^{-1}, respectively. Accordingly, the strongest adsorption of VSiT for MB caused a reduction in the light absorption, and led the low photodecomposition efficiency.

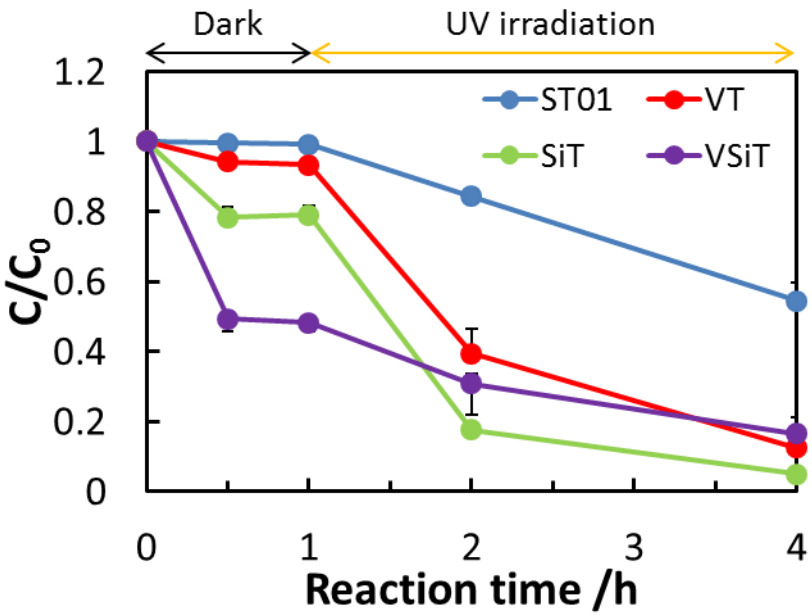

Fig. 3-5 Adsorptivity and photodecomposition efficiency of MB by each photocatalyst as a function of reaction time.

The efficiencies (C/C_0) as a function of reaction time were calculated from initial concentration of MB (C_0); and concentration of MB in each reaction time (C).

Reaction time: dark condition, 1 h; and UV light irradiation, 3 h.

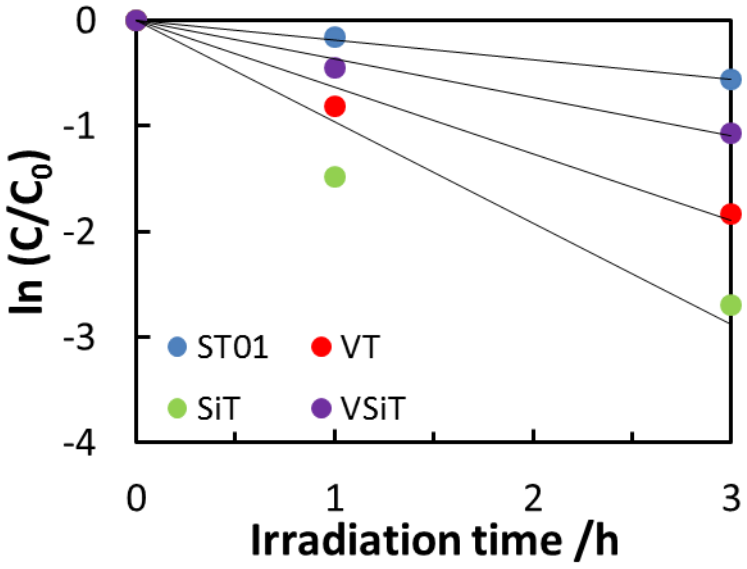

Fig. 3-6 The $\ln(C/C_0)$ of MB by each photocatalyst as a function of irradiation time of UV light. The $\ln(C/C_0)$ are obtained using C/C_0 in **Fig. 3-5**.

As mentioned above, the strongest adsorption of target compound, especially cationic dye, led the lowering of the photodecomposition ability. Therefore, we adjusted the molar ratio of vanadium to be modified to SiT, and compared these abilities for adsorption and photodecomposition of MB.

As shown in Fig. 3-7, in the dark conditions for 1 h, the adsorption efficiencies of SiT, V(0.001)-SiT, V(0.005)-SiT and V(0.01)-SiT for MB were 20.4%, 46.1%, 51.8% and 61.4%, respectively. The *k* values of SiT, V(0.001)-SiT, V(0.005)-SiT and V(0.01)-SiT were 1.29, 1.35, 0.350 and 0.841 h^{-1}, respectively. These results suggest that the decomposition efficiency is reduced when an adsorption rate is higher than 50% (adsorption amount: *ca.* 78.2 μmol/g).

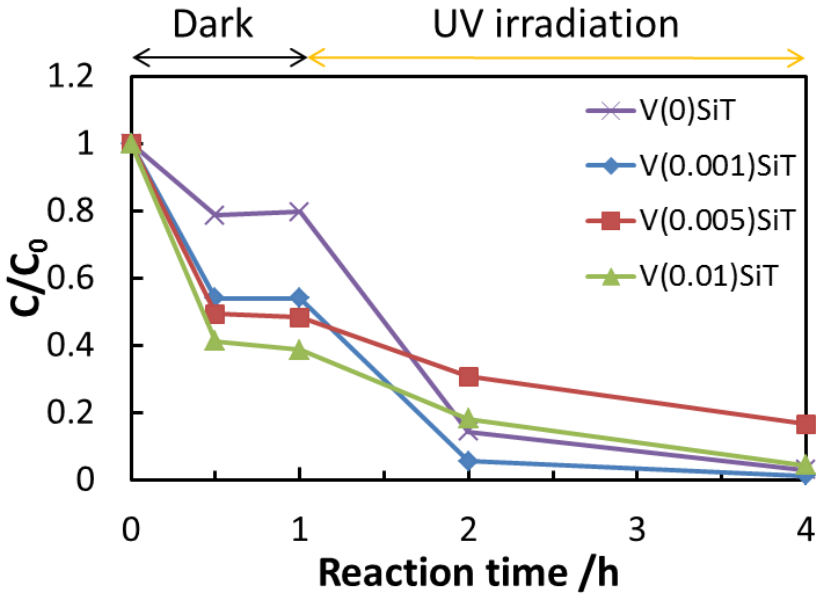

Fig. 3-7 Adsorption and photodecomposition of MB by each photocatalyst in various V content.

In contrast, in the dark conditions for 1 h, each photocatalyst did not adsorb InC. These results were based on the electrostatic repulsion between the negatively charged photocatalyst and negatively charged InC. The photodecomposition efficiencies of ST01, SiT, VT, and VSiT for InC were 99.3%, 72.7%, 8.23%, and 2.36%, respectively (**Fig. 3-8**). In addition, the photodecomposition efficiency (*k*) of the VT and VSiT under UV light irradiation of InC was found to be lower than those of ST01 and SiT, by photodecomposition rate (*k*) estimated from plots in **Fig. 3-9**. The *k* values of ST01, SiT, VT, and VSiT for InC were 2.46, 0.443, 0.0311, and 0.00900 h^{-1}, respectively. These results demonstrated that the repulsions of negatively charged photocatalyst for the anionic target compound attributed the insufficient photodecomposition.

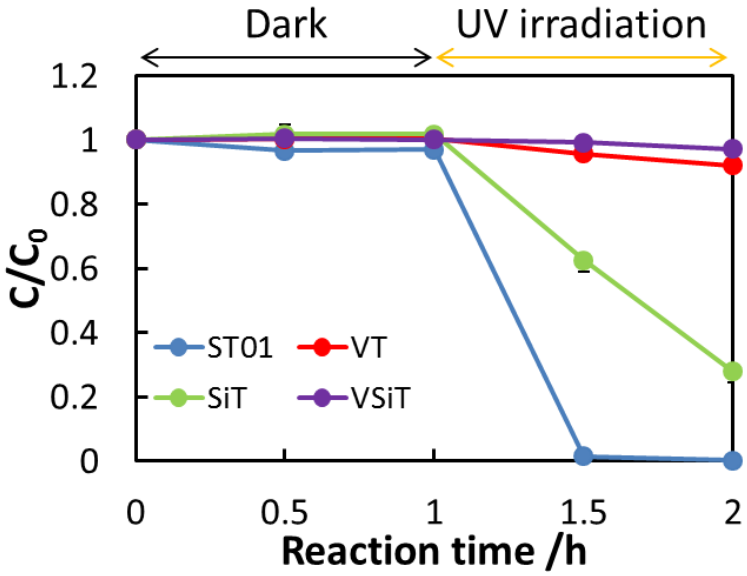

Fig. 3-8 Adsorptivity and photodecomposition efficiency of InC by each photocatalyst as a function of reaction time.

The efficiencies (C/C_0) as a function of reaction time were calculated from initial concentration of InC (C_0); and concentration of InC in each reaction time (C).

Reaction time: dark condition, 1 h; and UV light irradiation, 1 h.

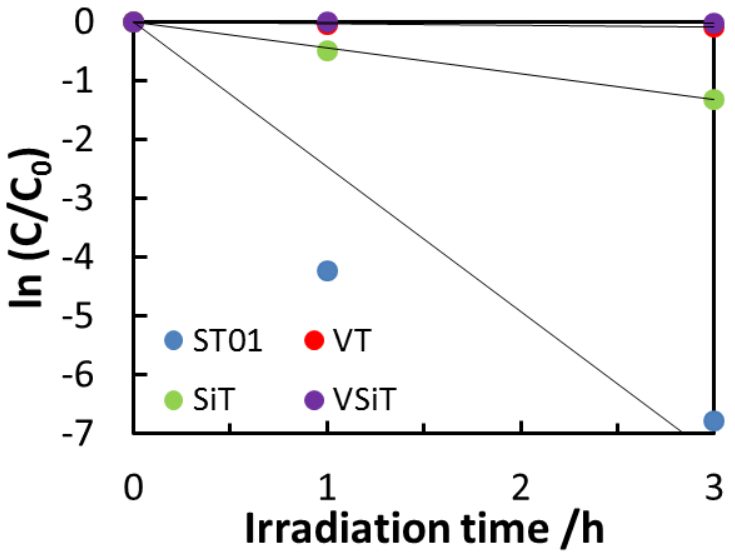

Fig. 3-9 The $\ln(C/C_0)$ of InC by each photocatalyst as a function of irradiation time of UV light. The $\ln(C/C_0)$ is obtained using C/C_0 in **Fig. 3-8**.

3.4. Conclusions

SiT photocatalyst exhibited high decomposition capacities for DMSO under UV light irradiation. The high negative charge of VSiT in aqueous solution attributed high adsorptivity for cationic MB but the too highest adsorptivity reduced the photocatalytic activity. Also, the photodecomposition abilities of the negatively charged photocatalyts for anionic dye such as InC were lower than that of anatase TiO_2 (ST01), due to the electrostatic repultion. Inversely, the negatively charged photocatalyst was considered to be selective for cationic species. These facts are concluded that the charged photocalytic materials are useful for photodecomposition of a targeted cationic compound.

3.5. References

[1] A. Mase, T. Sugita, M. Mori, S. Iwamoto, T. Tokutome, K. Katayama, H. Itabashi, Study of vanadium-modified N/Si co-doped TiO_2 in aqueous solution and its photocatalytic activity, Chem. Eng. J. 225 (2013) 440 – 446.

[2] R. Bruck, H. Aeed, H. Shirin, Z. Matas, L. Zaidel, Y. Avni, Z. Halpern, The hydroxyl radical scavengers dimethyl sulfoxide and dimethyl urea protect rats against thioacetamide-induced fulminant hepatic failure, J. Hepatol. 31 (1999) 27–38.

[3] M.N. Abellán, R. Dillert, J. Gimenez, D. Bahnemann, Evaluation of two types of TiO_2-based catalysts by photodegradation of DMSO in aqueous suspension, J. Photochem. Photobiol. A 202 (2009) 164 – 171.

[4] M. Mori, K. Tanaka, H. Taoda, M. Ikedo, H. Itabashi, Ion-exclusion/adsorption chromatography of dimethylsulfoxide and its derivatives for the evaluation to quality-test of TiO_2-photocatalyst in water, Talanta 70 (2006) 169 – 173.

[5] A. Syoufian, K. Nakashima, Degradation of methylene blue in aqueous dispersion of hollow titania photocatalyst: Optimization of reaction by peroxydisulfate electron scavenger, J. Colloid Interface Sci. 313 (2007) 213 – 218.

[6] Z. Liu, Y. Wang, W. Chu, Z. Li, C. Ge, Characteristics of doped TiO_2 photocatalysts for the degradation of methylene blue waste water under visible light, J. Alloys. Compd. 501 (2010) 54 – 59.

[7] Q.I. Rahman, M. Ahmad, S.K. Misra, M. Lohani, Efficient degradation of methylene blue dye over highly reactive Cu doped strontium titanate ($SrTiO_3$) nanoparticles photocatalyst under visible light, J. Nanosci. Nanotechnol. 12 (2012)

7181 – 7186.

[8] R. Vinu, S.U. Akki, G. Madreas, Investigation of dye functional group on the photocatalytic degradation of dyes by nano-TiO_2, J. Hazard. Mater. 176 (2010) 765 – 773.

[9] H. Ozaki, K. Saito, S. Iwamoto, M. Inoue, Photocatalytic activities of nanocrystalline Si-modified titania xerogels prepared by the glycothermal method, J. Mater. Sci. 43 (2008) 2286 – 2292.

[10] K. Kabra, R. Chaudhary, L.R. Sawhney, Treatment of hazardous organic and inorganic compounds through aqueous-phase photocatalysis: a review, Ind. Eng. Chem. Res. 43 (2004) 7683 – 7696.

[11] H. Ozaki, S. Iwamoto, M. Inoue, Effect of the addition of a small amount of vanadium on the photocatalytic activities of N- and Si-codoped titanias under visible-light irradiation, Catal. Lett. 113 (2007) 95 – 98.

[12] Japan Fine Ceramics Association, edt.: JIS R 1704 (2007)/ISO 10676 (2010), Fine Ceramics (advanced ceramics, advanced technical ceramics-Test method for water purification performance of semiconducting photocatalytic materials by measurement of forming ability of active oxygen).

[13] B.M. Weckhuysen, D.E. Keller, Chemistry, spectroscopy and the role of supported vanadium oxides in heterogeneous catalysis, Catal. Today 78 (2003) 25 – 46.

Chapter 4

Study of vanadium-modified N/Si co-doped TiO_2 in aqueous solution and its photocatalytic activity

4.1. Introduction

Chapters 2 and 3 described the addition of adsorptivity for photocatalyst to improve the organic matter decomposition efficiency in the aqueous phase. This chapter describes synthesis of visible light-induced photocatalyst with adsorptivity.

The present study aimed to characterize the capability of the visible light-induced photocatalyst vanadium-modified N/Si co-doped TiO_2 (VNSiT) for water purification. Two versions of VNSiT were synthesized, and their properties in water were investigated, including their photoabsorption in the visible region, isoelectric points, and average hydrodynamic diameters, which is the average size of the aggregated particles in an aqueous solution. In addition, the capacity of the VNSiTs for water purification via the photoactivated decomposition of dimethyl sulfoxide (DMSO, an OH radical scavenger) dissolved in water under visible light irradiation was evaluated. These results were compared with those for anatase phase TiO_2, SiT, NT, and NSiT, as mentioned above.

4.2. Experimental methods

4.2.1. Photocatalyst preparation

Si-doped titania with a Si/Ti charged ratio of 0.2 was prepared by the glycothermal method and collected as a xerogel [1]. The product was calcined in a box furnace in air at 500 °C for 30 min to remove surface organic species. This sample was designated as Si(0.2)–TiO_2. Next, SiT was heated to 600 °C at a rate of ~10 °C/ min under a 100 mL/min flow of argon gas and then exposed to NH_3 gas (100 mL/min) for 2 h, followed by annealing at 500 °C in air for 1 h. This sample was designated as NSiT [2]. The vanadium doping of NSiT was carried out using an impregnation method in which the NSiT was added to an ammonium vanadate solution. The samples were dried at 70 °C, followed by calcination at 600 °C for 30 min. The vanadium species were mounted on the NSiT in V/Ti ratios (v/v) of 0.005 in V(0.005)–NSiT and 0.02 in V(0.02)–NSiT, corresponding to values reported in previous studies by Ozaki et al. [3].

4.2.2. Photocatalyst characterization

The UV–Vis absorption spectra of the samples were acquired using a JASCO V-650 spectrophotometer. Crystalline phases in the samples were identified from powder diffraction patterns collected using X-ray diffraction (XRD, Cu Kα radiation, Rigaku RINT2200VF). Energy dispersive X-ray fluorescence spectroscopy (EDX) (Shimadzu EDX-800) was used for determination of the chemical composition of the samples. The distribution of vanadium in the VNSiTs was evaluated using transmission electron microscopy (TEM) at an analysis center (Sumika Chemical Analysis Service, Ltd., Japan). X-ray photoelectron spectroscopy (XPS) spectra were obtained on a

Shimadzu AXIS-NOVA with an Al Kα source operating at 15 kV and 10 mA and used to determine the atomic and chemical composition of the sample surface. Zeta potentials and hydrodynamic sizes were determined using a Zetasizer Nano ZS apparatus with an MRT-2 autotitrator (Malvern) through the measurement of the electrophoreticity and dynamic light scattering characteristics of the VNSiTs. For this experiment, a small amount of sample was dispersed in 10 mM NaCl, and the pH was adjusted with 0.1 M NaOH or 0.1 M HCl. The analysis was conducted after the suspension was ultrasonicated for 10 min.

4.2.3. Photocatalytic decomposition of DMSO

The ability of the photocatalysts to purify water under visible light was evaluated via their ability to decompose DMSO [4,5], which has been used as an indicator of water quality in such experiments.

The test for the photocatalytic decomposition of DMSO was conducted by dispersing the synthesized photocatalyst (10 mg) in a 10 ppm DMSO solution (100 mL) and then irradiating the suspension with blue light-emitting diodes (blue LEDs, NSPB510S, Nichia). Blue LEDs emit in the range 420–520 nm with an emission peak at 470 nm. The power of the blue LEDs used in this study was 72 mW, with 96 individual LEDs used as the light source (4 panels, each equipped with 24 LEDs).

The concentration of DMSO and its products in solution were determined by same method of chapter 2.

4.2.4. Photocatalytic decomposition of MB

The test for the decomposition of MB was conducted by dispersing the photocatalyst (10 mg) with stirring in a 5 ppm MB solution (100 mL), followed by irradiation of the suspension with 96 individual as the light source (4 panels, each equipped with 24 LEDs). The dye concentration was determined on the basis of the change in the absorbance at 660 nm as a function of the irradiation time using a Hitachi U-3500 UV–Vis spectrophotometer. The decomposition experiments were also performed in the dark to evaluate the adsorptivity of the catalyst particles.

4.3. Results and discussion

4.3.1. Characterization of the synthesized photocatalysts

The photocatalysts were initially characterized using XRD. The diffraction patterns revealed peaks originating from anatase phase TiO_2 in all samples, but peaks from SiO_2 and V_2O_5 were not observed in SiT, NSiT, V(0.005)–NSiT, or V(0.02)–NSiT because of their low abundance (**Fig. 4-1**).

The Brunauer–Emmett–Teller (BET) surface areas and crystal sizes of the photocatalysts are summarized in **Table 4-1**. Anatase phase TiO_2 prepared in this study had an average crystal size of 19 nm and a BET surface area of 87 m^2/g. The NT photocatalyst, which was nitrogen doped at 600 °C, had an average crystal size of 22 nm and a smaller BET surface area of 77 m^2/g. This smaller BET surface area was attributed to sintering of the TiO_2 particles during thermal treatment, which elevated the surface energy through ionic dispersion of the particles. The crystal size of SiT (11 nm),

which was obtained by doping small amounts of Si into TiO_2 (Si/Ti of 0.2), was smaller than that of TiO_2, and the BET surface area (183 m^2/g) was larger than that of TiO_2. These results suggest that the insertion of Si into the vacant tetrahedral holes in TiO_2 reduce the aggregation of the TiO_2 particles and consequently suppress sintering [6]. This behavior may be related to the formation of a negatively charged surface featuring OH groups resulting from the insertion of Si.

Furthermore, the crystal size and BET surface area of NSiT, which was obtained by nitrogen doping at 600 °C, were 11 nm and 182 m^2/g, respectively, indicating that sintering of the particles did not occur because of the high thermal stability of SiT. The VNSiTs, which were prepared by mounting a small amount of V_2O_5 on NSiT, exhibited a slightly larger crystal size (12 nm) and slightly smaller BET surface area (180 m^2/g) compared with those of SiT. Sintering may have caused an elevation in the surface energy because of modification of the SiT with V_2O_5, although the impact was minimal.

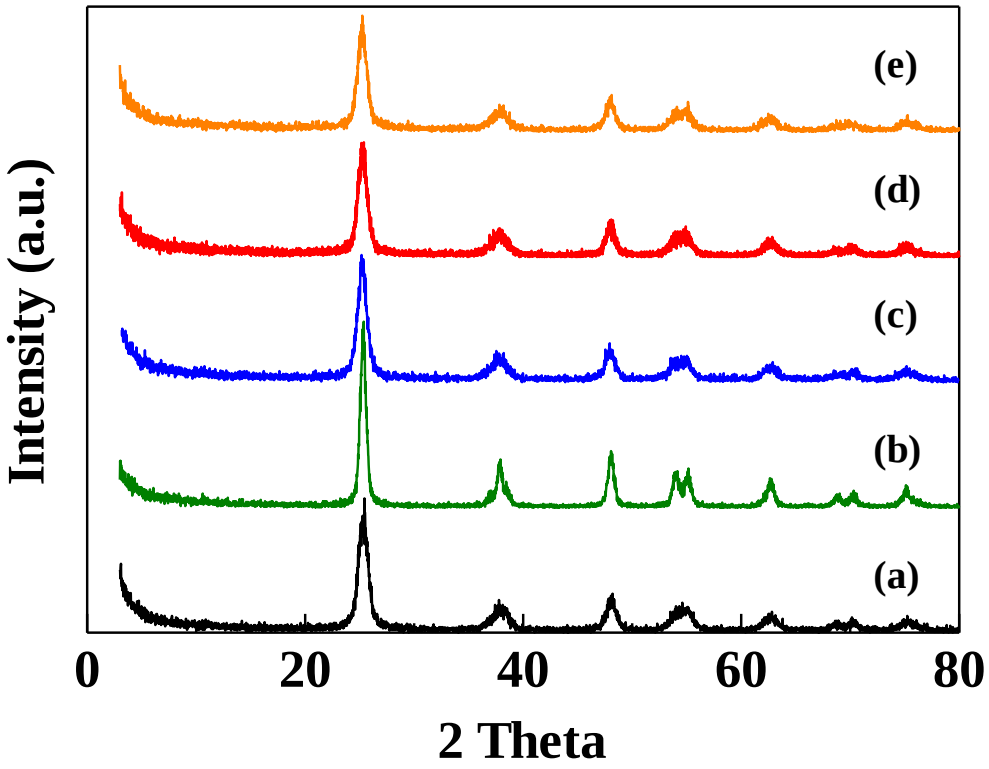

Fig. 4-1 XRD patterns for (a) SiT, (b) NT, (c) NSiT, (d) V(0.005)–NSiT, and (e) V(0.02)–NSiT.

Table 4-1 BET surface areas and crystal sizes of synthesized photocatalysts.

Sample	BET surface area (m^2/g)	Crystal size (nm)
Anatase TiO_2	87	19
NT	77	22
SiT	183	11
NSiT	182	11
V(0.005)-NSiT	180	12
V(0.02)-NSiT	180	12

4.3.2. UV–Vis characterization of photocatalysts

Initially a white powder, SiT turned yellow after NH_3 treatment and annealing. Whereas SiT absorbed only in the UV region (<400 nm), all of the nitrified samples absorbed in the visible light region (>400 nm). NSiT displayed a strong absorption band at 400–550 nm. In the case of unmodified anatase, the negative charges formed by the substitution from O^{2-} into N^{3-} are balanced by formation of oxygen vacancies. On the other hand, in the case of nitrified Si-modified titanias, the negative charge formed by the substitution from O^{2-} into N^{3-} can be compensated by the positive charge formed by the Si insertion, which explains the more stable doping of nitrogen in the Si-modified titanias than in titanias [2]. Conseqently, the visible-light responsivity of NSiT is expected to be enhanced compared with NT.

In addition, the spectra of the VNSiTs revealed that their absorption expanded into the visible region and became more intense depending on the amount of vanadium species mounted on NSiT. It has been reported that V_2O_5, which arises from a polymeric vanadium(V) species with a square-pyramidal VO_5 and/or highly distorted octahedral VO_6 structure, absorbs wavelengths lower than 570 nm, and that vanadium(IV) has an absorption band centered at 770 nm owing to a d–d transition [7,8]. Therefore, the UV–Vis spectra of the VNSiTs suggested the presence of both V^{5+} and V^{4+}. These results can be seen in **Fig. 4-2**. On the basis of spectral analysis, the band gap energy values of the photocatalysts were determined to be 3.2 eV for NT and 2.3 eV for NSiT, V(0.005)–NSiT, and V(0.02)–NSiT, as estimated from the Tauc plots (commonly used for the calculation of band gap energies) [9,10].

The difference in the band gap energies between NT and NSiT is likely due to the difference in the content of the nitrogen species doped into TiO_2. Namely, the band gap

energy decreases as the amount of nitrogen increases (band gap energies of 3.2 eV and 2.3 eV for NT and NSiT, respectively), and light absorption in the visible light region is enhanced consequently [9,10]. In addition, the band gap energies of the two VNSiTs were same as that of NSiT irrespective of the amount of vanadium mounted on the NSiT, because the band gap energy is dependent on the amount of doped nitrogen and not the amount of vanadium.

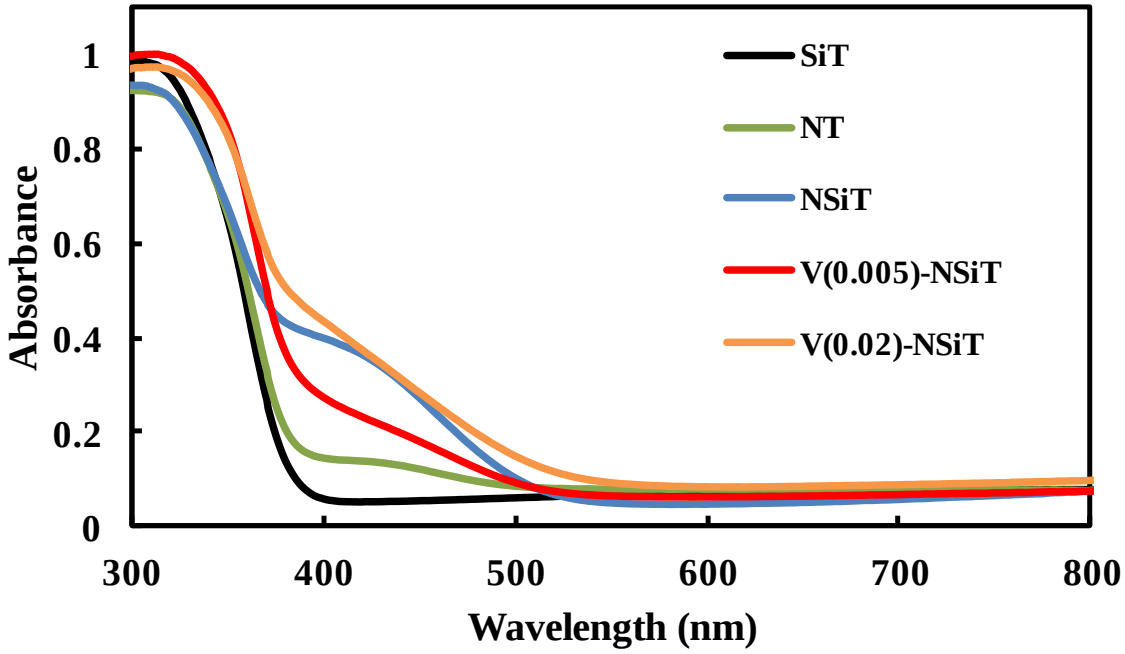

Fig. 4-2 UV–Vis spectra of the synthesized photocatalysts.

4.3.3. XPS characterization of the photocatalysts

The surfaces of the photocatalysts were characterized using XPS. All of the binding energies were referenced to the C(1s) peak at 285.0 eV, according to the values reported by Machold *et al.* [11]. **Fig. 4-3a** depicts the Ti($2p_{3/2}$) core level binding energy. The peak located at 458.8 eV indicates the presence of titanium in the Ti^{4+} state. The O(1s) XPS spectra of the VNSiTs are shown in **Fig. 4-3b**. Peak A located at 530.0 eV was assigned to the crystal lattice oxygens (Ti–O and V–O), while peak B located at 532.1 eV was assigned to the oxygen associated with the Si–O–Ti bridging bond. Moreover, **Fig. 4-3c** shows the V($2p_{3/2}$) core level binding energies at 517 and 516 eV, which correspond to V^{4+} and V^{5+} states, respectively, and indicate the formation of V_2O_5 [12–15]; these peaks were not observed in NSiT. The intensities of the V^{4+} and V^{5+} peaks were dependent on the amount of vanadium species mounted on the NSiT.

The N(1s) peaks at 396 eV shown in **Fig. 4-3d** were assigned to the nitrogen atoms doped into the TiO_2 lattice, that is, the negatively charged nitrogen species that substituted for oxygen in the lattice [16,17]. The concentration of N, as indicated by the 396 eV peak, increased with the Si/Ti charged ratio up to 0.2. These results are in accordance with those obtained from the UV–Vis spectra.

The abundance ratios of V/Ti in the V(0.005)–NSiT and V(0.02)– NSiT estimated from the XPS spectra were 0.011 and 0.041, respectively (**Table 4-2**). This result suggests that the orientation of the VNSiTs on the surface of the crystalline phases is likely dependent on the amount of vanadium.

Observation of the distribution of vanadium in the VNSiTs using TEM and EDX (**Table 4-3**) was also attempted, but the presence of vanadium was not detected. This result is largely due to the very small amount of vanadium species present in the

photocatalysts, combined with the fact that the vanadium was highly dispersed in the VNSiTs.

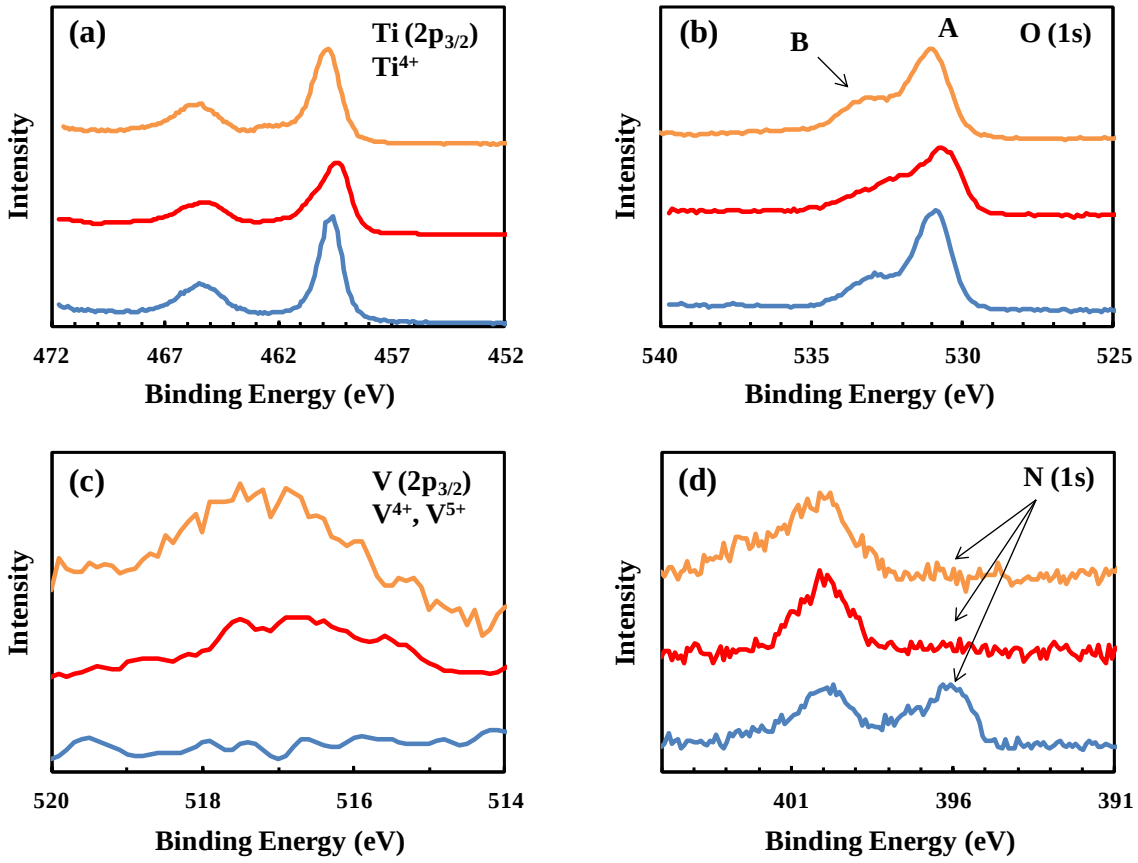

Fig. 4-3 XPS spectra of NSiT (blue line), V(0.005)–NSiT (red line), and V(0.02)–NSiT (orange line): (a) Ti($2p_{3/2}$), (b) O(1s), (c) V($2p_{3/2}$), and (d) N(1s) core levels.

Table 4-2 Si/Ti, N/Ti, and V/Ti ratios for each photocatalyst.

Sample	Si (103 eV)/Ti (459 eV)	N (396 eV)/Ti (459 eV)	V (518 eV)/Ti (459 eV)
Anatase TiO_2	-	-	-
SiT	0.32	-	-
NT		0.0047	
NSiT	0.34	0.0089	-
V(0.005)–NSiT	0.32	0.0025	0.011
V(0.02)–NSiT	0.35	0.0051	0.041

Table 4-3 Analytical results for the chemical composition of the photocatalysts by EDX.

Component element	Abundance ratio (%)				
	Anatase TiO_2	SiT	NT	NSiT	V(0.005)–NSiT
TiO_2	99.7	84.4	96.8	91.6	90.5
SiO_2	-	11.9	-	8.3	9.1
Others	0.3	3.7	3.2	0.1	0.4

4.3.4. Zeta potentials of the photocatalysts

Fig. 4-4a shows the zeta potentials of the photocatalysts as a function of pH. The isoelectric point (pI) of NSiT was 3.7, while that of TiO_2 was 5.8. The shift to lower values was caused by the addition of Si, and is believed to be related to the pI of pure SiO_2 (pI *ca.* 2.0) [18]. The pI values of V(0.005)–NSiT and V(0.02)–NSiT were 3.2 and 2.9, respectively, possibly because the vanadium mounted on the NSiT was converted to the negatively charged vanadic acid in water [19]. The average hydrodynamic diameters of the photocatalyst nanoparticles are presented in **Fig. 4-4b**, also as a function of pH. At lower pI values, the average hydrodynamic diameters dramatically increased owing to particle aggregation, as indicated by the gradual decline in the zeta potential, and the maximum diameters were obtained near the pI of each photocatalyst. However, the average hydrodynamic diameters decreased with increasing pH values, as indicated by the increasingly negative zeta potentials. From these results, it was apparent that modifying the surface with vanadium species significantly reduced the particle size and affected the dispersibility of the TiO_2 nanoparticles at neutral pH. Modifying the particle surface with the metal induced an effective electrostatic force that generated repulsion and prevented a decrease in the surface area [20].

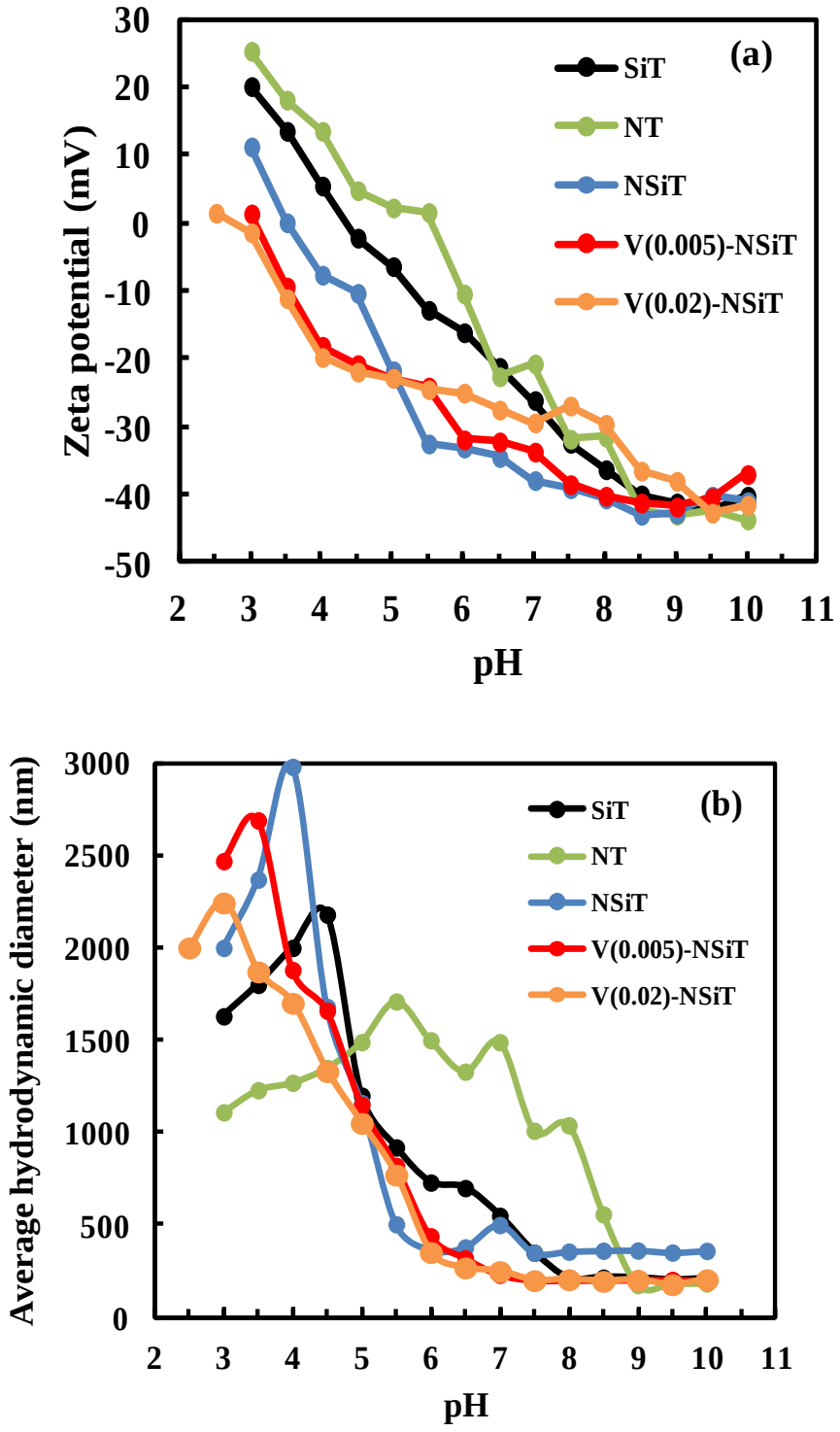

Fig. 4-4 (a) Zeta potentials and (b) average hydrodynamic diameters of the synthesized photocatalysts as a function of pH.

4.3.5. Photocatalytic decomposition of DMSO using VNSiTs

DMSO, a highly polar organic solvent, is known to be an OH radical scavenger [21]. Upon oxidation of DMSO, MSI, MSA, and SA are generated stoichiometrically [4,5]. Thus, the generation of OH radicals using photocatalysts under irradiation can be indirectly observed through the oxidation of DMSO to SA. Thus, the water purification potential of the photocatalysts was evaluated on the basis of their ability to decompose DMSO (initial concentration: C_0 = 10 ppm) by observing the formation of the decomposition products MSI, MSA, and SA under visible light irradiation. No decrease in the DMSO concentration was observed under dark conditions; that is, there was no adsorption of DMSO onto the photocatalysts under dark conditions. In addition, the self-decomposition of DMSO was not observed before or after light irradiation when no photocatalyst was present. In contrast, under visible light irradiation for 10 h in the presence of each N-doped photocatalyst, the concentration of DMSO decreased, as shown in **Fig. 4-5**. As the photocatalytic decomposition of DMSO proceeded, the formations of MSI and MSA was observed, but SA was not detected because the decomposition of MSA was insufficient during the irradiation for 10 h (**Fig. 4-5**). The vanadium-doped photocatalysts V(0.005)–NSiT and V(0.02)–NSiT exhibited high decomposition efficiencies for DMSO, attaining 40% and 29% decomposition, respectively, compared to 6.9% using NT and 15% using NSiT. The rate constants (*k*) for the decomposition of DMSO under visible light irradiation for 10 h were calculated from the slope of the approximate curves (**Fig. 4-6**) and found to be 0.0067 h^{-1} for NT, 0.014 h^{-1} for NSiT, 0.051 h^{-1} for V(0.005)–NSiT, and 0.032 h^{-1} for V(0.02)– NSiT.

The formation of MSI and MSA depended on the irradiation time (**Fig. 4-5**). In addition, the formation of MSA increased with the *k* value as the photocatalytic

decomposition of DMSO proceeded, as did the formation and decomposition efficiencies for MSI. The differences between V(0.005)–NSiTs and V(0.02)–NSiTs in the decomposition of DMSO were related to the different amounts of vanadium species mounted on the NSiT. Specifically, mounting an excess of vanadium reduced the efficiency for photocatalytic DMSO decomposition in the aqueous phase because the vanadium species blocked the ability of the photocatalyst to absorb light.

With V(0.02)–NSiT, the formation of MSI depended only on the irradiation time, while the formation of MSA continued to slightly increase after irradiation was halted at 10 h. This result indicated that the amount of OH radicals generated by the photocatalyst was insufficient for the decomposition of DMSO and/or MSI. Therefore, the formation of MSA was found to be related not only to the decomposition of DMSO but also that of MSI.

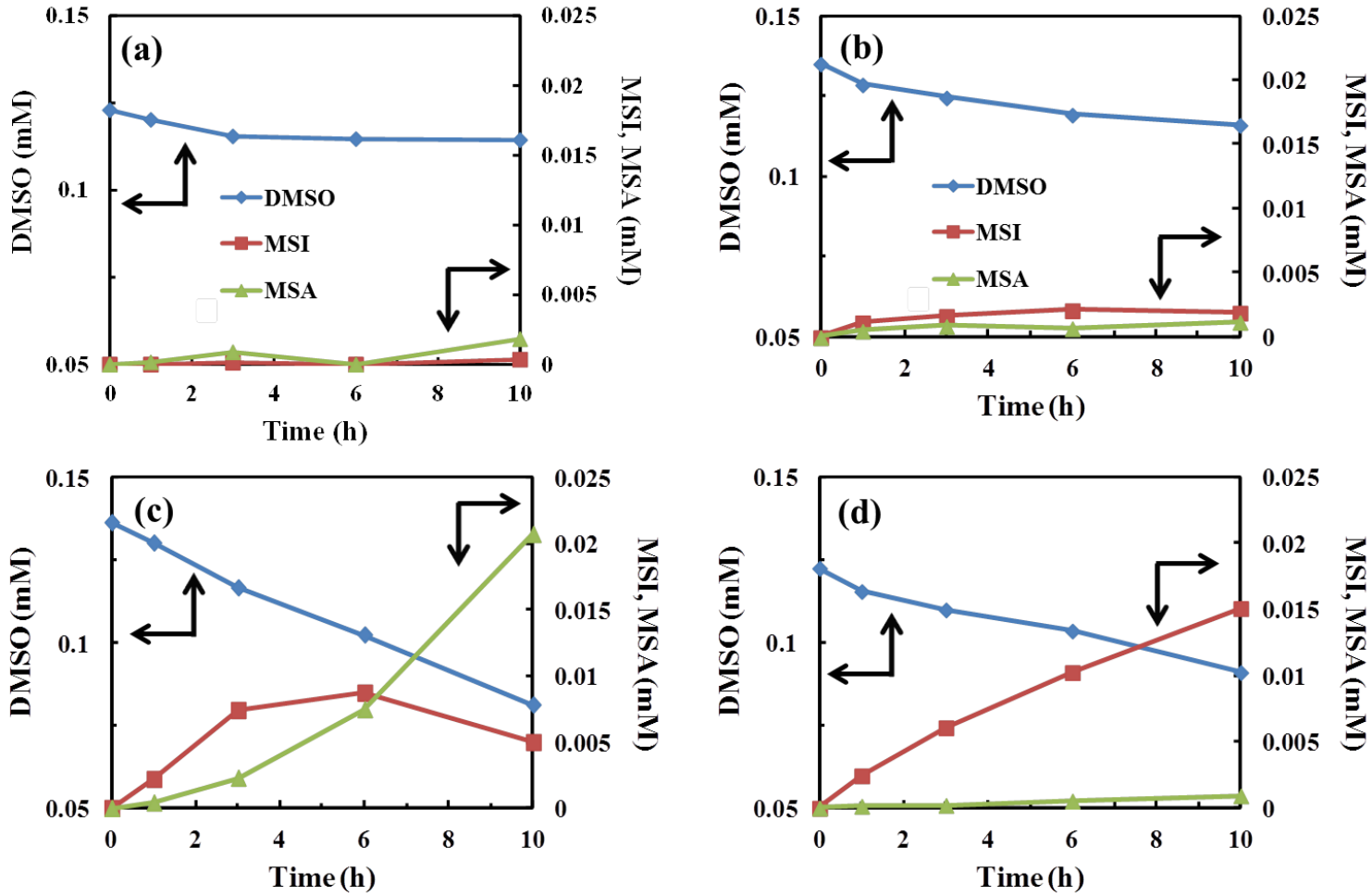

Fig. 4-5 Variation in the concentrations of MSI and MSA formed by photocatalytic decomposition of DMSO using (a) NT, (b) NSiT, (c) V(0.005)–NSiT, and (d) V(0.02)–NSiT.

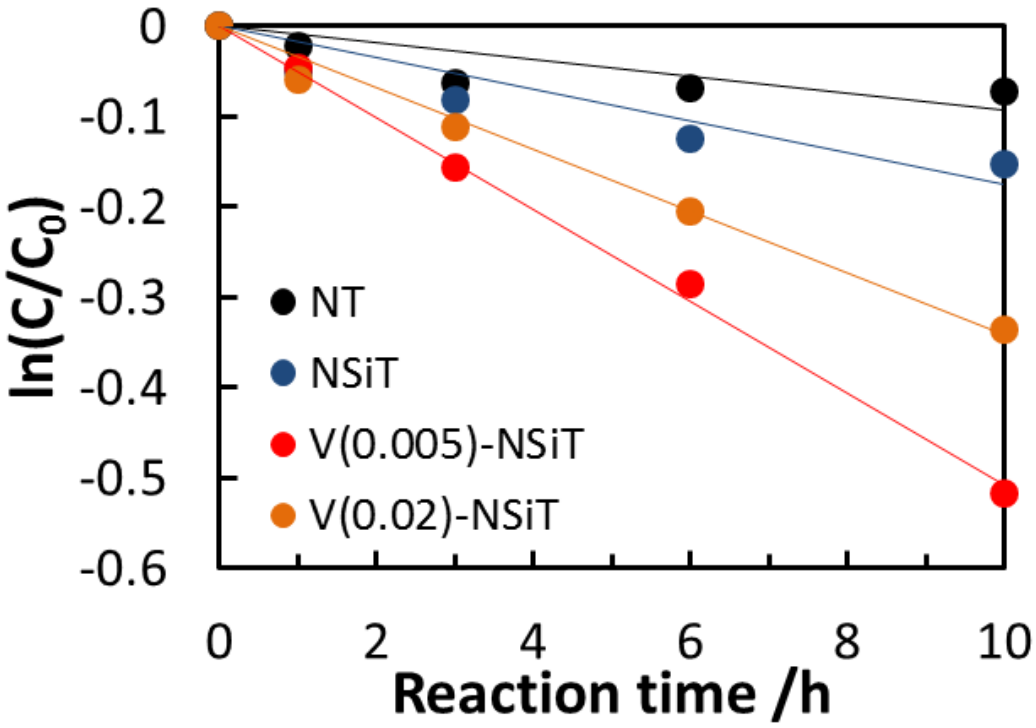

Fig. 4-6 Decomposition of DMSO using the photocatalysts under visible light irradiation for 10 h. Initial concentration (C_0): 10 ppm; Concentration at each irradiation time (C).

The photocatalytic decomposition of DMSO using V(0.005)– NSiT is possibly, therefore, a stoichiometric reaction first involving formation of MSI with a decrease in the concentration of DMSO, and subsequently formation of MSA with a decrease in the concentration of MSI [5]. The absorbance of V(0.005)–NSiT at 420–520 nm from the LEDs was lower than that of NSiT and V(0.02)–NSiT; however, the average hydrodynamic diameter and polydispersity index at pH 7 were smaller than those of the other photocatalysts, as summarized in **Table 4-4**. Additionally, after visible light irradiation for 10 h, the pH of the solution shifted to pH 4 as the DMSO decomposed and MSI and MSA were formed. At pH 4, the average hydrodynamic diameter of the VSNiTs was approximately half than that of NSiT. Generally, in an aqueous solution, higher photocatalytic activity corresponds to a smaller average hydrodynamic diameter and a larger BET surface area. Accordingly, the smaller average hydrodynamic diameter and the larger BET surface area of the VNSiTs in solutions at pH 4–7 are believed to give rise to the high DMSO decomposition efficiency.

Table 4-4 Isoelectric points and average hydrodynamic diameters of synthesized photocatalysts.

Sample	Isoelectric point	Average hydrodynamic diameter (nm)*
NT	5.8	1490
NSiT	3.7	500
V(0.005)-NSiT	3.2	230
V(0.02)-NSiT	2.9	250

* Values were obtained at pH 7.

4.3.6. Photocatalytic decomposition of MB

Compared to NT and NSiT, the VNSiTs exhibited high adsorptivity for MB in the MB decomposition experiment conducted under dark conditions; the percentage of MB adsorbed to the VNSiTs in the dark was 47% compared to 1% for NT and 32% for NSiT (**Fig. 4-7**). However, the photodecomposition activity of the VNSiTs under visible light irradiation after adsorbing MB was extremely low. In this case, the strong adsorption of MB by the VNSiTs owing to electric attraction may have caused a reduction in the light absorption. These results indicate that NSiT, which did not contain any vanadium species, was most useful for the adsorption and photodecomposition of MB.

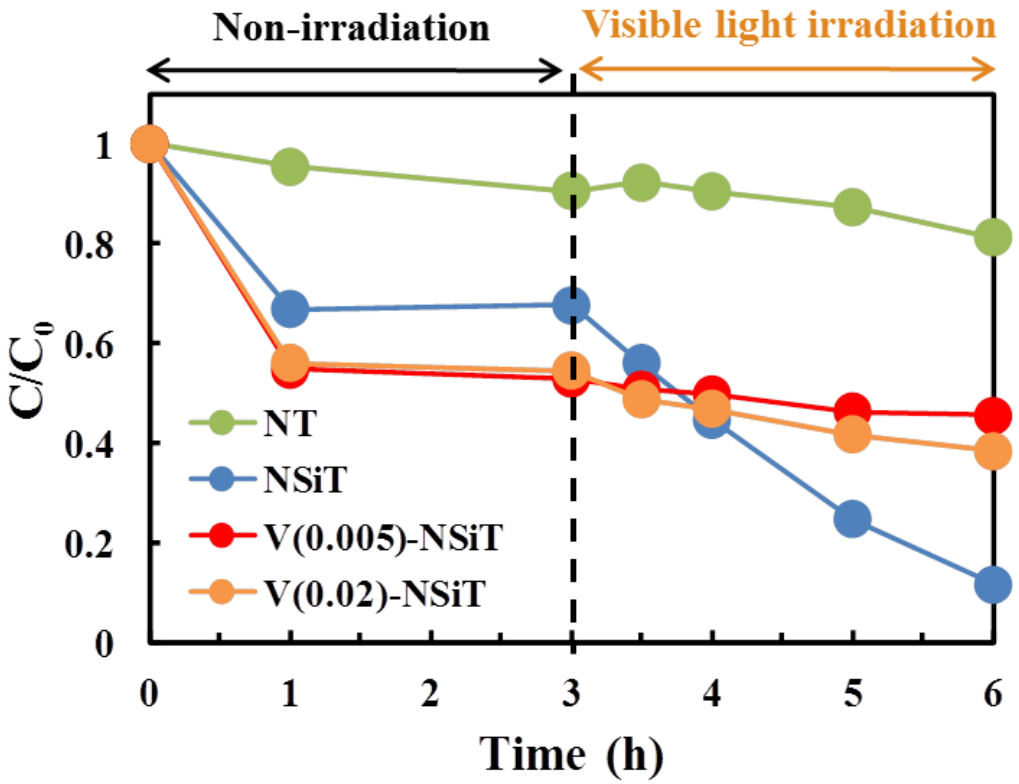

Fig. 4-7 Decomposition of MB by the photocatalysts in the dark conditions and visible light irradiation for 3 h. Initial concentration (C_0): 5 ppm.

4.4. Conclusions

VNSiT photocatalysts prepared by doping vanadium species on the surface of NSiT exhibited high decomposition capacities for DMSO in an aqueous solution under visible light irradiation. High activity is attributed to their higher dispersibility and smaller average hydrodynamic diameters in water compared to those of other photocatalysts. These features are believed to be due to the formation of negatively charged vanadic acid and hydration of the vanadium species. In addition, the vanadium species in the photocatalyst exhibited a promoter effect, enhancing contact with the substrate molecule because of its high dispersibility. Furthermore, a strong electrostatic effect of the VNSiTs in water was observed on the basis of the adsorption and photocatalytic decomposition of ionic species, such as the basic dye MB.

Further investigations will focus on characterization of VNSiT coated materials, such as glass plates, for application of the photocatalysts to water purification.

4.5. References

[1] H. Ozaki, K. Saito, S. Iwamoto, M. Inoue, Photocatalytic activities of nanocrystalline Si-modified titania xerogels prepared by the glycothermal method, J. Mater. Sci. 43 (2008) 2286 – 2292.

[2] H. Ozaki, S. Iwamoto, M. Inoue, Effects of amount of Si addition and annealing treatment on the photocatalytic activities of N- and Si-codoped titanias under visible-light irradiation, Ind. Eng. Chem. Res. 47 (2008) 2287 – 2293.

[3] H. Ozaki, S. Iwamoto, M. Inoue, Effect of the addition of a small amount of vanadium on the photocatalytic activities of N- and Si-codoped titanias under visible-light irradiation, Catal. Lett. 113 (2007) 95 – 98.

[4] M.N. Abellan, R. Dillert, J. Gimenez, D. Bahnemann, Evaluation of two types of TiO_2-based catalysts by photodegradation of DMSO in aqueous suspension, J. Photochem. Photobiol. A 202 (2009) 164 – 171.

[5] M. Mori, K. Tanaka, H. Taoda, M. Ikedo, H. Itabashi, Ion-exclusion/adsorption chromatography of dimethylsulfoxide and its derivatives for the evaluation to quality-test of TiO_2-photocatalyst in water, Talanta 70 (2006) 169 – 173.

[6] S. Iwamoto, S. Iwamoto, M. Inoue, H. Yoshida, T. Tanaka, K. Kagawa, XANES and XPS study of silica-modified titanias prepared by the glycothermal method, Chem. Mater. 17 (2005) 650 – 655.

[7] S. Higashimoto, W. Tanihata, Y. Nakagawa, M. Azuma, H. Ohue, Y. Sakata, Effective photocatalytic decomposition of VOC under visible-light irradiation on N-doped TiO_2 modified by vanadium species, Appl. Catal. A 340 (2008) 98 – 104.

[8] F. Amano, T. Yamaguchi, T. Tanaka, Photocatalytic oxidation of propylene with

molecular oxygen over highly dispersed titanium, vanadium, and chromium oxides on silica, J. Phys. Chem. B 110 (2006) 281 – 288.

[9] H. Irie, Y. Watanabe, K. Hashimoto, Nitrogen-concentration dependence on photocatalytic activity of $TiO_{2-x}N_x$ powders, J. Phys. Chem. B 107 (2003) 5483 – 5486.

[10] S.S. Thind, G. Wu, A. Chen, Synthesis of mesoporous nitrogen–tungsten codoped TiO_2 photocatalysts with high visible light activity, Appl. Catal. B Environ. 111 – 112 (2012) 38 – 45.

[11] T. Machold, W.Y. Suprun, H. Papp, Characterization of VO_x–TiO_2 catalysts and their activity in the partial oxidation of methyl ethyl ketone, J. Mol. Catal. A 280 (2008) 122 – 130.

[12] P. Oliveira, M.L. Rojas-Cervantes, A.M. Ramos, I.M. Fonseca, A.M. Botelho do Rego, J. Vital, Limonene oxidation over V_2O_5/TiO_2 catalysts, Catal. Today 118 (2006) 307 – 314.

[13] L.K. Boudali, A. Ghorbel, P. Grange, F. Figueras, Selective catalytic reduction of NO with ammonia over V_2O_5 supported sulfated titanium-pillared clay catalysts: influence of V_2O_5 content, Appl. Catal. B 59 (2005) 105 – 111.

[14] D.A. Bulushev, L. Kiwi-Minsker, V.I. Zaikovskii, A. Renken, Formation of active sites for selective toluene oxidation during catalyst synthesis via solid-state reaction of V_2O_5 with TiO_2, J. Catal. 193 (2000) 145 – 153.

[15] B. Liu, X. Wang, G. Cai, L. Wen, Y. Song, X. Zhao, Low temperature fabrication of V-doped TiO_2 nanoparticles, structure and photocatalytic studies, J. Hazard. Mater. 169 (2009) 1112 – 1118.

[16] A. Fujishima, X. Zhang, D.A. Tryk, TiO_2 photocatalysis and related surface

phenomena, Surf. Sci. Rep. 63 (2008) 515 – 582.

[17] Z. Wang, W. Cai, X. Hong, X. Zhao, F. Xu, C. Cai, Photocatalytic degradation of phenol in aqueous nitrogen-doped TiO_2 suspensions with various light sources, Appl. Catal. B 57 (2005) 223 – 231.

[18] G.A. Parks, The isoelectric points of solid oxides, solid hydroxides, and aqueous hydroxo complex systems, Chem. Rev. 65 (1965) 177 – 198.

[19] B.M. Weckhuysen, D.E. Keller, Chemistry, spectroscopy and the role of supported vanadium oxides in heterogeneous catalysis, Catal. Today 78 (2003) 25 – 46.

[20] S. Manoranjan, S. Komkrit, S. Sirikalaya, C. Tawatchai, B. Pratim, Characterization of doped TiO_2 nanoparticle dispersions, Chem. Eng. Sci. 66 (2011) 3482 – 3490.

[21] R. Bruck, H. Aeed, H. Shirin, Z. Matas, L. Zaidel, Y. Avni, Z. Halpern, The hydroxyl radical scavengers dimethyl sulfoxide and dimethyl urea protect rats against thioacetamide-induced fulminant hepatic failure, J. Hepatol. 31 (1999) 27 – 38.

Chapter 5

Photodecomposition of humic acid and natural organic matter in swamp water using a TiO_2-coated ceramic foam filter: Potential for the formation of disinfection byproducts

5.1. Introduction

In the chapters 2 – 4, we evaluated the water treatment ability of photocatalytic powder. However, when actually using the photocatalyst in water treatment, it should be used by immobilizing on a substrate.

In this study, we investigated the photocatalytic decomposition of humic acid (HA) in standard samples and natural organic matter (NOM) in swamp water by a TiO_2-coated ceramic foam filter (TCF, **Fig. 5-1**), in addition to the durability of the TCF reactor. We selected HA as the representative compound of NOM in water because it is a key component of humic substances derived from the decomposition of plants and animals [1]. Furthermore, HA has received much attention for water-treatment applications because it is a precursor of various disinfection byproducts (DBPs) [2-7].

Consequently, we explored and compared the capability and durability of TCF on the photodecomposition of HA as a standard sample and NOM in a swamp water sample collected from Gunma Prefecture (Japan). In addition, the potentials of DBP formation by the chlorination of HA and NOM in photocatalytically treated solutions were investigated.

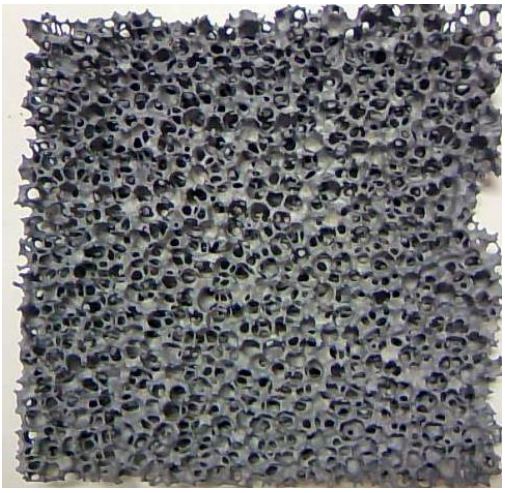

Fig. 5-1 Photograph of the TiO_2-coated ceramic filter (TCF). Size: 100 × 100 × 10 mm; crystalline form of TiO_2: anatase; amount of TiO_2 coated on Si-C ceramic foam filter: 0.01 % g^{-1}.

5.2. Experimental

5.2.1. Preparation of photocatalyst

TCF (**Fig. 5-1**; 100 × 100 × 10 mm, Photocatalytic Materials, Aichi, Japan) was prepared by supporting TiO_2 on a SiC-ceramic foam filter via a sol–gel method, as previously described [8]. Titanium tetraisopropoxide (28.4 g) and diethanolamine (10.6 g) were dissolved in ethanol (200 mL). After mixing vigorously at room temperature, water was added to the solution in a molar ratio of 1.0 with respect to the isopropoxide. An adequate amount of polyethylene glycol was then added to the solution. A SiC-foam plate used as the support substrate was subsequently dipped into the solution. The coated plate was dried at 100 °C for 1 h and then carefully heat-treated in air. The temperature was slowly increased (2 °C /min) to 650 °C and maintained at this level for 1 h. Three different TCF samples (surface thickness: *ca*. 0.3, 0.5, and 1.0 μm) were

prepared by varying the amount of TiO_2 coated on the ceramic filter (*ca.* 0.01%, 0.03% and 0.06% g^{-1}). The crystalline form of TiO_2 on the ceramic foam filter was anatase in all cases. A bare SiC-ceramic foam filter was used as the blank in the photocatalytic experiments.

5.2.2 Photodecomposition of HA and real samples

A 100 mg/L solution of HA sodium salt (Sigma–Aldrich) in deionized water was used as the stock solution to prepare dilute test standard samples (1–50 mg/L). The results of TOC analyses and UV_{254} absorption for the test standard samples are summarized in **Table 5-1**.

Real swamp water samples were collected from two different locations in Kiryu City, Gunma Prefecture (Japan), and filtered through a 0.45 μm membrane for the removal of suspended solids. TOC and UV_{254} for the swamp water samples were 2.7 mg/L and 0.11, for sample 1, and 1.6 mg/L and 0.063, for sample 2, respectively.

As shown in **Fig. 5-2**, the TCF reactor, along with the front and rear turbulence pieces, was placed in the acrylic-resin-based photocatalytic oxidation reactor (290 × 108 × 110 mm) over the reaction area (108 × 102 mm). Subsequently, 500 mL of the test standard solution was poured into the photocatalytic reactor. UV irradiation was carried out with a commercial black light blue lamp (National- FL20S-BLB lamp, spectral peak: around 350 nm). The light intensity incident on the surface of the TCF reactor was adjusted to 2.0 mW/cm^2 by using a hand-held illumination photometer UM-10 with a receptor head UM-360 (Konica Minolta, Japan). The standard solution in the reactor was circulated by a peristaltic pump (Cole-Parmer Master Flex 7518-10) at a flow rate of 500 mL/min. Reaction samples (10 mL) were periodically collected every 3 h.

The TOC and inorganic carbon (IC) dissolved in the reaction samples were measured by using a Shimadzu TOC-VCSH analyzer, while the UV_{254} absorbance was measured using a Hitachi U-3500 spectrometer.

Table 5-1 TOC and UV_{254} absorbance results for test standard solutions with different initial concentrations of HA.[a)]

Initial concentration of HA (mg/L)	TOC (mg/L)	UV_{254}
1.0	0.58	0.024
2.5	1.3	0.090
5.0	2.5	0.17
10	4.5	0.28
50	22.7	1.41

[a)] Values were obtained as the average of three measurements.

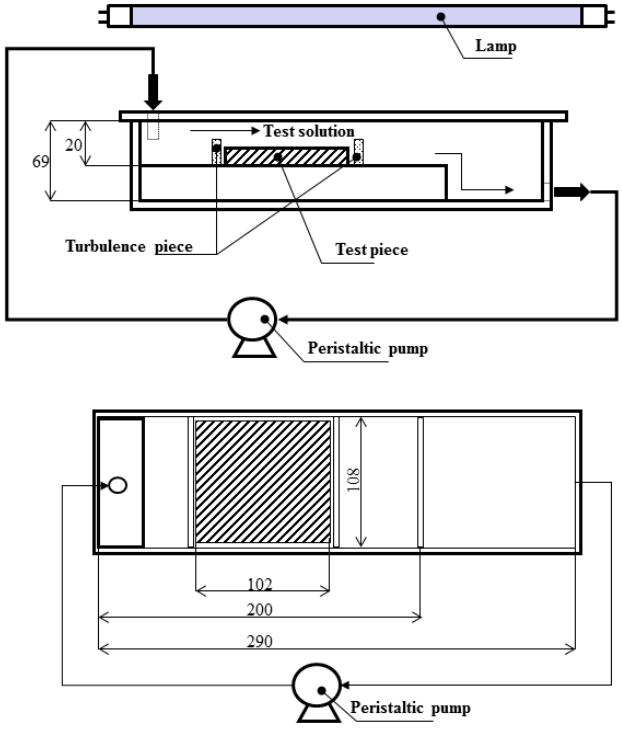

Fig. 5-2 Schematic illustration of the photocatalytic reactor used in the present study.

5.2.3. Chlorination of aqueous solutions and measurement of DBP formation potential

Chlorination of the reaction samples to generate THM and HAA products was carried out according to a test method proposed by Chang *et al.* [9] and standard methods for the examination of water in Japan [10]. Prior to chlorination, a sample solution (5 mL) was collected from the photocatalytic reactor and diluted ten-fold with deionized water. Subsequently, excess sodium hypochlorite was added to the sample solution, and the pH was adjusted to 6.8–7.2 with H_2SO_4. After incubation in a 100 mL incubator bottle at 20 °C for 24 h, the sample solution was quenched by the addition of 0.01–0.02 g sodium ascorbate. The THM products formed (e.g., chloroform, dichlorobromomethane, dibromochloromethane, and bromoform) were extracted with n-hexane (40 mL chlorinated aqueous solution, 5 mL *n*-hexane, 1 min extraction time). HAA products (e.g., chloroacetic acid, dichloroacetic acid, trichloroacetic acid, and bromoacetic acid) were extracted with methyl *tert*-butyl ether (MTBE). The extraction methodology was as follows. 40 mL of the chlorinated sample solution was adjusted to pH 0.5 with H_2SO_4 and then shaken with 20 g NaCl and 4 mL MTBE for 2 min. The organic phase containing the HAA products was collected and subsequently dehydrated with sulfuric acid anhydride. 0.2 mL diazomethane was added to the organic solution, which was finally allowed to settle for 60 min and warmed at 40 °C to decompose any remaining diazomethane.

THMs were determined by GC in a Shimadzu GC-2014 apparatus equipped with an electron capture detector (Shimadzu ECD-2014). The HAA products in the organic solution were determined by GC in a Shimadzu GCMS-QP2010 system.

5.3. Results and discussion

5.3.1. Optimization of the amount of TiO_2 on TCF reactors

The effect of the amount of TiO_2 coated on the ceramic foam filter on the extent of photodecomposition of HA is discussed in this chapter. Several TCF pieces were tested and compared in terms of TOC removal (%) from the HA standard solutions; the results are shown in **Fig. 5-3** as a function of reaction time. The initial concentration of HA in the solution was 10 mg/L, which corresponded to an initial TOC (TOC_0) of 4.5 mg/L. Under no-irradiation conditions (first 12 h), the TOC remained largely unchanged (0.7 – 3.4% decrease) in the case of all the TCF pieces studied, including the uncoated ceramic foam filter. The slight decrease in the TOC under dark conditions could be attributed to the weak physical adsorption of HA on the surface of the ceramic filters, since no IC was detected under these conditions.

Upon UV irradiation, the effective TOC removal was obtained using higher amount of TiO_2 incorporated-ceramic foam filter (**Fig. 5-3**). However, notable differences were observed when consecutive reactions were performed. Thus, a decrease in the TOC removal was observed after the second and third operation cycles for TCF samples containing 0.03% g^{-1} and 0.06% g^{-1} TiO_2. The TiO_2 loaded in these samples might partially come off by flowing water, thus leading to poor catalytic performance. This phenomenon was not observed, however, for the TCF sample containing 0.01% g^{-1} TiO_2. Consequently, this sample was selected for further experiments.

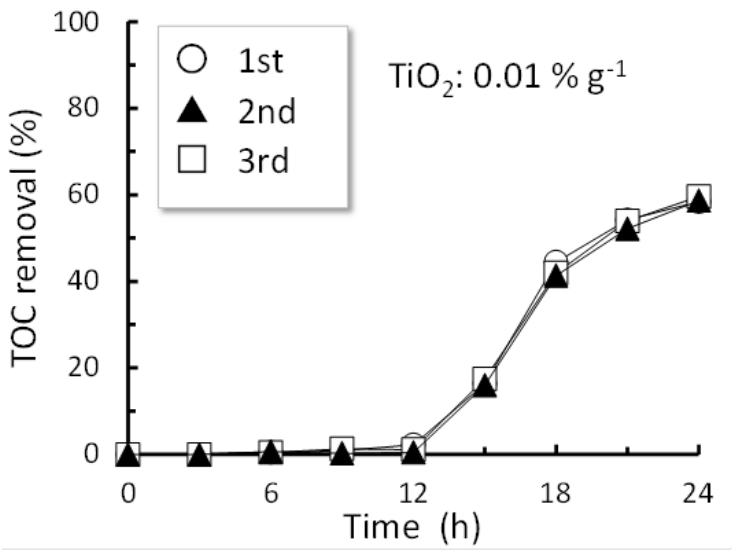

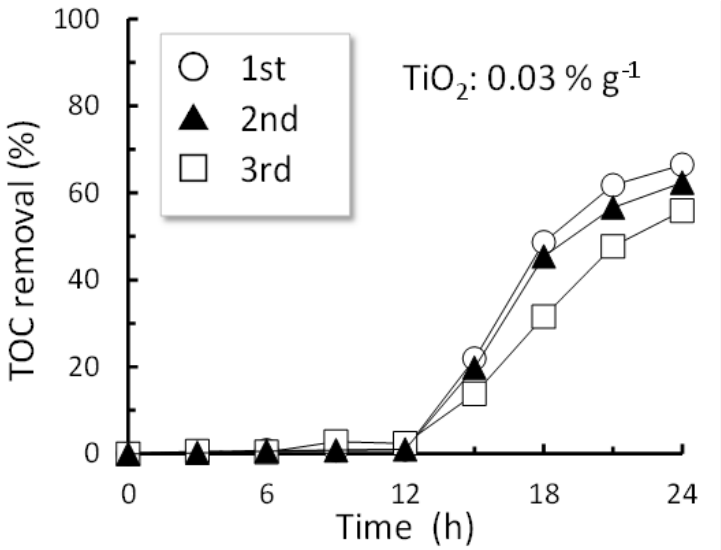

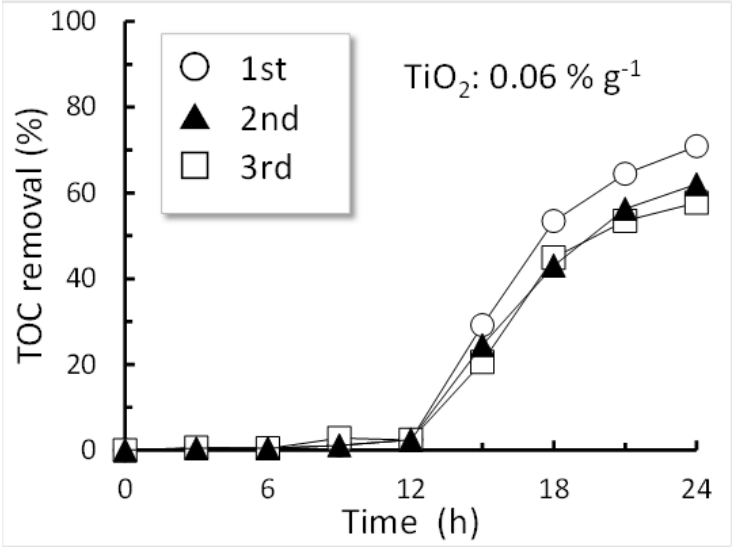

Fig. 5-3 TOC removal (%) as a function of reaction time for three consecutive reactions over TCF samples with varying amounts of TiO_2. Reaction conditions: initial concentration of HA: 10 mg/L. Total volume of the tested solution: 500 mL; flow rate: 500 mL/min. TOC removal is calculated according to the following equation: TOC removal percentage = $(C_0 / C)/C_0 \times 100$ (%), where C_0 is the initial TOC and C is the TOC at each sampling time

5.3.2. Effect of the initial concentration of HA in the solution

Fig. 5-4 shows the TOC removal percentage and UV_{254} as functions of irradiation time for initial HA concentrations ranging from 1 to 50 mg/L. As expected, HA was weakly adsorbed (0.5–4.0% TOC and 2.9–5.4% UV_{254}) under dark conditions. Under UV irradiation, the optimum TCF sample showed noticeable HA removal after 12 h of the reaction (44–61% TOC and 60–83% UV_{254}) over the entire range of initial concentrations studied. The TOC removal percentage and UV_{254} in the case of solutions containing very low and very high initial concentrations of HA (1 and 50 mg/L) were slightly lower as compared to those for the rest of the solutions (e.g., 2.5, 5.0, and 10 mg/L). In the case of the solution with the lowest concentration of HA, the poor decomposition efficiency observed could be explained in terms of the lower efficiency of contact with the TCF reactor surface. Since the solution with the highest concentration of HA was brown in color, it was expected to absorb UV light strongly, thereby weakening the intensity of UV radiation reaching the TCF surface.

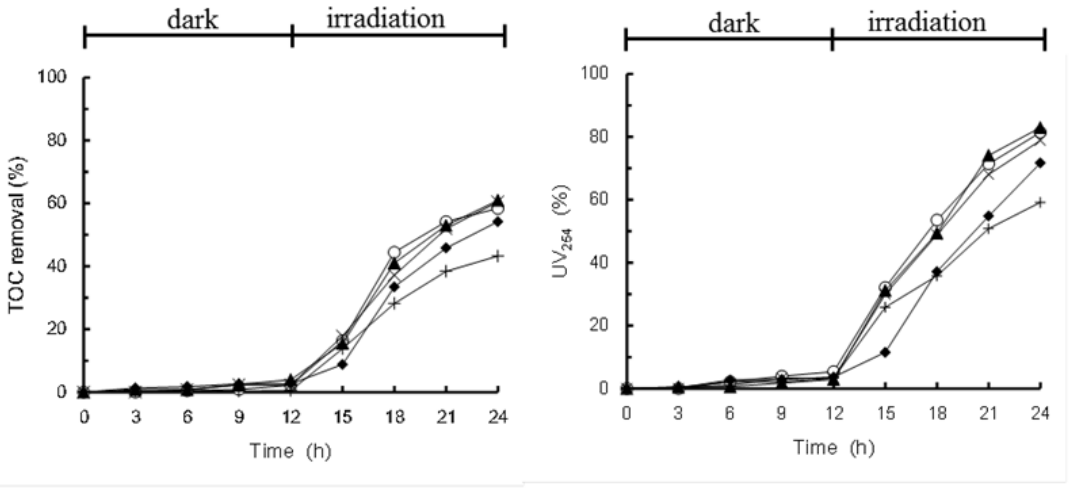

Fig. 5-4 Removal percentages of TOC (left) and UV_{254} (right) for different initial concentrations of HA as functions of reaction time. Initial concentration of HA: + = 1 mg/L, × = 2.5 mg/L, ▲ = 5 mg/L, ○ = 10mg/L, and ◆ = 50mg/L; total volume of test solution: 500 mL; flow rate: 500 mL/min. Removal percentage of analyte is calculated as TOC removal percentage = $(C_0 \times C)/C_0 \times 100$ (%), where C_0 is the initial TOC and C is the TOC at different sampling times, and UV_{254} removal percentage = $(A_0 - A)/A_0 \times 100$ (%), where A_0 is the initial absorbance at 254 nm and A is absorbance at 254 nm at different sampling times.

Fig. 5-5 and **Table 5-2** summarize the results of the linear fit to the logarithmic plot of C/C_0 (TOC) and A/A_0 (UV_{254}) vs. irradiation time for all the initial concentrations of HA. Decomposition rates (*k*) can be calculated from the slopes of these linear (**Table 5-2**). The *k* values for UV_{254} were 1.5 times higher than those for the TOC, indicating that the aromatic compounds and conjugations in HA was preferentially decomposed than the mineralization after 12 h of irradiation time. Similar results were also reported by Huang *et al.* [11] and Liu *et al.* [12], who observed that a fraction of the dissolved organic carbon could not be removed completely, thereby implying the presence of refractory compounds that existed before irradiation or were generated during the process.

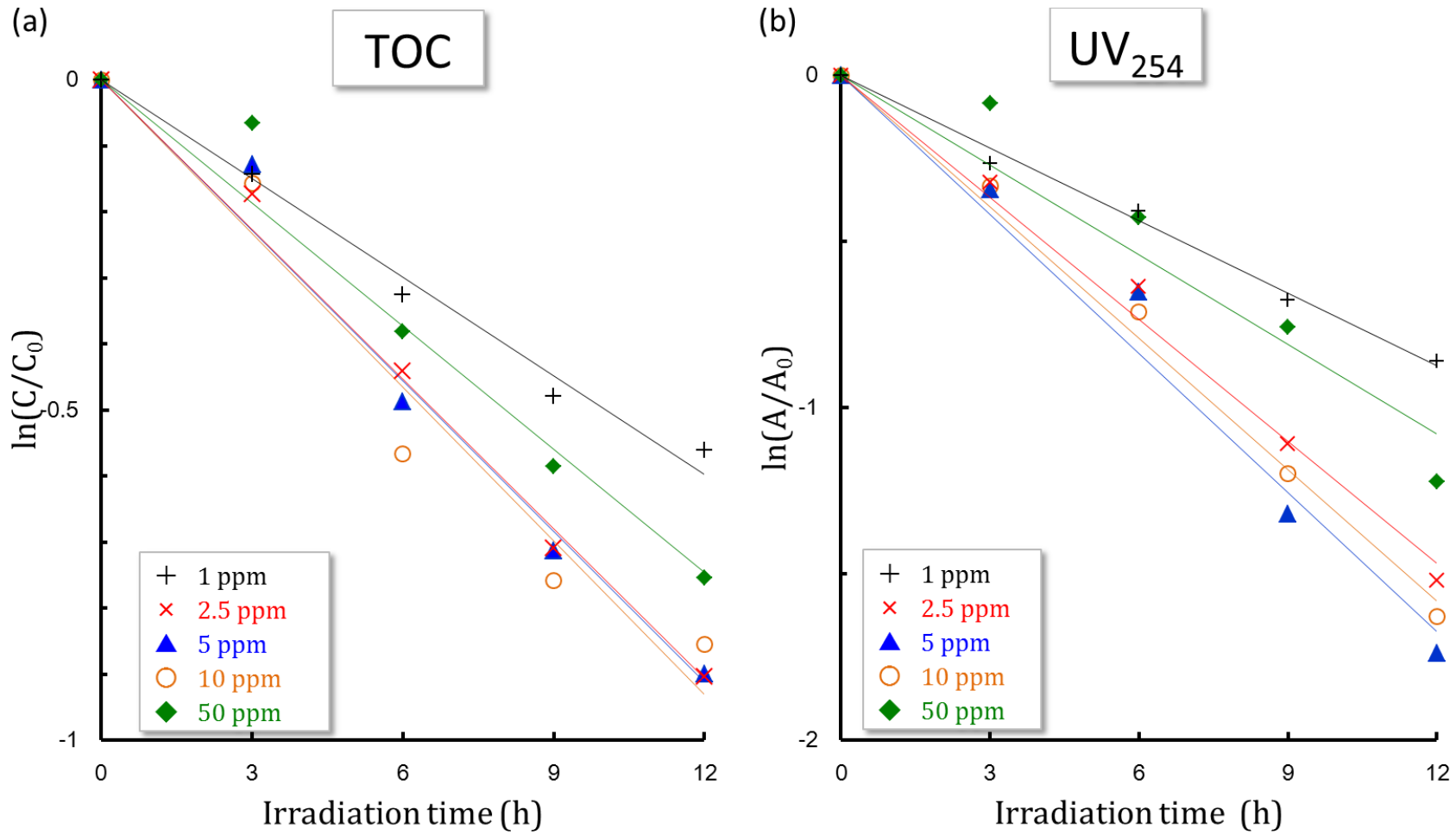

Fig. 5-5 (a) The $\ln(C/C_0)$ as a function of irradiation time (standard solution with HA); C_0: initial TOC; and C: TOC of solutions collected at different irradiation times, (b) The $\ln(A/A_0)$ as a function of irradiation time (standard solution with HA);A_0: initial UV_{254}; A: UV_{254} of solutions collected at different irradiation times.

Table 5-2 Linear fits and decomposition rates (k) from the logarithmic scale of C/C_0 of TOC and A/A_0 of UV_{254} as a function of irradiation time [a)].

TOC or UV_{254}	Initial concentration of HA (mg/L)	Approximation	Correlation coefficient (r^2)	k (h^{-1})
TOC	1	$y = -0.0504x$	0.985	0.0504
	2.5	$y = -0.0782x$	0.995	0.0782
	5	$y = -0.0806x$	0.982	0.0806
	10	$y = -0.0801x$	0.953	0.0801
	50	$y = -0.0652x$	0.971	0.0652
UV_{254}	1	$y = -0.0767x$	0.984	0.0767
	2.5	$y = -0.126x$	0.993	0.126
	5	$y = -0.143x$	0.979	0.143
	10	$y = -0.138x$	0.995	0.138
	50	$y = -0.0942x$	0.944	0.0942

[a)]The linear fit was obtained as follows: $\ln(C/C_0) = -k\mathrm{t} + \text{intercept}$, and $\ln(A/A_0) = -k\mathrm{t} + \text{intercept}$, respectively. C_0 is the initial TOC; C, the TOC in the solution at different sampling times; A_0, the initial absorbance at 254 nm; and A, the absorbance at 254 nm in the solution, at different sampling times (see **Fig. 5-5**)

The IC concentration increased with the irradiation time during the photodecomposition of HA, probably because of partial mineralization of some of the organic compounds [13]. The total carbon (TC, sum of TOC and IC) upon irradiation for 6–12 h, that is, after a reaction time for 18–24 h, was slightly lower than the initial TOC in the standard solutions (**Table 5-3**, and **Fig. 5-6**), and this could be attributed to the partial evaporative loss of IC as CO_2.

The TOC removal percentage and UV_{254} were observed to increase with the flow rate. Thus, the TOC removal percentage and UV_{254} for the solution containing 1 mg/L HA were 43% and 59%, respectively, at a flow rate of 500 mL/min, and these values increased to 57% and 78% when flow rate was doubled. However, operation at high flow rates was technically difficult because the pump could not function efficiently at high flow rates.

Table 5-3 TOC, IC, and TC in HA solutions irradiated for 12 h.

Initial concentration of HA (mg/L)	Initial TOC (mg/L)	TOC after irradiation for 12h (mg/L)	IC after irradiation for 12 h (mg/L)	TC (mg/L)
1	0.58	0.33	0.18	0.51
2.5	1.3	0.51	0.51	1.02
5	2.5	0.98	1.45	2.43
10	4.5	1.88	2.38	4.26
50	21	10.4	7.17	17.6

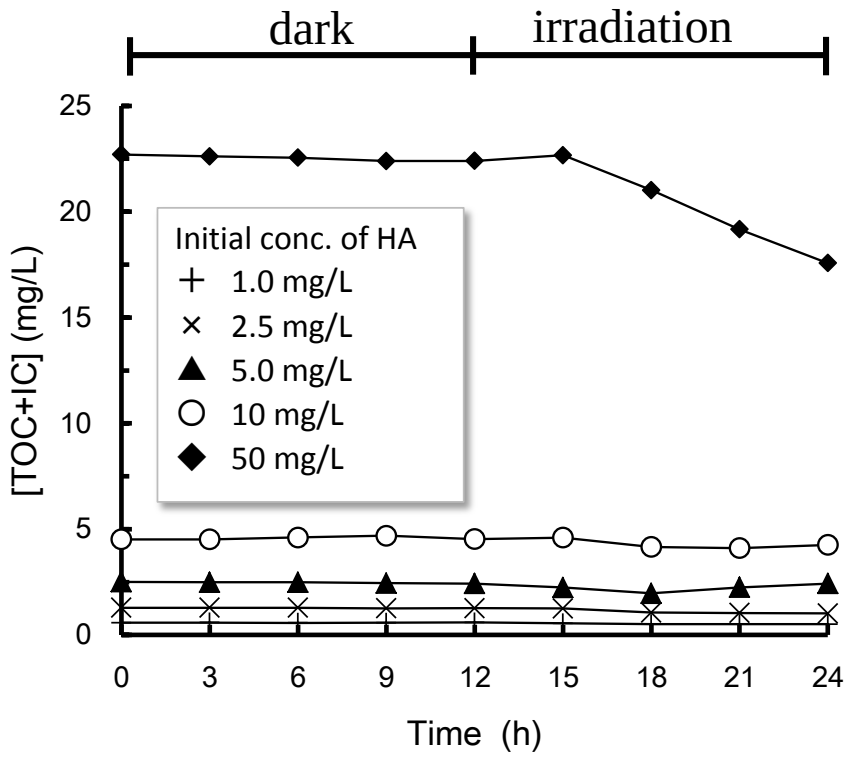

Fig. 5-6 Total carbon (TC) in the tested solutions as a function of reaction time. TC was calculated as the sum of TOC and IC.

5.3.3. Photodecomposition of HA and potential for formation of DBPs by chlorination

The potential for the formation of DBPs such as THMs and HAAs by chlorination of the photocatalytically treated solution is discussed in this section. **Fig. 5-7** presents the concentration of DBPs in the irradiated HA solutions as a function of TOC or UV_{254}. As expected, the concentration of DBPs after the chlorination process was dependent on the TOC and UV_{254} values in the HA solutions. Thus, the larger TOC and UV_{254} of the solutions was the higher DBP concentration. The DBP formation potentials (FPs) upon chlorination, which were obtained from the slopes of the linear fits [14] in **Fig. 5-7**, were 20–22 for THMs and 54–56 for HAAs to TOC; and 239–288 for THMs and 610–863 for HAAs to UV_{254}. Remarkably, the HAAFP were found to be approximately twice of the THMFP. Although the reasons for this difference are unclear, the DBP formation potential has been found to be strongly dependent on the chlorination method employed, as previously described by Ueda *et al.* [15].

The concentrations of THMs followed the trend chloroform > bromodichloromethane > dibromochloromethane > bromoform as THMs, and those of HAAs followed the trend dichloroacetic acid > trichloroacetic acid > chloroacetic acid. These trends remained unaltered before and after the photocatalytic decomposition of HA solutions by the TCF materials (**Fig. 5-8**). The THMs including bromide made only a small contribution to the THMFP since the original HA samples had low concentrations of bromide (<10 μg/L in 10 mg/L HA used in this study) [16].

The decrease ratio in DBPFP, $P/P_0 \times 100$ (%), can be obtained from the THMFP and HAAFP values before (P_0) and after (P) irradiation for 12 h. The ratios for the THMs followed the order chloroform (49%) > bromodichloromethane (33%) > dibromochloromethane (29%), while bromoform was not detected. In contrast, those for

the HAAs followed the order dichloroacetic acid (43%) > trichloroacetic acid (34%) > chloroacetic acid (21%). These results led us to conclude that HA was a precursor of DBPs and that photodecomposition could inhibit the DBP formation potential.

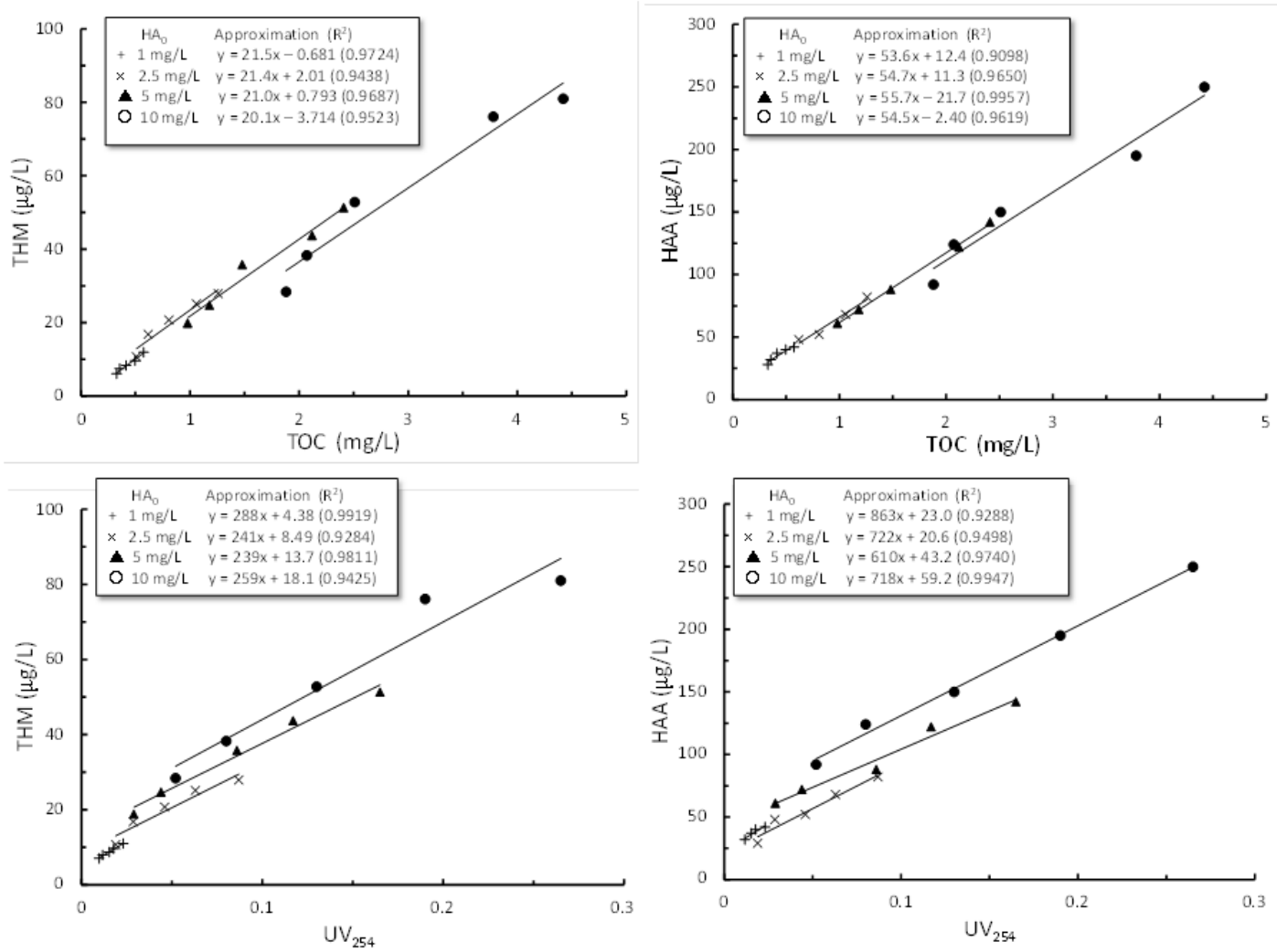

Fig. 5-7 Concentration of DBPs as a function of TOC and UV_{254} decrease for HA solutions irradiated for 12 h. Upper plot: total THM and HAA concentrations vs. TOC; lower plot: total THM and HAA concentrations vs. UV_{254}.

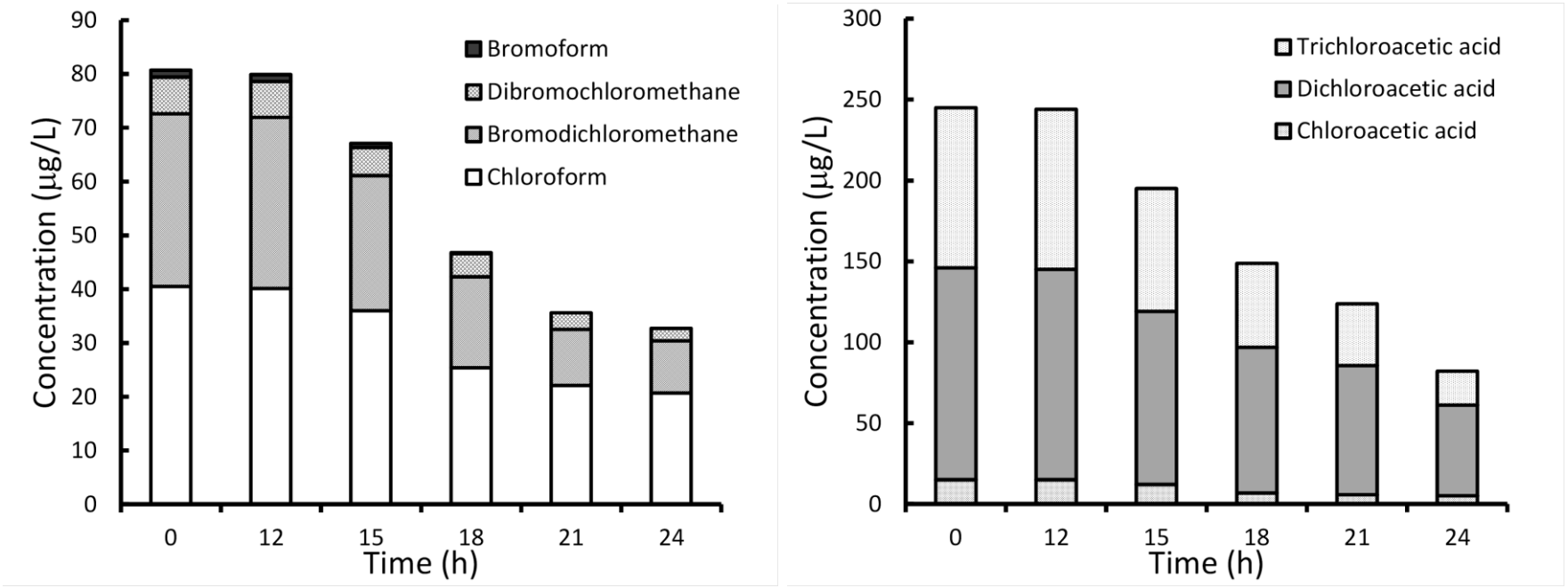

Fig. 5-8 Concentration of THMs (left) and HAAs (right) obtained by chlorination of the photocatalytic treated water samples at different irradiation times. Tested solution: 10 mg/L HA solution.

5.3.4. Durability

The durability of the TCF for HA decomposition (initial concentration = 10 mg/L) and the DBPFP were investigated to evaluate the stability and long-term applicability of the reactor. A commercial TiO_2-coated glass sheet (100 × 100 × 5 mm) was used for the sake of comparison. Both the TCF and the TiO_2-glass sheet were repeatedly used for 30 consecutive experiments; the rate of TOC removal in the HA solution is shown in **Fig. 5-9**. The TOC removal percentage in the case of the TCF reactor remained almost unchanged (59→57%) after 30 consecutive experiments, whereas the stability of the TiO_2-coated glass sheet decreased notably after 20 consecutive runs (63→2%), although the same coating method was adopted for both reactors. This large decrease in the photocatalytic activity was probably due to the release of TiO_2 from the glass sheet. Such TiO_2 release was not observed in the case of the TCF.

The relative standard deviation (RSD) of TOC removal in the TCF reactor for 12 h of irradiation was 2.6% (n = 30). This high durability of TiO_2 coated on the solid was related to the surface appearance, although the surface appearance could not be understood completely. Additionally, the formation of THMs and HAAs was found to be dependent on the TOC in HA, and the concentrations of THMs and HAAs were ca 34 mg/L (RSD = 4%, n = 30) and ca 99 mg/L (RSD = 4%, n = 30), respectively. Thus, TCF has certain features suitable for the photodecomposition of water contaminants, including high repeatability and ease of handling (e.g., washing, recovery, and recycling).

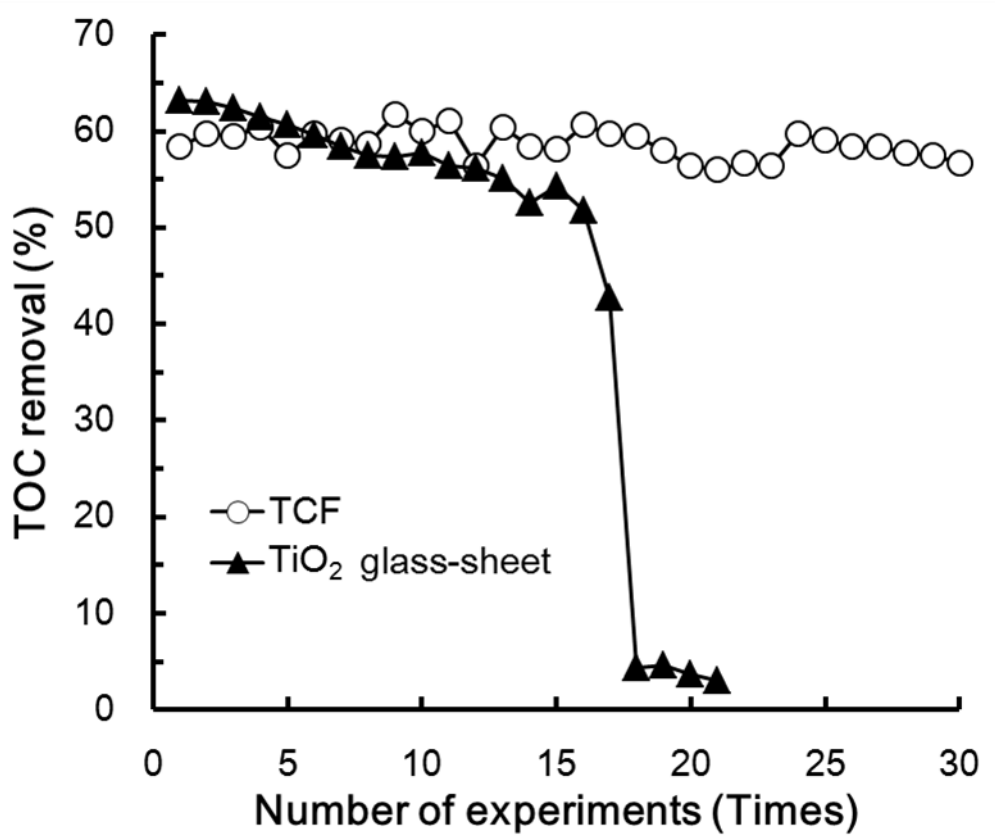

Fig. 5-9 TOC removal percentage by TCF and TiO_2-glass sheet to different cycles. Irradiation time: 12 h. Removal percentage was calculated from equation obtained in **Fig. 5-3**.

5.3.5. Photodecomposition of NOMs in swamp water samples and formation of DBPs by chlorination

As shown in **Fig. 5-10**, the TOC removal percentage and UV_{254} after 12 h under dark conditions were 0.7% and 4.1% for sample 1, and 0.4% and 1.4% for sample 2, respectively. These values increased to 58% and 74% for sample 1 and to 41% and 61% for sample 2, respectively, after irradiation for 12 h. As in the case of the HA standard solutions, *k* values could be obtained from the slope of the linear fit in the logarithmic representation (**Fig. 5-11**, and **Table 5-4**). Sample 1 showed TOC and UV_{254}-based *k* values of 0.073 and 0.11 h^{-1}, respectively, while these values decreased to 0.047 and 0.083 h^{-1} for sample 2 (**Fig. 5-11**). The *k* values for the swamp samples were found to be in the same range as those for the HA-dissolved standard solutions.

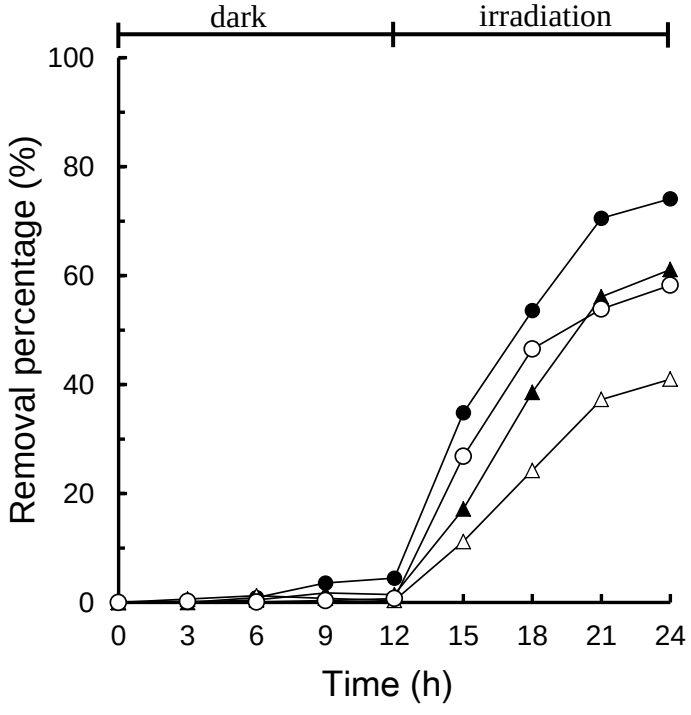

Fig. 5-10 TOC removal percentage and UV_{254} in swamp water samples as functions of reaction time. Experimental conditions are the same as those in **Fig. 5-4**. ○ = sample 1 to TOC; △ = sample 2 to TOC; ● = sample 1 to UV_{254}; and ▲ = sample 2 to UV_{254}.

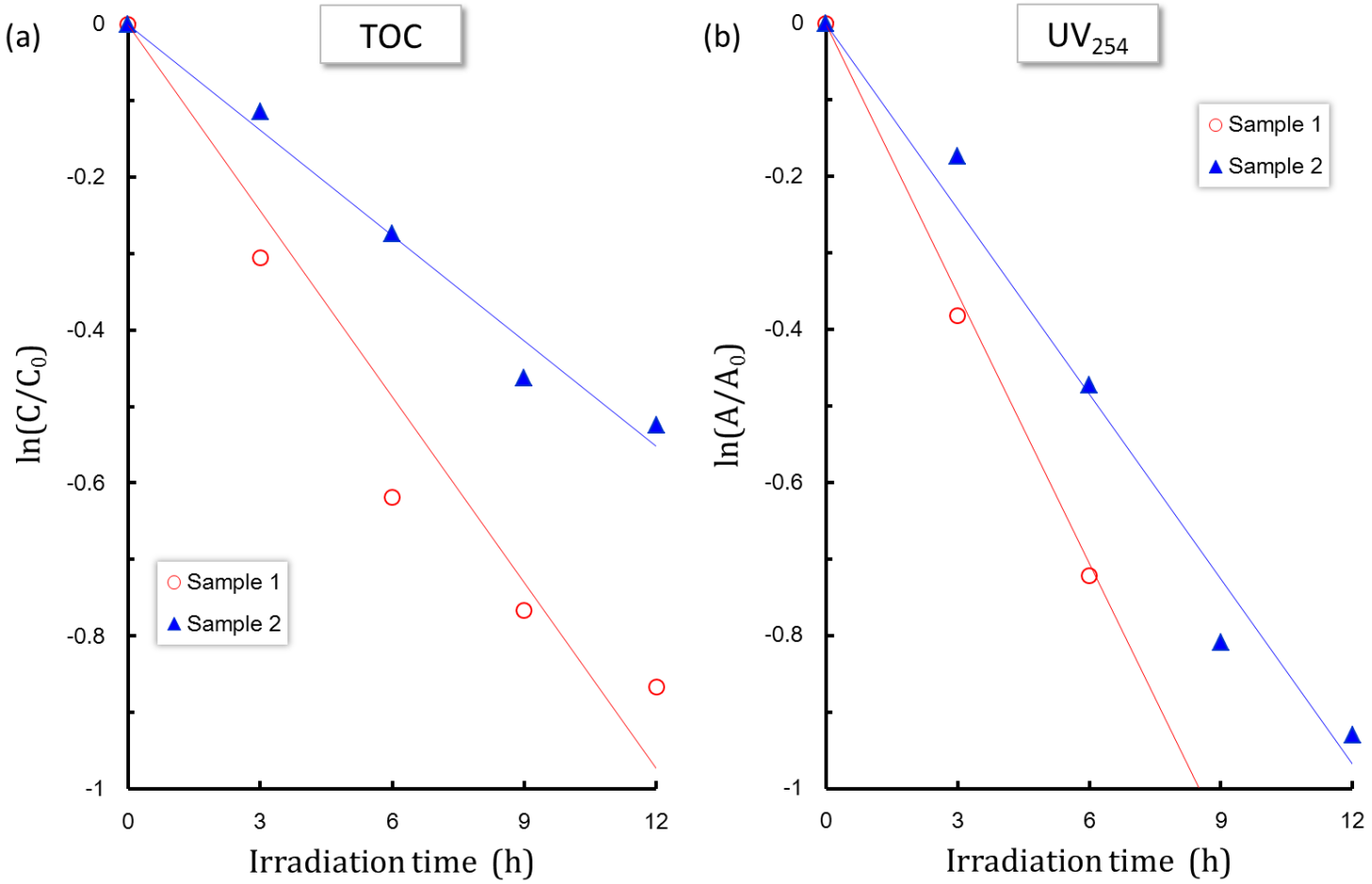

Fig. 5-11 (a) $\ln(C/C_0)$ as a function of irradiation time (swamp water), C_0: initial TOC; C: TOC in solution collected at different irradiation times, and (b) $\ln(A/A_0)$ as a function of irradiation time (swamp water);A_0: initial UV_{254}; A: UV_{254} in solution collected at different irradiation times.

Table 5-4 Linear fits and decomposition rates (k) from the logarithmic scale of C/C_0 of TOC and A/A_0 of UV_{254} as a function of irradiation time for swamp water samples.[a)]

TOC or UV_{254}	Sample	Approximation	Correlation coefficient (r^2)	k (h^{-1})
TOC	1	$y = -0.0820x$	0.929	0.0820
	2	$y = -0.0465x$	0.982	0.0465
UV_{254}	1	$y = -0.123x$	0.970	0.123
	2	$y = -0.0823x$	0.980	0.0823

[a)]The linear fit was obtained as follows: $\ln(C/C_0) = -k\mathrm{t} + \mathrm{intercept}$ and $\ln(A/A_0) = -k\mathrm{t} + \mathrm{intercept}$ (see **Fig. 5-11**)

IC increased with the irradiation time during the decomposition of NOM in the swamp water samples. As in the case of the HA solutions, TC in the swamp water after irradiation was lower than the initial TOC (**Table 5-5**).

The THMFP and HAAFP values after the chlorination of photocatalytically treated swamp water samples were also measured; the results are summarized in **Table 5-6**. Several DBP products were detected in the swamp water samples, including chloroform, bromodichloromethane, and dibromochloromethane as THMs and dichloroacetic acid and trichloroacetic acid as HAAs. Remarkably, the bromoform and chloroacetic acid concentrations were below the limit of quantitative determination for the GC system employed. It is worth mentioning that this composition is typical of chlorinated lake or river waters. The THMFP and HAAFP largely decreased after the photodecomposition process was applied to the swamp water samples. The concentrations of THMs and HAAs after irradiation were below the water quality standards imposed by the Ministry of Health, Labour and Welfare of Japan [17].

The THMFP/HAAFP ratio remained, irrespective of the type of sample analyzed and the occurrence of photocatalytic reactions. These ratios were similar to those published by the Kiryu City Water Bureau (*ca.* 0.3). This composition was typical of chlorinated swamp waters, and it did not change due to photodecomposition.

Table 5-5 TOC, IC, and TC in swamp water samples irradiated for 12 h.

Sample	Initial TOC (mg/L)	TOC after irradiation for 12h (mg/L)	IC after irradiation for 12 h (mg/L)	TC (mg/L) [a)]
1	2.67	1.55	0.92	2.47
2	1.61	0.66	0.81	1.49

a) TC was estimated as the sum of TOC and IC in each tested solution.

Table 5-6 Formation potentials of THMs and HAAs upon chlorination of swamp water samples after UV irradiation for 12 h.

Sample	DBPs	DBPs before irradiation (μg/L): P_0	DBPs after irradiation for 12 h (μg/L): P	Inhibition ratio in DBP formation potential (%) [a)]
1	Chloroform	23.4	10.3	56
	Bromodichloromethane	18.8	6.2	67
	Dibromochloromethane	7.6	2.5	67
	Total THM	49.8	19.0	62
	Dichloroacetic acid	143	31.5	78
	Trichloroacetic acid	58.4	22.3	62
	Total HAA	201	53.8	73
2	Chloroform	16.3	7.3	55
	Bromodichloromethane	10.5	3.8	64
	Dibromochloromethane	n.d.[b)]	n.d.	-
	Total THM	26.8	11.1	59
	Dichloroacetic acid	38.1	16.4	57
	Trichloroacetic acid	45.7	21.8	52
	Total HAA	83.8	38.2	54

[a)] The decrease in the DBP formation potential was obtained as $\text{Inhibition ratio } (\%) = (P_0 - P)/P_0 \times 100$.

[b)] n.d. = not detected

5.4. Conclusions

Photodecomposition of NOM in swamp water by a TCF reactor was found to follow the same trend as the photodegradation of a HA, which is a precursor of THMs and HAAs. The DBP formation potential after chlorination of the photocatalytically treated water samples was strongly dependent on TOC and UV_{254}. Accordingly, the TOC and UV_{254} values in aqueous solution were concluded to be key indicators of the photodecomposition efficiency.

Additionally, the TCF reactor used in this study was shown to be an efficient photocatalytic material for the decomposition of pollutants such as HA and NOM. The TCF reactor showed high stability in consecutive operation cycles.

Further investigations will be devoted to confirm the feasibility of using the TCF for NOM removal in a treatment plant (e.g., Water Work Bureau) and to determine the DBPFP under these conditions.

5.5. References

[1] S. Nagao, H. Kodama, T. Aramaki, N. Fujitake, M. Uchida, Y. Shibata, Carbon isotope composition of dissolved humic and fulvic acids in the Tokachi river system, Radiat. Prot. Dosim. 146 (2011) 322 – 325.

[2] Y. Cho, W. Choi, Visible light-induced reactions of humic acids on TiO_2, J. Photochem. Photobio. A Chem. 148 (2002) 129 – 135.

[3] J. Fu, M. Ji, Y. Zhao, L. Wang, Kinetics of aqueous photocatalytic oxidation of fulvic acids in a photocatalysis-ultrafiltration reactor (PUR), Sep. Purif. Technol. 50 (2006) 107 – 113.

[4] S. Liu, M. Lim, R. Fabris, C. Chow, M. Drikas, R. Amal, TiO_2 photocatalysis of natural organic matter in surface water: impact on trihalomethane and haloacetic acid formation potential, Environ. Sci. Technol. 42 (2008) 6218 – 6223.

[5] H. Selcuk, M. Bekbolet, Photocatalytic and photoelectrocatalytic humic acid removal and selectivity of TiO_2 coated photoanode, Chemosphere 73 (2008) 854 – 858.

[6] B. Tryba, P. Brozek, M. Piszcz, W. Morawski, New photocatalyst for decomposition of humic acids in photocatalysis and photo-Fenton processes, Pol. J. Chem. Technol. 13 (2011) 8 – 14.

[7] X.W. Zhang, A.J. Du, P.F. Lee, D.D. Sun, J.O. Leckie, TiO_2 nanowire membrane for concurrent filtration and photocatalytic oxidation of humic acid in water, J. Membrane Sci. 313 (2008) 44 – 51.

[8] K. Kato, A. Tsuzuki, Y. Torii, H. Taoda, T. Kato, Y. Butsugan, Morphology of thin anatase coating prepared from alkoxide solutions containing organic polymer,

affecting the photocatalytic decomposition of aqueous acetic acid, J. Material. Sci. 30 (1995) 837 – 841.

[9] C.-Y. Chang, Y.-H. Hsieh, S.-S. Hsu, P.-Y. Hu, K.-H. Wang, The formation of disinfection by-products in water treated with chlorine dioxide, J. Hazard. Mater. 79 (2000) 89 – 102.

[10] Japan Water Works Association, 2001. Standard Methods for the Examination of Water. Tokyo (In Japanese).

[11] X. Huang, M. Leal, Q. Li, Degradation of natural organic matter by TiO_2 photocatalytic oxidation and its effect on fouling of low-pressure membrane, Water Res. 42 (2008) 1142 – 1150.

[12] S. Liu, M. Lim, R. Fabris, C. Chow, K. Chiang, M. Drikas, R. Amal, Removal of humic acid using TiO_2 photocatalytic process – fractionation and molecular weight characterization studies, Chemosphere 72 (2008) 263 – 271.

[13] T.S. Natarajan, M. Thomas, K. Natarajan, H.C. Bajaj, R.J. Tayade, Study on UV-LED/TiO_2 process for degradation of Rhodamine B dye, Chem. Eng. J. 169 (2011) 126 – 134.

[14] S. Ohara, T. Uehara, K. Kimura, T. Yoshida, S. Fujiwara, H. Mizuguchi, Y. Fuse, E. Yamada, Behavior of humic substances and algal dissolved organic matter as precursors of trihalomethane in Lake Biwa, Bunseki Kagaku (Japanese) 58 (2009) 231 – 240.

[15] Y. Ueda, Y. Itoh, T. Tsuzuki, Concentration of some chlorination disinfection by-products in tap water and relationship among them in Hokkaido, Hokkaido Institute of Public Health Report (Japanese) 45 (1995) 76 – 79.

[16] L. Liang, P.C. Singer, Factors influencing the formation and relative distribution of

haloacetic acids and trihalomethanes in drinking water. Environmental Science and Technology 37 (2003) 2920 – 2928.

[17] The Ministry of Health, (2008) Labour and Welfare of Japan HP, Water Quality, Chap. 4: http://www.mhlw.go.jp/english/policy/health/water_supply/4.html. (accessed 04.04.12).

Chapter 6

Development of an online flow evaluation system for water treatment ability of a photocatalytic material using ionic dye and ibuprofen as indicator

6.1. Introduction

In chapter 5, we demonstrated usefulness of photocatalyst-coated material for decompositions of HA and NOM. In the evaluation of quality test for water treatment of photocatalysts and the materials, the photocatalytic reactions and the analyses of target compound concentrations were separately performed. Thus, the samplings at a constant period during the photocatalytic reactions were needed, and the solution volumes in the photocatalytic reactor were consequently consumed. The contamination of the analyte sample was often caused, and it was conducted to the analytical errors.

In this study, we equipped the flow analytical system with an online-combined photocatalytic reactor and spectrophotometer. This system can continuously monitor the absorbance of analytes in the tested solution circulating in the reactor without consumption of the solution owing to sampling. The availability of this system is demonstrated through decomposition of methylene blue (MB) and indigo carmine (InC) using ST01-, vanadium-modified TiO_2 (VT)-, silica-doped TiO_2 (SiT)- and vanadium-modified silica-doped TiO_2 (VSiT)-mounted glass plate. Finally, the decomposition of ibuprofen (IBP) by ST01-plate and VT-plate under UV-irradiation was assessed as the application of the flow analytical system with photocatalytic plate.

6.2. Experimental

6.2.1. Preparation of photocatalytic platews

A typical anatase-type TiO_2 photocatalyst ST01 was purchased from Ishihara Sangyo Kaisha Ltd. (Osaka, Japan). About VT, SiT and VSiT photocatalytic powders, as described in chapter 3.

Each photocatalytic plate was prepared by evaporation to dryness with suspension of photocatalytic powder. A borosilicate glass plate (35 mm × 50 mm × 2 mm; Sekiya Rika Co., Ltd, Tokyo, Japan) was dipped in a 2.5 mol/L NaOH solution for 2 h at 80 °C and was ultrasonically washed with water for 10 min. Next, the plate was dipped in 1.0 mol/L HCl for 30 min at 80 °C, ultrasonically washed with water for 10 min, and dried at 40–50 °C for 3 h in a drying oven (DX402, Yamato Scientific Co., Ltd, Tokyo, Japan). The glass plate was dipped in a 2 g/L suspension of each photoatalytic powder (100 mL) until the solvent is eliminated at 80 °C and dried at 60 °C for 1 h in a drying oven.

6.2.2. Evaluation of photocatalytic plates in aqueous solutions

The water treatment abilities of the photocatalytic plates were evaluated by measuring the changes in the absorbance of MB and InC as a function of irradiation time. Specifications of photocatalysts coated onto glass plate in this experiment are summarized in **Table 6-1**. ST01- and VT-plates were used for the MB and InC decomposition reactions in aqueous solutions under UV irradiation.

Table 6-1 Specifications of photocatalysts coated onto glass plates.

	Average of crystal size (nm)	Amount on glass plate (mg)	Charge at pH 6
ST01	7.0	13.5	Neutral
VT	8.0	18.7	Negative
SiT	11	28.9	Negative
VSiT	12	19.1	Negative

6.2.3. Online flow evaluation system

Flow analytical system consisting of the homemade reactor (80 mm × 115 mm × 20 mm) and a spectrophotometer (S-3250, Soma Optics Co. Ltd., Japan) (**Fig. 6-1**). During the tests, 5 mg/L MB or 20 mg/L InC test solutions (50 mL) were poured into the homemade reactor and circulated at a flow rate of 1.6 mL/min using a peristaltic pump. The flow rate had chosen the speed that could obtain reproducible circulation of the tested solution using the pump.

The adsorptions of the analyte dyes on the plates were initially determined for 5 h in the dark, and the photodecompositions were continuously monitored as a function of UV irradiation for 19 h using a LogStick LS200-V voltage data logger (Osaka Micro Computer. Inc., Osaka, Japan). The monitoring wavelengths were 660 and 610 nm for MB and InC, respectively. The proposed system could continuously determine the changes in absorbance of organic compounds without sampling, that is, without consumption of the solution.

Decomposition of 10 mg/L IBP (50 mL) using photocatalytic plate was performed by the same system, except for the detector. In this experimental, Hitachi U-3500 UV–Vis spectrophotometer was used, for the purpose of monitoring of intermediates during photocatalytic reaction (**Fig. 6-2**). In these experiments, two UV lamps (λ_{Max}: 352 nm)

(National-FL20S-BLB lamp, Matsushita Electric Industrial Co., Ltd., Osaka, Japan) were arranged in parallel to generate a light irradiance of 2.0 mW/cm^2.

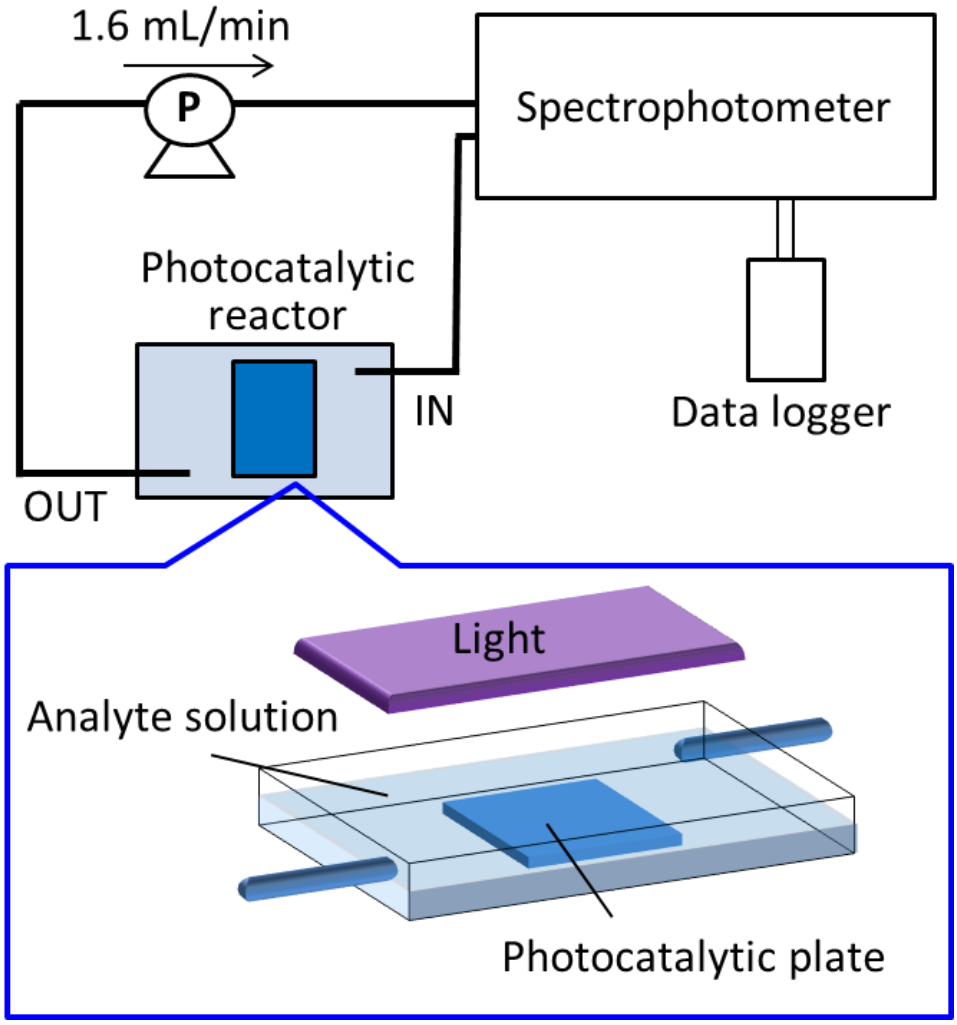

Fig. 6-1 Schematic illustration of flow analytical system for photocatalytic evaluation.

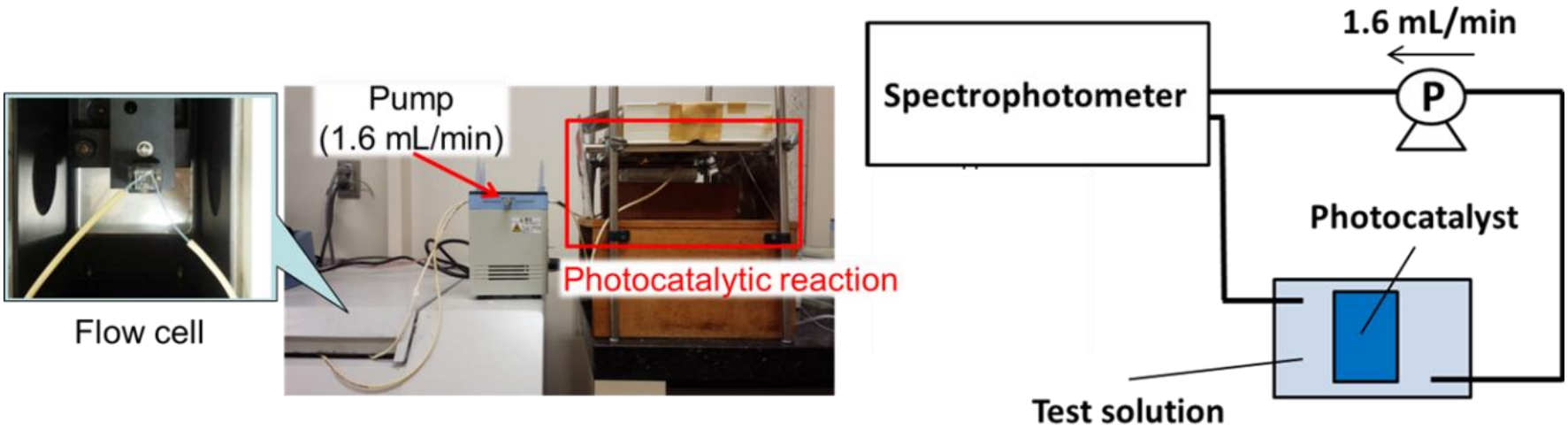

Fig. 6-2 The flow analytical system of photocatalytic material in IBP decomposition.

6.3. Results and discussion

6.3.1. Characterization of photocatalytic material

Firstly, we characterized the plates coating different types of photocatalysts. **Fig. 6-3** shows the photographs of the four different plates. The photocatalysts could be successfully coated onto glass plates without regarding to types of photocatalysts, though the coatings were performed without modification of any spacers between glass plate and photocatalyst. Also, through this experiment, the detachment of the photocatalytic from the plate was not observed during photocatalytic reaction.

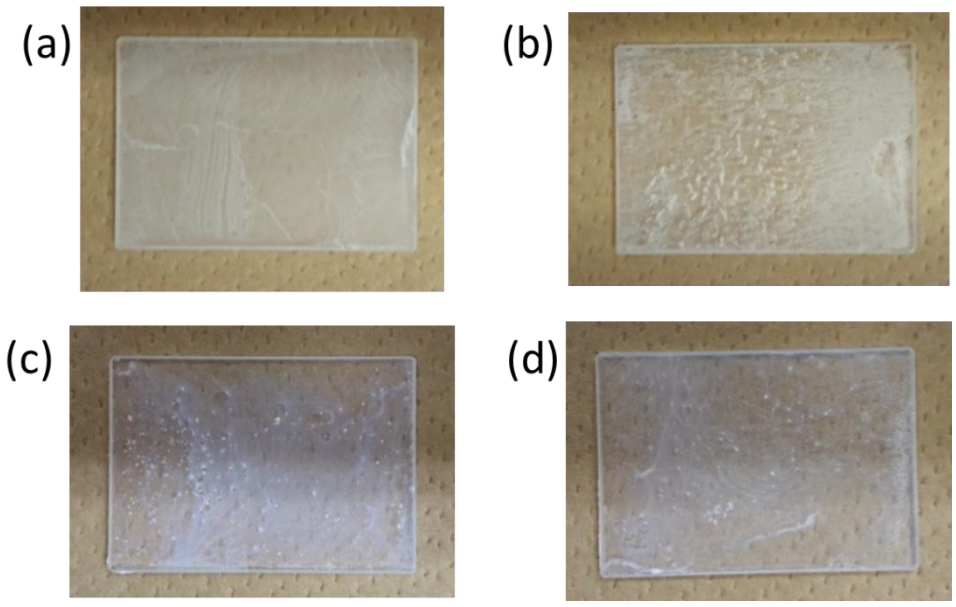

Fig. 6-3 Prepared photocatalytic-plate. (a) ST01-, (b) VT-, (c) SiT-, and (d) VSiT-plate.

6.3.2. Decomposition of organic dye using photocatalytic plate

The adsorptivity in the dark and the photocatalytic activity under light-irradiation of the prepared photocatalytic plates was evaluated by the evaluation system equipped in this study. **Fig. 6-4** shows changes in concentration ratios of MB using each photocatalytic plate in dark condition for 5 h and in the UV irradiation. The concentration ratios were calculated from the concentration of MB as functions of reaction time (C) and the initial concentration (C_0). As the result, the VT-, SiT- and VSiT-plate exhibited high adsorptivity for MB in the dark condition, against ST01-plate did not provide the adsorptivity. Especially, by using VSiT-plate, the concentration ratio of MB was decreased to 54.7% for 5 hours. SiT- and VT adsorbed 15.8% and 14.6% of MB, respectively. The tendency that photocatalytic-plate co-doping vanadium and silica showed the highest adsorptivity for MB was parallel to the results by the particle obtained in Chap. 3.

Under UV irradiation condition, MB was almost decomposed by VSiT-plate for 18 h including the adsorption in the dark condition. In Chap. 3, the particle of vanadium-silica-TiO_2 that provided high adsorptivity for MB was lower photodecomposition ability. When the particle was coated onto glass plate, the decomposition ability was maintained. Although the chemical mechanism was not cleared at this stage, the design of photocatalytic material and/or the reaction condition would be affected for the photocatalytic decompositions.

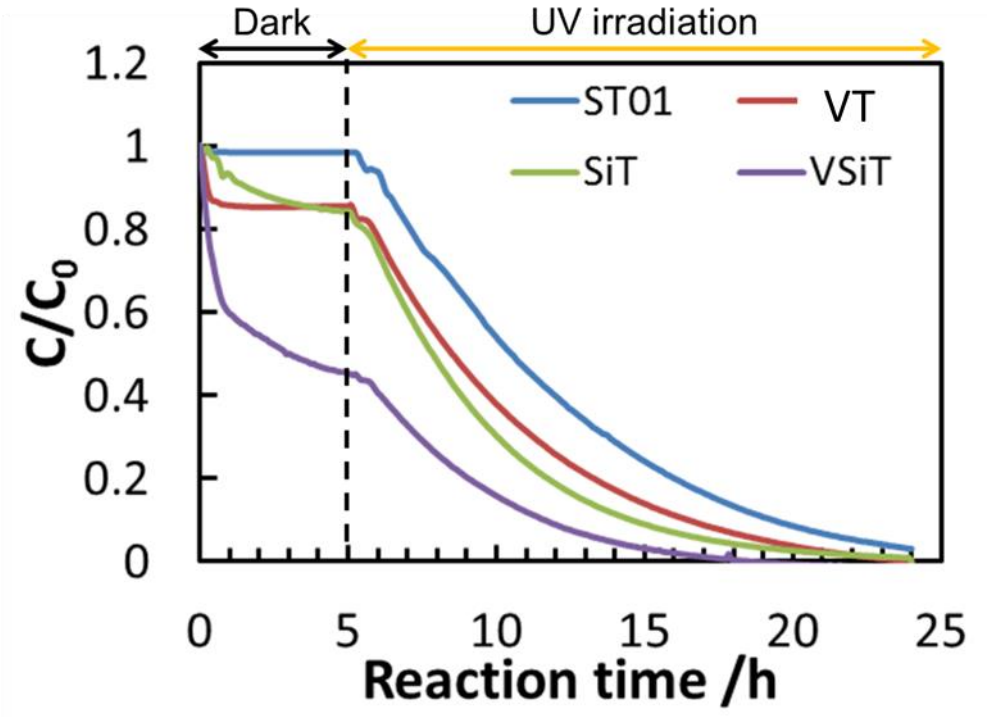

Fig. 6-4 Decompositions of MB by each photocatalytic plate.

Next, the photocatalytic activities of the plates were evaluated by the photodecomposition constant (*k*) using the changes in concentration ratio of MB shown in **Fig. 6-4**. **Table 6-2** summarizes the constants (*k*) estimated from an apparent pseudo-first-order model using Eq. (1), as well as adsorptivity of MB.

$$\ln(C/C_0) = kt + a \qquad (1)$$

where *t* is UV-irradiation time, and a is the intercept. The *k* values were calculated from linearly fitting plots of ln (C/C_0) as a function of *t*.

In addition, each half-life time ($t_{1/2}$) was calculated using Eq. (2), and each obtained value was summarized in **Table 6-2**.

$t_{1/2} = 0.693/k$ (2)

The k values for MB under UV irradiation for 19 h were in the order of VSIT- (0.271 h^{-1}) > SiT- (0.233 h^{-1}) > VT- (0.187 h^{-1}) > ST01- (0.148 h^{-1}) each photocatalytic plate. This would be because the stronger acidity of as-prepared photocatalytic powders would lead strong electrostatic attraction for positively charged MB in the solution than ST01, which is anatase TiO_2.

In addition, the rapid adsorption of MB to VSiT-plate was found to be in 1 h after beginning the reaction in the dark condition. This means that the adsorption rate of VSiT-plate for MB is relatively fast, though the kinetic adsorption constant.

Table 6-2 Adsorptivity, kinetic constant and half-life time of each plate for MB.

	Adsorptibity (%)	k (h^{-1})	$t_{1/2}$ (h)
ST01-plate	1.58	0.148	4.68
SiT-plate	15.8	0.233	2.98
VT-plate	14.6	0.187	3.71
VSiT-plate	54.7	0.271	2.56

Conditions are described in section 6.2.3.

In the other hand, the adsorption and photodecomposition of InC, which is an acidic dye, obtained different results with that of MB as mentioned above. As shown in **Fig. 6-5**, the adsorption for InC was not almost observed without regarding to types of photocatalysts, and the complete photodecomposition could be achieved in 19 hours of UV-irradiation.

Also, as summarized in **Table 6-3**, the *k* values for InC under UV irradiation for 19 h were order of ST01-plate (0.270 h^{-1}) > SiT-plate (0.205 h^{-1}) > VSiT-plate (0.171 h^{-1}) > VT-plate (0.134 h^{-1}). The highest decomposition efficiency of ST01-plate for InC is related to be weaker electrostatic repulsion than other plates, because isoelectric point (pI) of ST01 is *ca.* 6. In contrast, the fact that obtained the relative high decomposition efficiencies of SiT-, VT- and VSiT-plates for InC implied that InC was easily decomposed by photocatalytic activity.

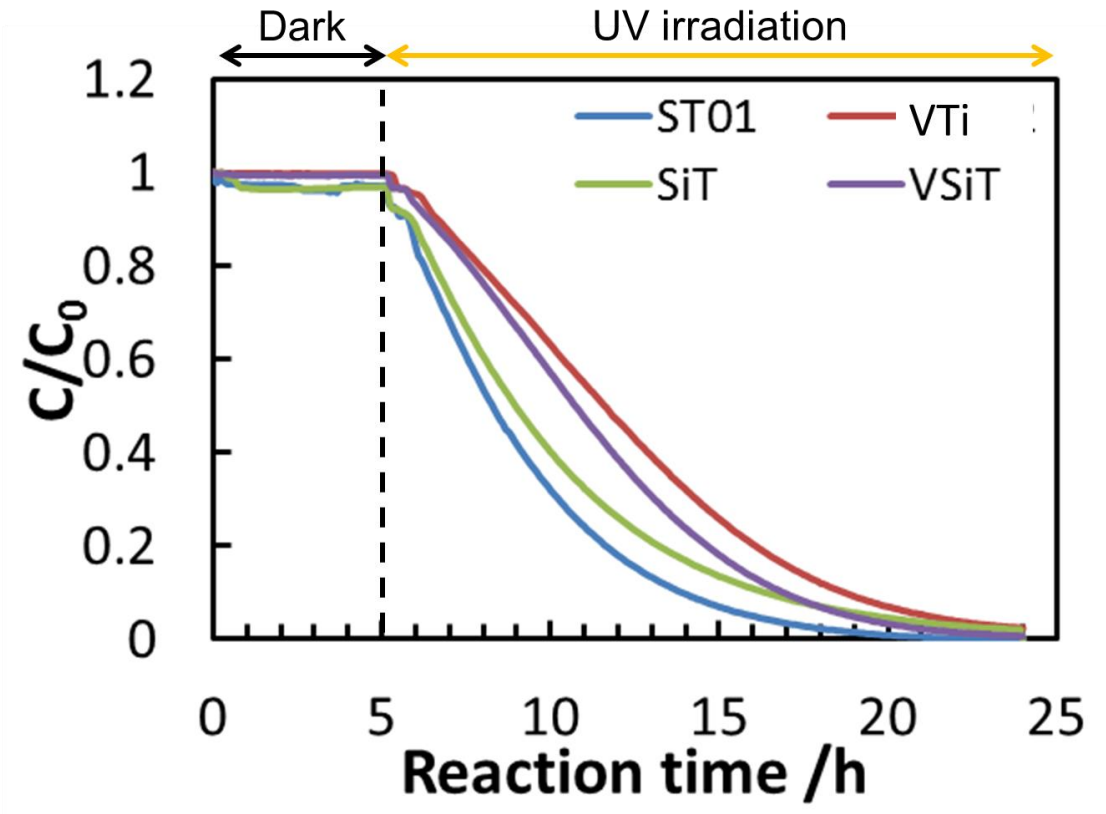

Fig. 6-5 Decompositions of InC by each photocatalytic plate.

Table 6-3 Adsorptivity, kinetic constant and half-life time of each plate for InC.

	Adsorptibity (%)	k (h^{-1})	$t_{1/2}$ (h)
ST01	2.90	0.270	2.57
SiT	3.14	0.205	3.37
VT	0.348	0.134	5.17
VSiT	0.709	0.171	4.05

Conditions are described in section 6.2.3.

6.3.3. Decomposition of IBP using ST01- and VT-plate

Ibuprofen (IBP) belongs to a new class of widely used water pollutants, which is biological active and has strong impact on the environment even in small concentrations [1,2]. This is unchanged form and incompletely metabolized medicines [3]. Although by-products of IBP, which are present in the aquatic environment in low concentration are still harmful for human and animals. The removal of IBP in wastewater has mainly been carried out by advanced oxidation processes [4-6]. The occurrence of these side products has been often reported in the literature. However, only high concentrated, polluted solutions were investigated so far [3,7].

Fig. 6-6 show the decomposition of IBP by ST01- and VT-plate using online flow system equipped UV–Vis spectrophotometer (**Fig. 6-2**). This system is able to monitoring both decomposition of IBP and production of its intermediates. **Fig. 6-7** shows the plots of absorption at 222 nm (analyte) and 262 nm (intermediates) during the decomposition of IBP. There was no adsorption of IBP onto the photocatalytic plates under dark conditions. In contrast, under UV light irradiation, production of the intermediates with the decrease of IBP was confirmed. When comparing ST01- and VT-plates, the VT-plate exhibited lower decomposition rate than the ST01-plate but it exhibited large production volume of intermediates. The results indicate that VT-plate might be not suitable for photodecomposition of IBP, because it has the potential of producing the hazardous substance.

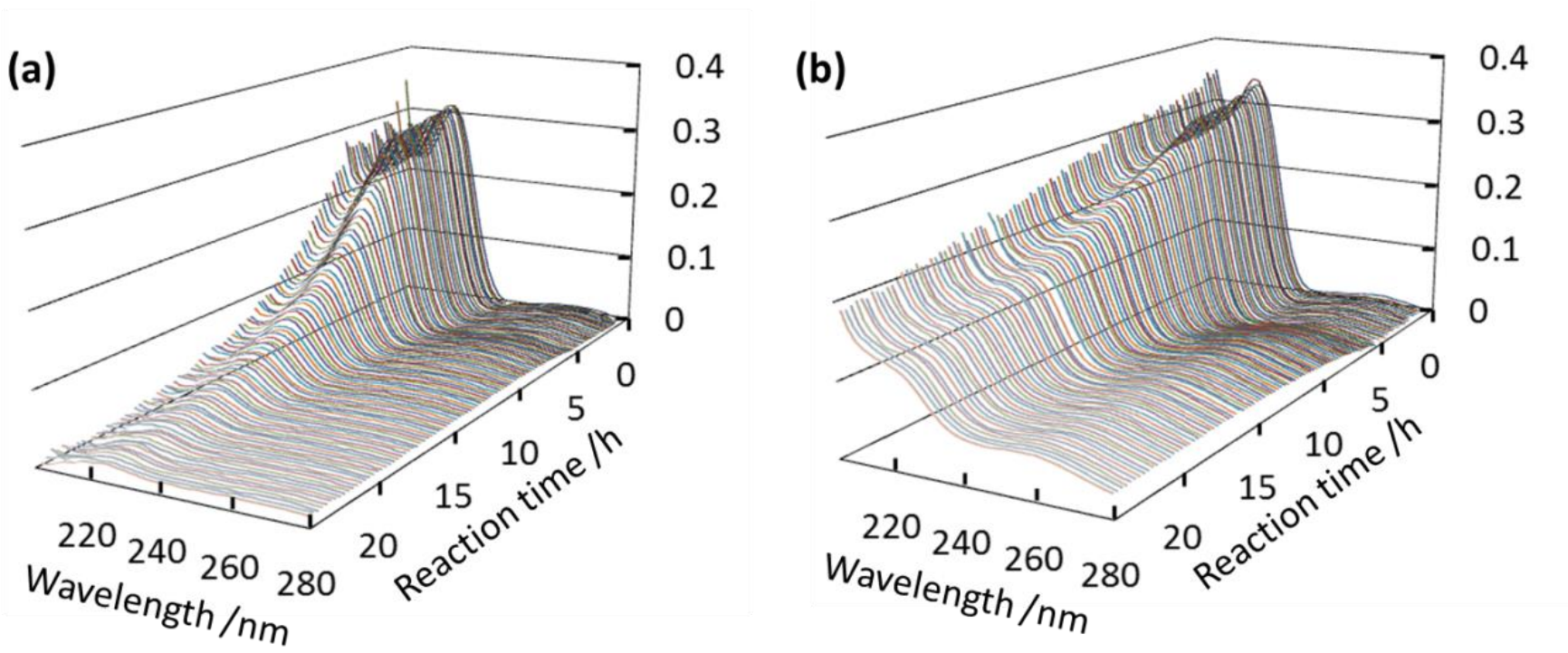

Fig. 6-6 Spectral changes in photodecomposition of IBP by (a) ST01- and (b) VT-plates as a function of reaction time.

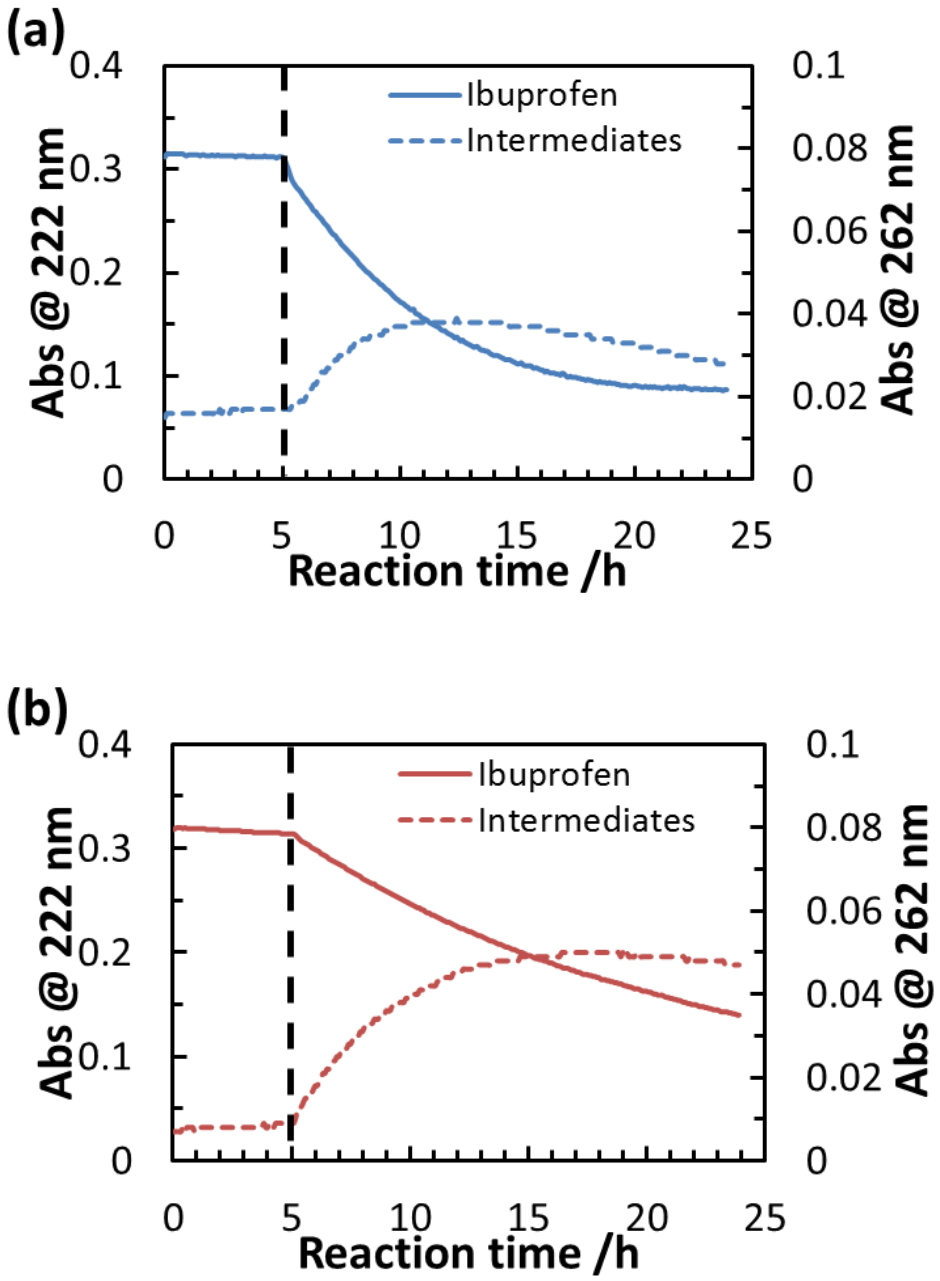

Fig. 6-7 Changes in absorptions at 222 nm and 262 nm during the decomposition of IBP by (a) ST01- and (b) VT-plate.

6.4. Conclusions

In this study, the photocatalyst-glass plate was evaluated for applications in water treatment by the continuous monitoring in the flow evaluation system, which does not consume the test solution volume. The VT particles facilitated stable photodecompositions regardless of the reactant charge under UV light irradiations. The plates decomposed a cationic dye (MB) and anionic dye (InC), without regarding to their charges. Also the electrostatic adsorptions of SiT-, VT-, VSiT-plates to cationic species could be conducted to the efficient photodecomposition. Furthermore, we could successfully analyze simultaneous monitoring of decrease in IBP and formation of its by-product, by using flow evaluation system.

6.5. References

[1] N. Miranda-García, S. Suárez, B. Sánchez, J.M. Coronado, S. Malato, M.I. Maldonado, Photocatalytic degradation of emerging contaminants in municipal wastewater treatment plant effluents using immobilized TiO_2 in a solar pilot plant, Appl. Catal. B 103 (2011) 294 – 301.

[2] N. Klamerth, L. Rizzo, S. Malato, M.I. Maldonado, A. Agüera, A.R. Fernández-Alba, Degradation of fifteen emerging contaminants at μg L^{-1} initial concentrations by mild solar photo-Fenton in MWTP effluents, Water Res. 44 (2010) 545 – 554.

[3] J. Choina, H. Kosslick, Ch. Fischer, G.-U. Flechsig, L. Frunza, A. Schulz, Photocatalytic decomposition of pharmaceutical ibuprofen pollutions in water over titania catalyst, Appl. Catal. B Environ. 129 (2013) 589 – 598.

[4] S-P. Sun, X. Zeng, A.T. Lemley, Nano-magnetite catalyzed heterogeneous Fenton-like degradation of emerging contaminants carbamazepine and ibuprofen in aqueous suspensions and montmorillonite clay slurries at neutral pH, J. Molecul. Catal. A Chem. 371 (2013) 94 – 103.

[5] Y. Lee, U.V. Gunten, Oxidative transformation of micropollutants during municipal wastewater treatment: Comparison of kinetic aspects of selective (chlorine, chlorine dioxide, ferrate^{VI}, and ozone) and non-selective oxidants (hydroxyl radical), Water Res. 44 (2010) 555 – 566.

[6] M.M. Huber, S. Canonica, G-Y, Park, Oxidation of pharmaceuticals during ozonation and advanced oxidation processes, Environ. Sci. Technol. 37(5) (2003) 1016 – 1024.

[7] F. Méndez-Arriaga, R.A. Torres-Palma, C. Pétrier, S. Esplugas, J. Gimenez, C. Pulgarin, Ultrasonic treatment of water contaminated with ibuprofen, Water Res. 42 (2008) 4243 – 4248.

Chapter 7

Immobilization method of photocatalyst onto glass plate using electrostatic interaction and its evaluation of photocatalytic activity for water treatment using flow evaluation method

7.1. Introduction

In Chap. 6, we described the adsorption and photocatalytic abilities for the photocatalyst coated on the glass plate, which were prepared by dipping method without any spacers to connect between photocatalyst and glass plate. However, coating of photocatalyst onto solid phase without chemical interactions such as electrostatic or coordination bindings was not stable for the successive uses of water treatment for long time, *e.g.*, 1 week to 1 month.

Existing photocatalyst immobilization techniques include sol–gel processing [1,2], sputtering [3,4], and a hydrothermal method [5]. Sol–gel processing, the most convenient method, requires a calcination step to deposit the photocatalyst on the substrate, which limits the types of viable substrates to those displaying high thermal resistance, such as silica glass beads. Although sputtering has effectively produced homogeneous photocatalyst films, it requires the use of a dedicated device to sputter the photocatalyst. The hydrothermal method is conveniently applicable to a variety of substrates, but particle–substrate interactions promote aggregation and impede uniform particle deposition. Photocatalytic coating materials that respond to visible light are

needed to expand the scope of applications. In general, the synthesis of visible light-responsive TiO_2 photocatalysts involves ionized nitrogen and argon doping of photocatalyst-coated membranes using sophisticated ion-imprinting equipment [6,7]. Recently, a one-step procedure based on sol–gel processing [8], sputtering [9], and sonochemistry [10] was shown to form visible light-responsive photocatalytic films. However, this approach also involves a calcination step, which restricts its implementation to heat-resistant materials.

To address the limitations of current photocatalyst immobilization techniques, a simple and stable calcination-free photocatalytic coating method was developed using electrostatic interactions with the cationic silane coupling reagent trimethoxysilylpropyldiethylenetriamine (dien) as a spacer. In this approach, highly dispersible silica-doped TiO_2 (SiT) photocatalyst particles [11] were uniformly deposited onto dien-functionalized glass plates (dien-plate) in an aqueous solution. The zeta potential of SiT exhibited an isoelectric point (pIs) at 4.0, while that of anatase TiO_2 is 6.1. The increased negative zeta potential of SiT induces electrostatic dispersion in neutral and basic solutions [12]. The negatively charged SiT is expected to adsorb positively charged chemicals via electrostatic attractions, rather than hydrophobic interactions which are involved in activated carbon/TiO_2 composites [13,14]. This coating method was also applied to a visible light-responsive vanadium-modified nitrogen/silica co-doped TiO_2 (VNSiT) photocatalyst, which exhibits a higher negative charge than SiT.

Following the characterization of the prepared photocatalytic plates, their water treatment abilities were evaluated by monitoring the photodecomposition of methylene blue (MB) and indigo carmine (InC), basic and acidic dyes, respectively. These dyes

have often been utilized to assess synthetic photocatalysts [15-18] under UV and visible light irradiation. The evaluation method employed the flow evaluation system that was introduced in Chap. 6.

7.2. Experimental

7.2.1. Preparation and characterization of photocatalysts

A typical anatase-type TiO_2 photocatalyst ST01 was purchased from Ishihara Sangyo Kaisha Ltd. (Osaka, Japan). SiT and VNSiT was obtained and characterized by same procedures as described in Chap. 3 and 4, respectively.

7.2.2. Preparation of photocatalyst-coated plates with and without silane coupling reagent

A borosilicate glass plate (35 mm × 50 mm × 2 mm; Sekiya Rika Co., Ltd, Tokyo, Japan) was dipped in a 2.5 mol/L NaOH solution for 2 h at 80 °C and was ultrasonically washed with water for 10 min. Next, the plate was dipped in 1.0 mol/L HCl for 30 min at 80 °C, ultrasonically washed with water for 10 min, and dried at 40–50 °C for 3 h in a drying oven (DX402, Yamato Scientific Co., Ltd, Tokyo, Japan). The glass plate was dipped in a mixture of dien (10 mL), acetic acid (5 mL), and distilled-deionized water (50 mL) for 24 h at 60 °C and dried at 110 °C for 1 h in a drying oven. The dien-coated glass plate (dien-plate) was dipped in a 0.2 wt% photocatalyst suspension in water for 3 h at room temperature and was subsequently dried at 100 °C for 1 h. The procedures used to form the photocatalyst–dien-coated glass plates are illustrated in **Scheme 7-1**.

To assess the durability of the photocatalyst–dien-plates, photocatalyst-coated glass plates without the silane coupling reagent (photocatalyst–plate) were also prepared by dipping the base/acid etched glass plates into a 0.2 wt% photocatalyst powder suspension for 3 h at room temperature.

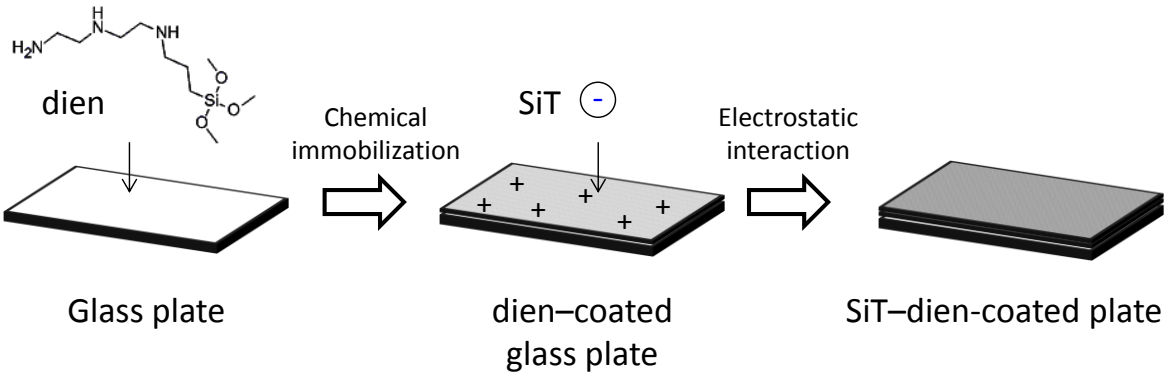

Scheme 7-1 Preparation of photocatalyst–dien-coated glass plates.

7.2.3. Characterization of photocatalyst-dien-plates

The amounts of the photocatalyst deposited on the glass plates were estimated using a JASCO V-650 spectrophotometer (JASCO, Tokyo, Japan) equipped with an integrating sphere unit. The crystalline phases were identified by X-ray diffraction (XRD) using an RINT2200VF apparatus (Rigaku, Japan) with Cu Kα radiation. The surface states of the plates were investigated by scanning electron microscopy coupled with energy dispersive X-ray fluorescence spectroscopy (SEM-EDX) using a Hitachi S-3000N and EX-200K instrument (Ibaraki, Japan). The weights of the photocatalysts deposited on the glass plate and the dien-coated glass plate were quantified using a CPA225D semi-micro analytical electronic balance (Sartorius Inc., Germany).

7.2.4. Evaluation of photocatalyst-dien-plates in aqueous solutions

The water treatment abilities of the photocatalytic plates were evaluated by measuring the changes in the absorbance of MB and InC as a function of irradiation time. While ST01–dien and SiT–dien-coated glass plates (ST01– and SiT–dien-plates) were used for the MB and InC decomposition reactions in aqueous solutions under UV irradiation, the VNSiT–dien-coated glass plate (VNSiT–dien-plate) was utilized to evaluate the photodecompositions under visible light irradiation.

The photodecomposition of MB and InC were conducted in a flow evaluation system (Chap. 6).

Furthermore, before and after photoirradiation, the change in total organic carbon (TOC) was measured to confirm the photodecomposition-induced mineralization of MB and InC using a TOC-UVA analyzer (Kyoritsu Chemical-Check Lab. Co., Tokyo, Japan) [19]. The analyzer presented a linear range between 3.0 and 30 mg/L and a limit of

quantification of 3.0 mg/L for TOC measurements.

In these experiments, two UV lamps emitting at 352 nm (National-FL20S-BLB lamp, Matsushita Electric Industrial Co., Ltd., Osaka, Japan) were arranged in parallel to generate a light irradiance of 2.0 mW/cm^2.

The photodecompositions of MB and InC using the photocatalytic plates were also carried out under visible light irradiation. The visible light responsiveness of the VNSiT–dien-plate in aqueous media was tested by irradiating the reactor with 96 blue light-emitting diodes (LEDs, NSPB510S, Nichia) emitting between 420 and 520 nm (4 panels equipped with 24 LEDs each, **Fig. 7-1**) for a light irradiance of 42 mW/cm^2. Adsorption tests were conducted in the dark for 5 h for MB and for 1 h for InC. The decomposition of MB and InC were evaluated for 24 h. With the exception of the different irradiation wavelengths, the experimental conditions and measurement methods were the same as those described above.

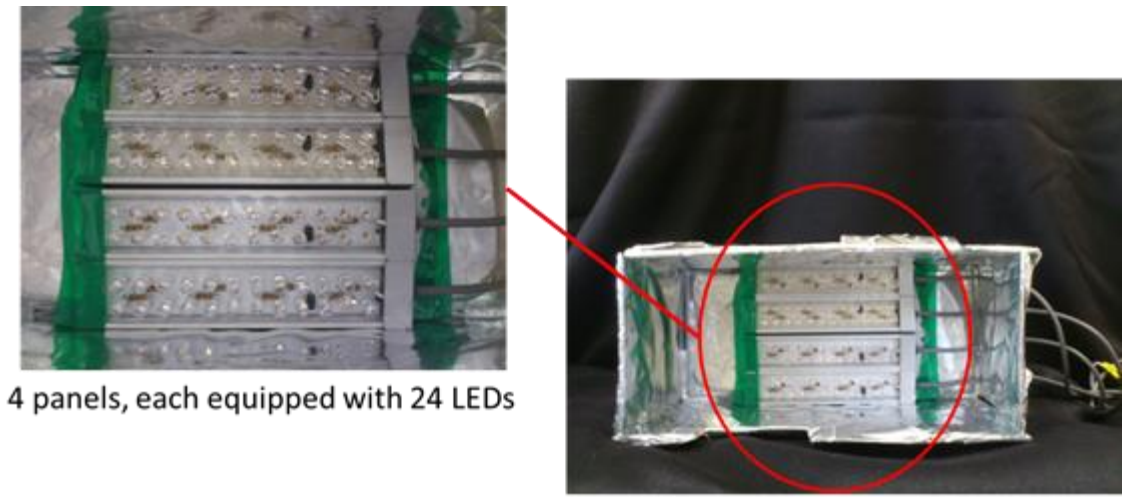

Fig. 7-1 Visible light source.

7.2.5. Application to photodecomposition of humic substances

The ability of the photocatalytic plate to decompose dissolved humic substances isolated from peaty soils (Uighur, Middle West China) was evaluated. The sample was magnetically stirred for 1 d and filtered using a 0.45 μm-membrane filter to remove solid materials. The initial TOC and pH were 15 mg/L and 6.1, respectively. The humic substances in water (50 mL) were circulated at a flow rate of 0.6 mL/min in the flow system shown in **Fig. 7-2**. The changes in absorbance at 254 nm (UV_{254}) were continuously monitored by the flow system as a function of reaction time. Adsorption tests were conducted in the dark for 5 h on the SiT–dien-plate, and the photodecomposition test was performed for 18 h under UV irradiation.

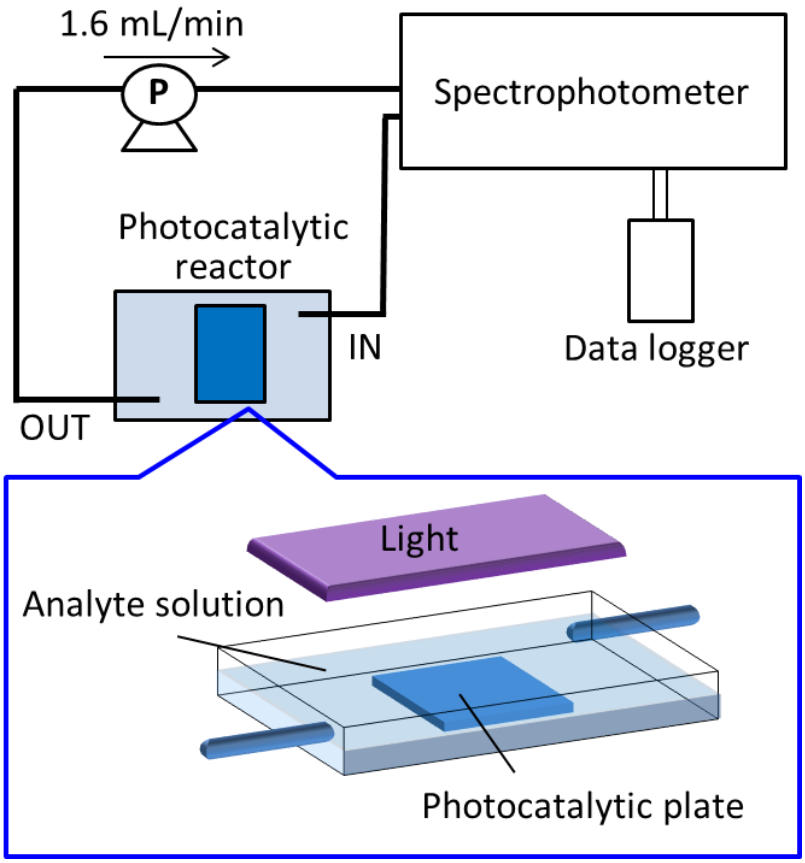

Fig. 7-2 Schematic illustration of flow analytical system for photocatalytic evaluation.

7.3. Results and discussion

7.3.1. Characterization of photocatalyst-dien-plates

First, the weights of deposited photocatalysts and UV–visible absorbance spectra were determined for each of the photocatalyst–dien-plates. **Fig. 7-3** compares the weights of the photocatalysts on the dien-plates to those on uncoated glass plates. The weight of ST01 was 1.2 times larger on the dien-plate than on uncoated glass, indicating that the effect of the dien coating was small. In contrast, the weights of SiT and VNSiT were 5.6 and 7.8 times higher, respectively, on the dien-plates than on the uncoated glass plates. These results may stem from the surface charges of the photocatalysts deposited on the dien-plates.

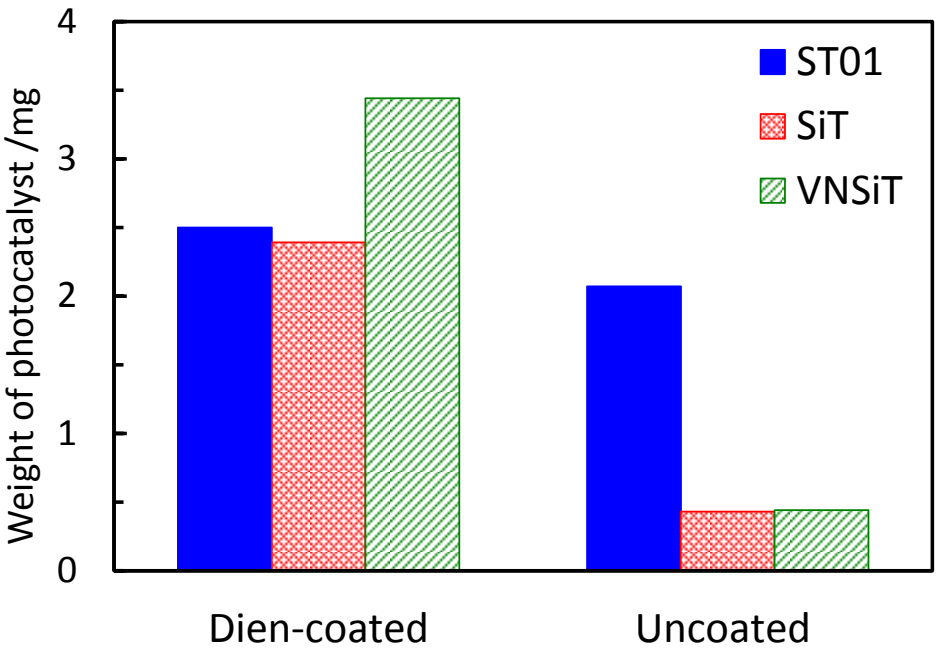

Fig. 7-3 Weights of photocatalyst deposited on dien-coated and uncoated glass plates.

SEM images revealed that SiT and VNSiT were more uniformly spread on the dien-plate surfaces than on ST01 (**Fig. 7-4**). The thicknesses of SiT and VNSiT ranged from 1 to 3 nm on the dien-plates (**Figs. 7-4B-2** and **7-4C-2**), while that of ST01 exceeded 3 nm (**Fig. 7-4A-2**).

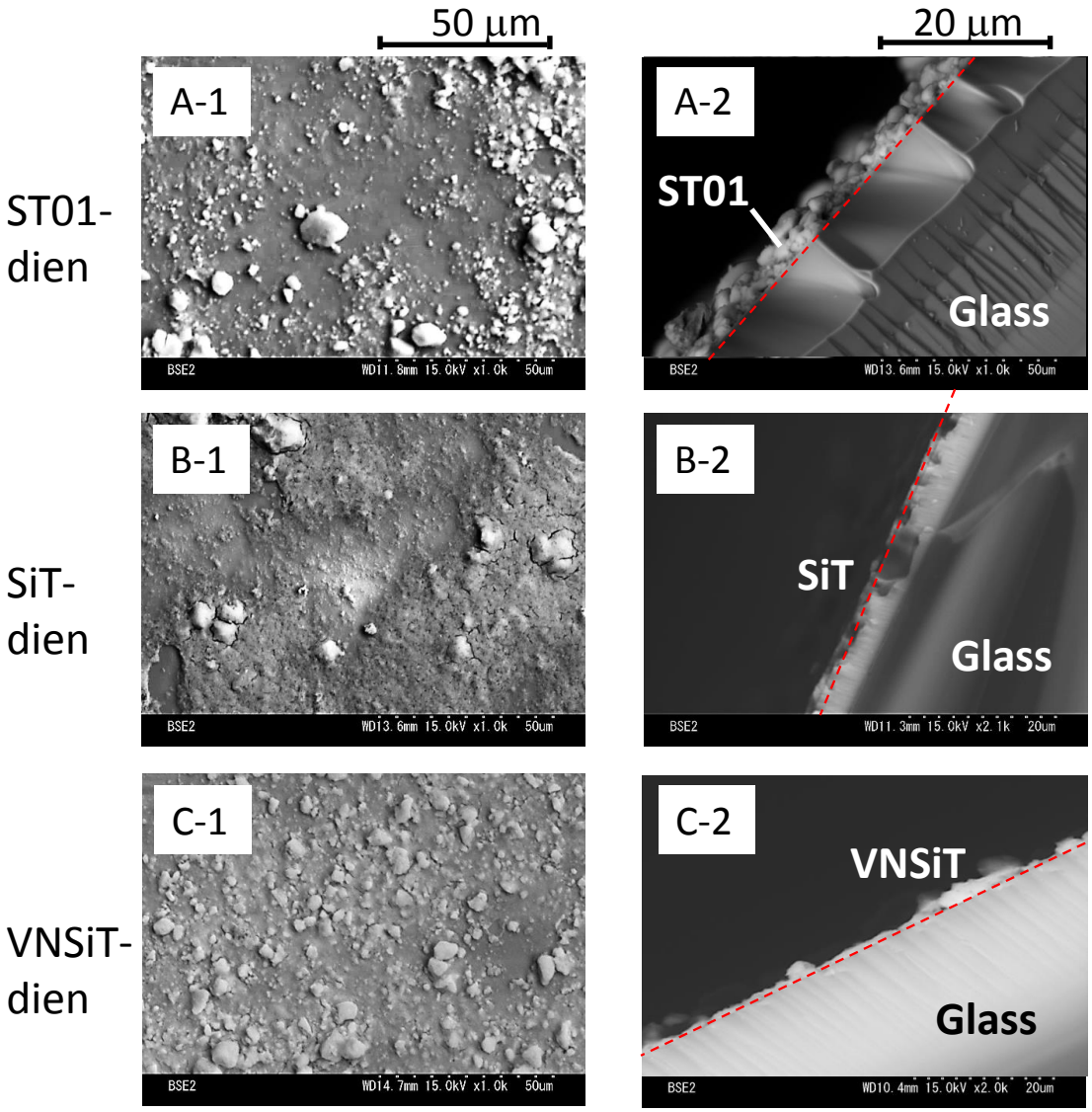

Fig. 7-4 SEM images of photocatalytic dien-coated glass plates.
(A) ST01–dien-, (B) SiT–dien-, and (C) VNSiT–dien-plates. (A1), (B1), and (C1) surface images. (A2), (B2), and (C2) cross-sectional images.

The transmission spectra of the prepared photocatalyst–dien-plates were obtained by UV–visible absorption spectrometry. The transmissions of the photocatalyst–dien-plates ranged from 300 to 450 nm (**Fig. 7-5**). The VNSiT–dien-plate exhibited the lowest transmission, consistent with its high visible light responsiveness.

Adsorbed ST01, SiT, and VNSiT were retained on the dien-coated glass plates after passing water (50 mL) at a flow rate of 1.6 mL/min for 24 h, but were removed from their uncoated counterparts. The amounts of deposited photocatalyst may be related to the uniform SiT and VNSiT coatings on the entire glass plate surface resulting from the high dispersibility of the particles in solution compared with that of ST01 particles, which partially aggregated on the glass plate.

In contrast, after circulating 50 mL water for 24 h, the photocatalyst–dien-plates showed XRD peaks corresponding to anatase TiO_2 (**Fig. 7-6**), indicating that photocatalyst deposition on the dien-plates did not alter the crystalline states.

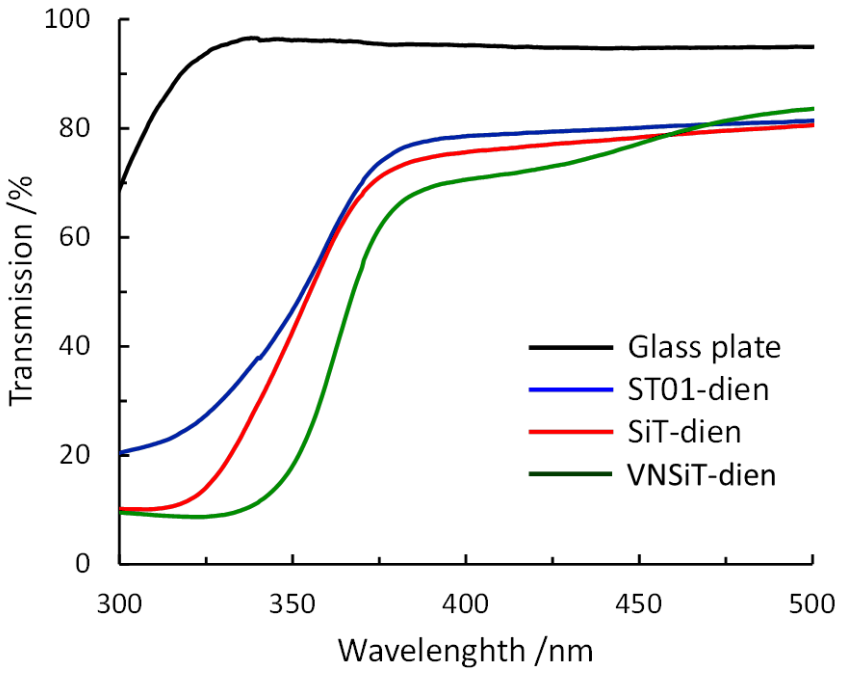

Fig. 7-5 UV–visible spectra of photocatalytic glass plates. Spectra of the glass plates were estimated using a JASCO V-650 spectrophotometer (JASCO, Tokyo, Japan).

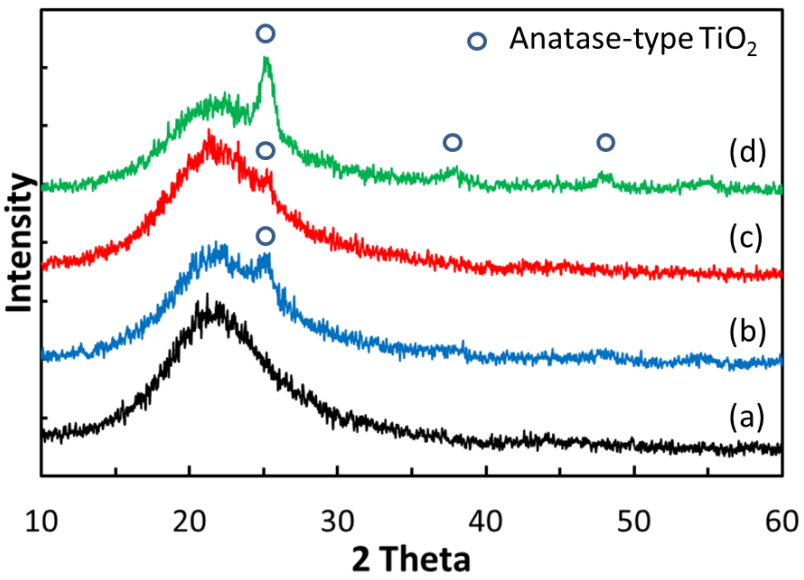

Fig. 7-6 XRD patterns of (a) bare glass-, (b) ST01–dien-, (c) SiT–dien-, and (d) VNSiT–dien-plates after circulating 50 mL water for 24 h.

ST01, SiT, and VNSiT displayed pH values of 6.0, 4.0, and 3.0, respectively, at the pI values estimated from previous zeta potential measurements (**Fig. 7-7**). Although the analytical instrument could not provide actual pI values, these results were assumed to be parallel to the pI values of the photocatalysts deposited on the dien-plates. Therefore, the negatively charged SiT and VNSiT particles were more strongly attracted to the positively charged dien, as compared to ST01 particles.

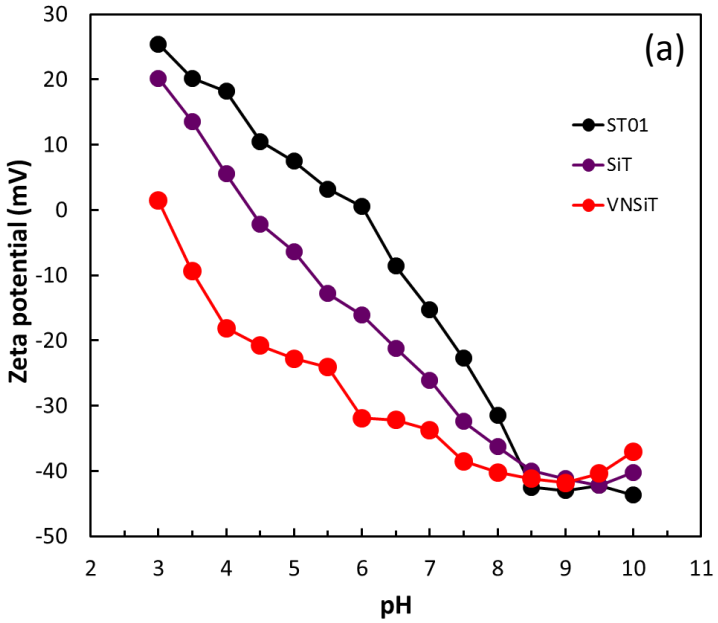

Fig. 7-7 Zeta potentials of ST01, SiT, and VNSiT particles.

7.3.2. Photocatalytic activity of SiT-dien-plate under UV irradiation

Changes in the concentration of MB on the ST01–dien- and SiT–dien-plates were investigated as a function of UV irradiation time. Adsorption experiments performed in the dark for 2 h showed that the SiT–dien-plate adsorbed 5.7% of the initial amount of MB (**Fig. 7-8a**), owing to weak electrostatic attractions between MB and SiT on the plate. After UV irradiation for 18 h, the SiT–dien-plate quantitatively decomposed MB,

while the ST01–dien-plate led to approximately 60% MB decomposition, suggesting that the electrostatic attractions between the SiT–dien-plate and MB were sufficient for photodecomposition. Furthermore, the TOC (3.6 mg/L) in the test solution following UV irradiation was the same as that prior to irradiation regardless of the photocatalyst, indicating that the organic transformation products generated from the decomposition of MB were not further mineralized. This was consistent with several studies, which reported that the mineralization of MB was difficult using common TiO_2 photocatalysts under UV irradiation [20, 21].

Changes in the concentration of InC on ST01–dien- and SiT–dien-plates were also monitored as a function of UV irradiation time. As shown in **Fig. 7-8b**, although neither plate exhibited InC adsorption in the dark after 2 h (mainly because of electrostatic repulsion between negatively charged functional groups ($–SO_3^-$) in InC), the complete decomposition of InC was achieved under UV irradiation for 10 and 14 h, respectively.

Furthermore, the TOC in the test solution (6.0 mg/L) did not change on the ST01–dien-plate (6.0 mg/L), but decreased to 3.1 mg/L on the SiT–dien-plate after 18 h of UV irradiation, demonstrating that the organic transformation products generated by the decomposition of InC were further decomposed and mineralized on the SiT–dien-plate.

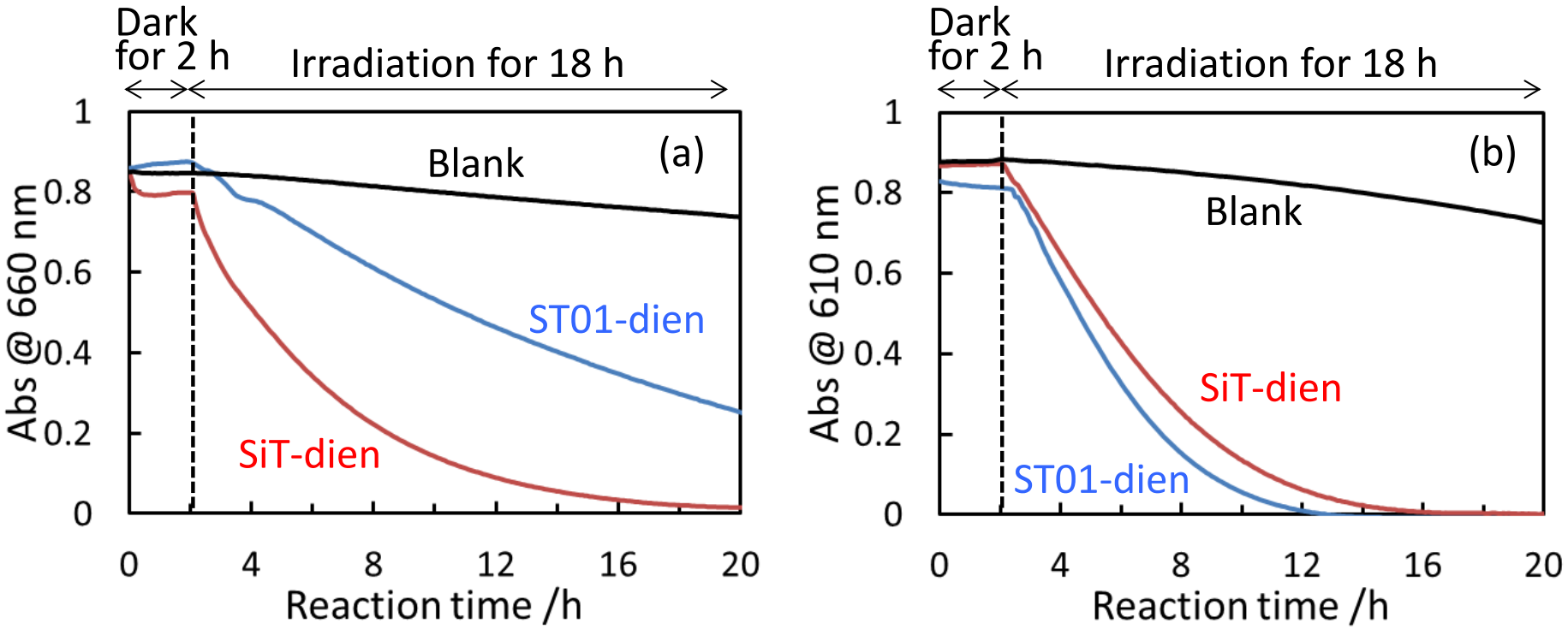

Fig. 7-8 Photocatalytic decompositions of (a) MB and (b) InC on photocatalyst–dien-plates under UV irradiation.

7.3.3. Photocatalytic activity of VNSiT–dien-plate under visible light irradiation

The photodecompositions of MB and InC on the VNSiT–dien-plate under visible light irradiation were evaluated using the flow analytical system.

As shown in **Fig. 7-9**, MB and InC were not completely decomposed on the VNSiT–dien-plate after visible light irradiation for 24 h. The photocatalytic glass adsorbed 18% MB in the dark, and photo-decomposed 70% InC and 83% MB. Additionally, no changes in the TOC were observed upon exposure to visible light on the VNSiT–dien-plate.

The photocatalytic decomposition of MB basically consisted of demethylation involving MB, azure B, azure A, and azure C [20,21]. On the other hand, indigo, 2-nitro benzaldehyde, anthranilic acid, 2-nitro benzoic acid, and nitro benzene have been observed in the photocatalytic decomposition of InC [22].

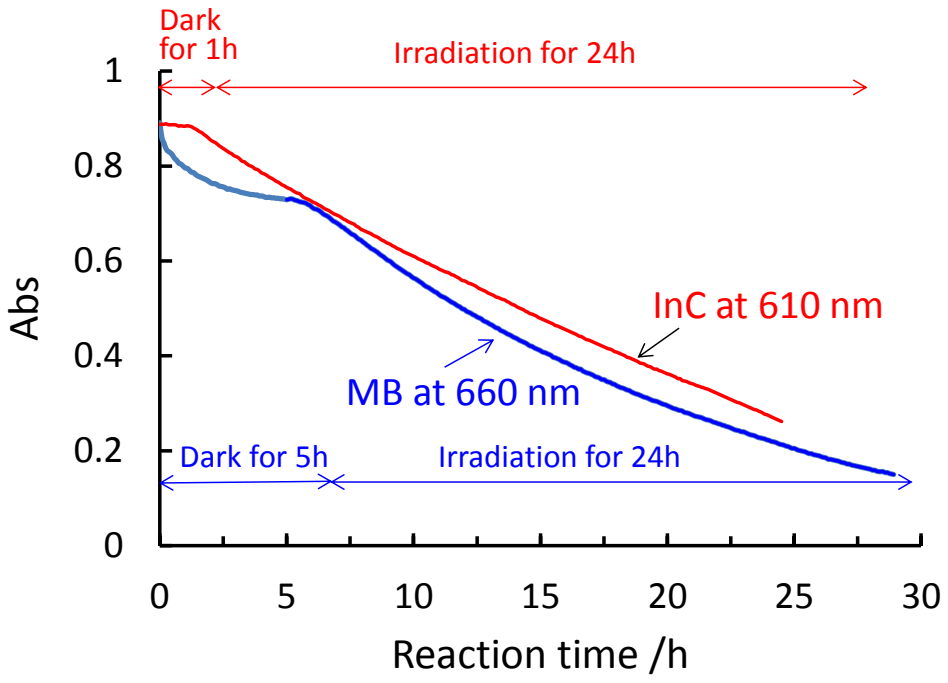

Fig. 7-9 Adsorption in the dark and photodegradation of MB and InC under visible light irradiation on VNSiT–dien-plate.

7.3.4. Photodecomposition rate constants

To understand the reaction kinetics of the decomposition of MB and InC on the ST01–dien- and SiT–dien-plates under UV irradiation and on the VNSiT–dien-plate under visible light irradiation, the photodecomposition rate constants (k) for an apparent pseudo-first-order model were calculated using Eq. (1):

$$\ln (C/C_0) = kt + a \qquad (1)$$

where C is the concentration of solute remaining in solution at irradiation time t, C_0 is the initial concentration (t = 0), and a is the intercept. The k values were estimated by linearly fitting plots of ln (C/C_0) as a function of t. SiT–dien-coated glass, which exhibited highly dispersed photocatalysts and a negative charge at neutral pH, displayed a rate constant that was 2.8 times higher than that of the ST01–dien-plate for the decomposition of positively charged MB under UV irradiation. The linear fits, correlation coefficients (r^2), half-life time ($t_{1/2}$) and k are summarized in **Table 7-1**. The photocatalytic plate prepared under mild conditions (non-calcination) facilitated the decomposition of MB under a lower light intensity as compared to those of typical materials prepared with calcination [23,24], as summarized in **Table 7-2**. The electrostatic adsorption of cationic dyes in the dark may contribute to the effective photodecomposition under light irradiation. The experimental results also suggested that the SiT–dien-plate may be useful for the decomposition of acidic InC dye. Although InC did not adsorb on the photocatalytic glass plate in the dark, OH radicals generated from the plate surface may effectively induce the desulfonation of InC. The k value for

the decomposition of InC was lower for the SiT–dien-plate than for the ST01–dien-plate, even though the decomposition rate was higher than that for MB. This may originate from electrostatic repulsion between the negatively charged SiT–dien-plate and InC.

The photodecomposition rate constants on the VNSiT–dien-plate under visible light irradiation decreased in the following order: MB (k = 0.0673 h^{-1}) > InC (k = 0.0502 h^{-1}) (**Table 7-3**). The plate did not facilitate the decomposition of MB as efficiently as some other visible light-responsive photocatalytic materials [25,26], as summarized in **Table 7-4**, primarily because MB strongly adsorbed on the VNSiT–dien-plate, which reduced the photoactivity under visible light irradiation, which has a weaker light intensity than UV-light irradiation. This implies that the valence between the adsorptivity and photoactivity of photocatalysts towards target species is important in highly efficient water treatment systems.

Table 7-1 Linear fits[a], correlation coefficients (r^2), photodegradation rate constants (k), and half-life times ($t_{1/2}$)[b] of MB and InC using ST01–dien- and SiT–dien-plates under ultraviolet irradiation.

	ST01-dien				SiT-dien			
Analyte	Approximation	r^2	k / h^{-1}	$t_{1/2}$ / h	Approximation	r^2	k / h^{-1}	$t_{1/2}$ / h
MB	y = –0.0783x + 0.223	0.9963	0.0783	11.7	y = –0.223x + 0.403	0.9972	0.223	4.91
InC	y = –0.305x + 0.817	0.9805	0.305	4.95	y = –0.235x + 0.616	0.9865	0.235	5.57

[a] Estimated using Eq. (1).

[b] Half-life times were calculated assuming that C/C_0 was 0.5.

Table 7-2 Comparative data of photodecomposition rate constants (k) of MB using SiT–dien-plate and previous methods under UV light irradiation.

Photocatalyst	Immobilization method	Plate	Light intensity	Initial concentration of MB	k /h^{-1}
This study (Si-TiO_2)	Self-assemble without calcination	Glass	2.0 mW/cm^2	1.56×10^{-5} M	0.223
Ref. 28 (TiO_2-SiO_2)	Sol-gel at 550 °C calcination	Glass	600 mW/cm^2	1.00×10^{-5} M	0.204
Ref. 29 (TiO_2)	Sol-gel at 600 °C calcination	Glass	80 mW/cm^2	3.13×10^{-4} M (with 8×10^{-3} M H_2O_2)	0.156

Table 7-3 Linear fits[a)], correlation coefficients (r^2), photodegradation rate constants (k), and half-life times ($t_{1/2}$)[b)] of MB and InC using VNSiT–dien-plate under visible light irradiation.

Analyte	Approximation	r^2	k / h^{-1}	$t_{1/2}$ / h
MB	y = –0.0673x + 0.251	0.9974	0.0673	14.0
InC	y = –0.0502x + 0.108	0.9929	0.0502	15.6

[a)] Estimated using Eq. (1).

[b)] Half-life times were calculated assuming that C/C_0 was 0.5.

Table 7-4 Comparative data of photodecomposition rate constants (k) of MB using VNSiT–dien-plate and previous methods under visible light irradiation.

Photocatalyst	Immobilization method	Plate	Light intensity	Initial concentration of MB	k /h^{-1}
This study (VNSiT)	Self-assemble without calcination	Glass	42.0	1.56×10^{-5} M	0.0673
Ref. 30 (N-TiO_2)	Atomic-layer deposition at 450 °C calcination	FTO glass	600	Unknown	0.108
Ref. 31 (C-TiO_2)	Sputtering of photocatalyst to 250 °C of Si-quartz substrate	Si and quartz	1.51	1.56×10^{-5} M	0.108

7.3.5. Photodecomposition of humic substances under UV-irradiation

The photocatalytic plates were used in the treatment of humic substances in waste water. In this case, to estimate the changes in the concentration of humic substances as a function of reaction time, the absorbance at 254 nm (UV_{254}), which is commonly used as an indicator of aromatic compounds in water, was continuously monitored by the flow analytical system. Additionally, the TOC values were analyzed by a TOC analyzer. In this study, the SiT–dien-plate was employed as the test plate under UV-irradiation.

As shown in **Fig. 7-10**, the UV_{254} of the sample solution decreased by about 2% after 5 h in the dark, and the UV_{254} and TOC after 18 h of UV irradiation decreased by 75% and 48%, respectively. The *k* value calculated using Eq. (1) for the UV_{254} values amounted to 0.083 h^{-1} for the SiT–dien-plate under UV irradiation, suggesting that the waste-water treatment performance of the photocatalytic materials was less than their ability to decompose MB and InC standard solutions, potentially owing to influences from matrices coexisting in the waste-water sample, though it could not be confirmed at this stage.

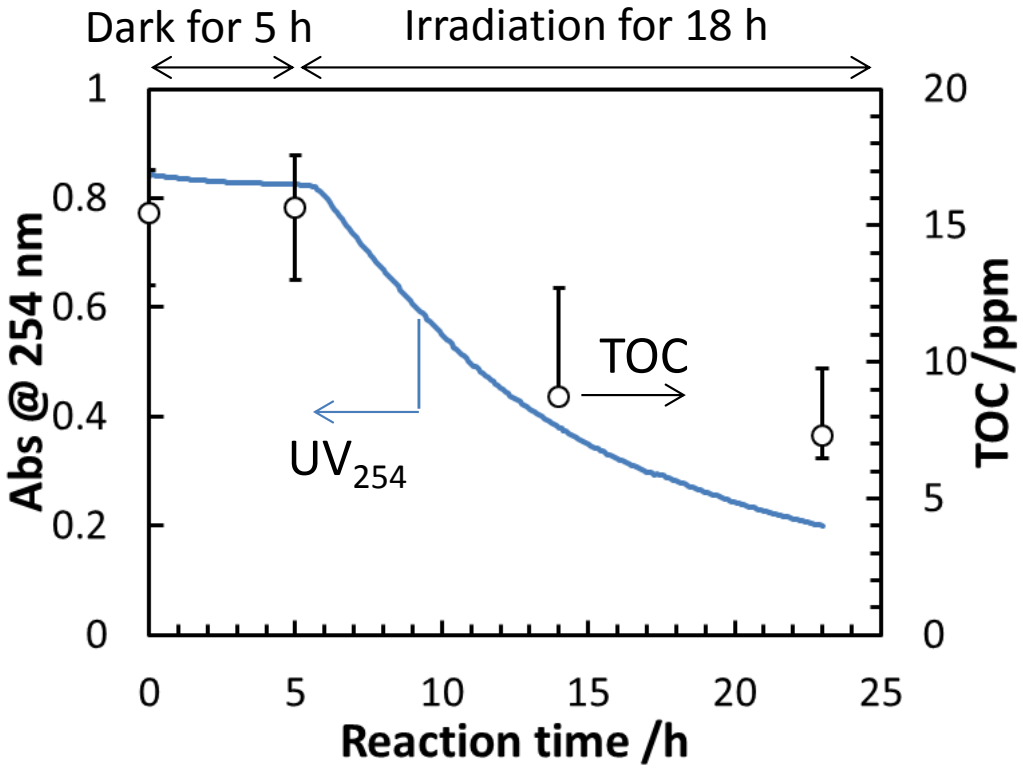

Fig. 7-10 Changes in UV_{254} and TOC during the treatment of humic substances in waste water using SiT–dien-plate under UV irradiation.

7.4. Conclusions

In this study, a photocatalyst–dien-plate was evaluated for applications in water treatment by the continuous monitoring of the flow analytical system without consumption of the test solution. The highly dispersible SiT particles facilitated stable photodecompositions regardless of the reactant charge under UV and visible light irradiations. The plates decomposed a cationic dye (MB) and anionic dye (InC), and the efficiencies were enhanced by electrostatic adsorption of cationic species. In the photodecomposition of dissolved humic substances, the *k* value obtained from the UV_{254} values on the SiT–dien-plate under UV irradiation was lower than its ability to decompose MB and InC standard solutions.

Consequently, the use of the flow analytical system provided the effective of SiT–dien-plate not only for photodecomposition of ionic dyes but also for that of dissolved humic substance. As next stage, the system will be applied to treatment of practical water samples, as well as the evaluation of novel phocatalytic materials developed.

7.5. References

[1] T. Ban, Y. Tanaka, Y. Ohya, Fabrication of titania films by sol–gel method using transparent colloidal aqueous solutions of anatase nanocrystals, Thin Solid Films 519 (2011) 3468 – 3474.

[2] Z. Liu, X. Zhang, T. Murakami, A. Fujishima, Sol– gel SiO_2/TiO_2 bilayer films with self-cleaning and antireflection properties, Sol. Energ. Mat. Sol. C. 92 (2008) 1434 – 1438.

[3] M. Kitano, K. Funatsu, M. Matsuoka, M. Ueshima, M. Anpo, Preparation of nitrogen-substituted TiO_2 thin film photocatalysts by the radio frequency magnetron sputtering deposition method and their photocatalytic reactivity under visible light irradiation, J. Phys. Chem. B. 110 (2006) 25266 – 25272.

[4] Y. Yasuda, M. Tobisaka, K. Kamikuri, Y. Hoshi, Effect of ion bombardment on low-temperature growth of TiO_2 thin films in DC reactive sputtering with two sputtering sources, Surf. Coat. Tech. 231 (2013) 439 – 442.

[5] J.H. Lee, M. Kang, S.J. Choung, K. Ogino, S. Miyata, M.S. Kim, J.Y. Park, J.B. Kim, The preparation of TiO_2 nanometer photocatalyst film by a hydrothermal method and its sterilization performance for *Giardia lamblia*, Water Res. 38 (2004) 713 – 719.

[6] R. Fernandes, N. Patel, R. Dholam, M. Adami, A. Miotello, Low energy ion-beam modification of TiO_2 photocatalyst thin film for visible light absorption, Surf. Coat. Technol. 203 (2009) 2579 – 2583.

[7] M. Takeuchi, Y. Onozaki, Y. Matsumura, H. Uchida, T. Kuji, Photoinduced hydrophilicity of TiO_2 thin film modified by Ar ion beam irradiation, Nucl. Instrum.

Methods Phys. Res. B 206 (2003) 259 – 263.

[8] W. Mekprasart, T. Khumtong, J. Rattanarak, W. Techitdheera, W. Pecharapa, Effect of nitrogen doping on optical and photocatalytic properties of TiO_2 thin film prepared by spin coating process, Energ. Procedia 34 (2013) 746 – 750.

[9] M. Kitano, K. Iyatani, E. Afsin, Y. Horiuchi, M. Takeuchi, S.H. Cho, M. Matsuoka, M. Anpo, Photocatalytic oxidation of 2-propanol under visible light irradiation on TiO_2 thin films prepared by an RF magnetron sputtering deposition method, Res. Chem. Intermed. 38 (2012) 1249 – 1259.

[10] R. Velmurugan, B. Krishnakumar, B. Subash, and M. Swaminathan, Preparation and characterization of carbon nanoparticles loaded TiO_2 and its catalytic activity driven by natural sunlight, Sol. Energ. Mater. Sol. Cells 108 (2013) 205 – 212.

[11] S. Iwamoto, W. Tanakulrungsank, M. Inoue, K. Kagawa, P. Praserthdam, Synthesis of large-surface area silica-modified titania ultrafine particles by the glycothermal method, J. Mater. Sci. Lett. 19 (2000) 1439 – 1443.

[12] A. Mase, T. Sugita, M. Mori, S. Iwamoto, T. Tokutome, K. Katayama, H. Itabashi, Study of vanadium-modified N/Si co-doped TiO_2 in aqueous solution and its photocatalytic activity, Chem. Eng. J. 225 (2013) 440 – 446.

[13] F. Kojin, M. Mori, Y. Noda, and M. Inagaki, Preparation of carbon-coated $W_{18}O_{49}$ and its photoactivity under visible light, Appl. Catal. B-Environ. 78 (2008) 202 – 209.

[14] D. Rajamanickam, and M. Shanthi, Photocatalytic degradation of an azo dye Sunset Yellow under UV-A light using TiO_2/CAC composite catalysts, Spectroc. Acta Pt. A-Molec. Biomolec. Spectr. 128 (2014) 100 – 108.

[15] A. Syoufian, K. Nakashima, Degradation of methylene blue in aqueous dispersion of hollow titania photocatalyst: Optimization of reaction by peroxydisulfate electron scavenger, J. Colloid Interface Sci. 313 (2007) 213 – 218.

[16] Z. Liu, Y. Wang, W. Chu, Z. Li, C. Ge, Characteristics of doped TiO_2 photocatalysts for the degradation of methylene blue waste water under visible light, J. Alloys. Compd. 501 (2010) 54 – 59.

[17] Q.I. Rahman, M. Ahmad, S.K. Misra, M. Lohani, Efficient degradation of methylene blue dye over highly reactive Cu doped strontium titanate ($SrTiO_3$) nanoparticles photocatalyst under visible light, J. Nanosci. Nanotechnol. 12 (2012) 7181 – 7186.

[18] R. Vinu, S.U. Akki, G. Madreas, Investigation of dye functional group on the photocatalytic degradation of dyes by nano-TiO_2, J. Hazard. Mater. 176 (2010) 765 – 773.

[19] S. Ishii, H. Okumura, S. Okauchi, K. Okuchi, K. Kato, S. Urano, K. Urano, New method of analyzing TOC by efficient UV oxidation and turbidity measurement, Jpn. Soc. Water Environ. (Japanese) 36 (2013) 183 – 190.

[20] M.A. Rauf, M.A. Meetani, A. Khaleel, A. Ahmed, Photocatalytic degradation of Methylene Blue using a mixed catalyst and product analysis by LC/MS, Chem. Eng. J. 157 (2010) 373 – 378.

[21] S. Horikiri, N. Teshima, Y. Saruki, H. Nishikawa, T. Sakai, Decomposition of methylene blue by new porous photocatalysts and analysis of decomposed products using high-performance liquid chromatography and mass spectrometry, Bunseki Kagaku (Japanese) 52 (2003) 881 – 885.

[22] M. Vautier, C. Guilland, J. Herrmann, Photocatalytic degradation of dyes in water: Case study of indigo and indigo carmine, J. Catal. 201 (2001) 46 – 59.

[23] P. Klankaw, C. Chawengkijwanich, N. Grisdanurak, and S. Chiarakorn, The hybrid photocatalyst of TiO_2–SiO_2 thin film prepared from rice husk silica, Superlattice. Microst 51 (2012) 343 – 352.

[24] N. R. Mathews, E. R. Morales, M. A. Cortés-Jacome, and J. A. T. Antonio, TiO_2 thin films – Influence of annealing temperature on structural, optical and photocatalytic properties, Sol. Energ. 83 (2009) 1499 – 1508.

[25] V. J. Babu, M. K. Kumar, A. S. Nair, T. L. Kheng, S. I. Allakhverdiev, and S. Ramakrishna, Visible light photocatalytic water splitting for hydrogen production from N-TiO_2 rice grain shaped electrospun nanostructures, Int. J. Hydrog. Energ. 37 (2012) 8897 – 8904.

[26] S. Wang, T. Chen, K. K. Rao, and M. Wong, Nanocolumnar titania thin films uniquely incorporated with carbon for visible light photocatalysis, Appl. Catal. B Environ. 76 (2007) 328 – 334.

Chapter 8

Conclusion and future prospect

8.1. Conclusions

In this thesis, we mainly described study on syntheses and characterizations of photocatalytic materials and development of its evaluation system for water purification. We could enhance the adsorptivity of the photocatalyst by modifying silica, vanadium and hydroxyl apatite onto TiO_2 particle. The obtained photocatalyst were found to be suitable as particles to assist water treatment. In addition, the flow evaluation system developed in this study was usefulness to know water treatment capabilities of the photocatalyst-coating materials such as glass-plate or ceramic foam types.

In this chapter, the conclusions in each previous chapter are summarized as described below.

Chapter 1 summarized the recent study of photocatalyst and the approaches to water treatment technologies. This chapter was concluded that the addition of adsorptivity to photocatalyst and the immobilization onto any materials were required when applying photocatalyst to water treatment.

Chapter 2 described the coating method of hydroxyapatite onto TiO_2 particle using photoinduced superhydrophilic reaction, and its water treatment ability under irradiation

of UV-light. The attractive point was that the coating method using light irradiation could effectively coat a biomimetic compound to photocatalyst, which cannot apply to the coating process with calcination. Additionally, this synthesis method has advantages that indicates short synthesis time, lower precursor concentration and high crystalline.

Chapter 3 described the syntheses and the capabilities of photocatalysts modifying vanadium and silica to TiO_2, in order to obtain high-adsorptivity for cationic species in aqueous solution. The synthesized VT, SiT and VSiT particles have negative charge at weak-acidic pH, and can effectively adsorb cationic species such as methylene blue (MB), compared to bare TiO_2 partcile. Especially, VT and SiT could effectively decompose MB because of good valance between the adsorptivities and photoactivities. In contrast, VSiT exhibited the lower decomposition efficiency of MB. This result showed the strongest adsorptivity lead to the lower decomposition efficiency. For anionic dye InC, the negatively charged photocatalysts showed the lower decomposition efficiencies, due to the electrostatic repulsion between them. Those results imply to be necessary to select a photocatalyst in accordance with the target species.

Chapter 4 described the photocatalytic ability of vanadium modified-N/Si-codoped TiO_2 (VNSiT) in order to obtain visible light responsive as well as high-adsorptivity for cationic species in aqueous solution. VNSiT exhibited high decomposition capacities for DMSO in an aqueous solution under visible-light irradiation. The high activity was related to their higher dispersibility and smaller average hydrodynamic diameters in water, compared to those of other photocatalysts. The vanadium species in the VNSiT

exhibited a promoter effect, enhancing contact with the substrate molecule because of its high dispersibility.

Chapter 5 described the water treatment ability of TiO_2–coated ceramic foam filter (TCF), as a high-efficient photocatalytic-coating material. Photodecomposition of natural organic matter (NOM) in swamp water by a TCF was found to follow the same trend as the photodegradation of a humic acid (HA), which is a precursor of THMs and HAAs. The disinfection byproducts (DBPs) formation potential after chlorination of the photocatalytically treated water samples was strongly dependent on TOC and UV_{254}. Accordingly, the TOC and UV_{254} values in aqueous solution were concluded to be key indicators of the photodecomposition efficiency.

Chapter 6 described the establishment of novel evaluation system for water treatment efficiency using photocatalyst-coating glass plate. The photocatalyst-glass plate was obtained by dipping glass plate in the suspended photocatalyst solution. The plates decomposed MB and InC, without regarding to their charges. Also the electrostatic adsorptions of SiT-, VT-, VSiT-plates to cationic species could be conducted to the efficient photodecomposition. Furthermore, we could successfully analyze simultaneous monitoring of decrease in IBP and formation of its by-product, by using flow evaluation system.

Chapter 7 described the coating method by electrostatic interaction using cationic silane-coupling reagent as a spacer to bind between photocatalyst particle and glass plate. The highly dispersible SiT particles facilitated the stable coating onto glass plate,

and the plate provided the photodecompositions of MB and InC under UV and visible light irradiations. In the photodecomposition of dissolved humic substances, the *k* value obtained from the UV_{254} values on the SiT–dien-plate under UV irradiation was lower than its ability to decompose MB and InC standard solutions.

Through these results, I believe that our developed photocatalyst and its materials can play the role for the construction of a water treatment system using a photocatalyst.

8.2. Future prospect

Water treatment using photocatalytic material has been attracting attention. This attention has been expected to be even greater in future. Through this study, we are considering that photocatalyst can be applied to 1) maintenance of cyclic water in plant factory and 2) treatment of industrial wastewater is expected.

1) In plant factory, water containing the nutrients needed for plant growth is circulated. Under this condition, it is necessary to sterilize the cyclic water with bacteria-prone [1]. By applying the photocatalytic to sterilization of water, it can keep the constant water quality in the maintenance-free. At this stage, the flow evaluation system described in Chaps. 6 and 7 is considered to be useful to introduce the sterilization system, because it can monitor the quality of cyclic water.
2) For treatment of industrial waste water, it has been performed by oxidation degradation using Fenton reaction [2] and biological removal [3]. However, those methods have some problems such as mass consumption of chemicals and

generation of sludge. If the photocatalyst-coating materials to water treatment can easily decompose the persistent substances, it should suppress the cross-contamination owing to the mass consumption of chemicals and the generation of sludge.

To achieve the future prospects as mentioned above will be next subjects to enhance the affinity to photocatalyst for target materials, and to consider shape of substrate coating photocatalyst. In our laboratory, to solve this problem, we will develop anion-adsorptive photocatalyst and establish water treatment system combining various photocatalysts.

8.3. References

[1] Patent licensing support chart: Hydroponic culture (Plant factory), (2006) Industrial property rights information: Training Hall, Tokyo, p. 4.

[2] T-W. Hao, P-Y. Xiang, R. Mackey, K. Chi, H. Lu, H-K. Chui, M. C.M. V. Loosdrecht, G-H. Chen, A review of biological sulfate conversions in wastewater treatment, Water Res. 65 (2014) 1 – 21.

[3] H. Zangeneh, A.A.L. Zinatizadeh, M. Feizy, A comparative study on the performance of different advanced oxidation processes ($UV/O_3/H_2O_2$) treating linear alkyl benzene (LAB) production plant's wastewater, J. Ind. Eng. Chem. 20 (2014) 1453 – 1461.

Acknowledgment

Foremost, I wish to express my sincere gratitude, appreciation and thanks to the promoter of the dissertation, Prof. Dr. ***Hideyuki Itabashi***, and Assoc. Prof. Dr. ***Masanobu Mori***, Graduate School of Science and Technology, Gunma University for their numerous helpful suggestions on this work, and their generous guidances, advices and encouragement throughout my course of study.

I would like also to express my deepest gratitude to Prof. Dr. ***Hideki Amii***, Prof. Dr. ***Hiroaki Ozaki***, Prof. Dr. ***Masashi Sonoyama***, and Assoc. Prof. Dr. ***Hideyuki Morimoto***, Graduate School of Science and Technology, Gunma University for their valuable suggestion and constructive comments during the course of this work and the preparation of this dissertation.

I wish to express my deep tratitude to Assoc. Prof. Dr. ***Shinji Iwamoto***, Mr. ***Toru Tokutome***, and Mr. ***Shin-Nosuke Noguchi***, Graduate School of Science and Technology, Gunma University, who give me constructive opinions and suggestion on my study.

I am also deeply indebted to Prof. Dr. ***Kenji Katayama***, Department of Applied Chemistry, Chuo University, who gave me constructive opinions and novel knowledge of photocatalyst.

I am also extended to Dr. ***Shigekazu Kato***, Photocatalytic Materials Inc., and Dr. ***Yoichi Saito*** for many helpful advice and discussions.

Finally, my deepest gratitude and appreciation are for my parents and friends, who at great sacrifice made it possible for me to have the luxury of length education.

March, 2015, Gumma

Tsuyoshi Sugita